Brazilian Journal of Medical and Biological Research (2007) 40: 1149-1157
ISSN 0100-879X

Preparation and cytotoxicity of cisplatin-containing liposomes

A.D. Carvalho Júnior[1], F.P. Vieira[1], V.J. De Melo[3], M.T.P. Lopes[3], J.N. Silveira[2], G.A. Ramaldes[1], A. Garnier-Suillerot[5], E.C. Pereira-Maia[4] and M.C. De Oliveira[1]

[1]Departamento de Produtos Farmacêuticos, [2]Departamento de Análises Clínicas e Toxicológicas, Faculdade de Farmácia, [3]Departamento de Farmacologia, Instituto de Ciências Biológicas, [4]Departamento de Química, Instituto de Ciências Exatas, Universidade Federal de Minas Gerais, Belo Horizonte, MG, Brasil
[5]Laboratoire BioMoCeTi UMR 7033, Université Paris 13, Paris, France

Abstract

We encapsulated cisplatin into stealth pH-sensitive liposomes and studied their stability, cytotoxicity and accumulation in a human small-cell lung carcinoma cell line (GLC4) and its resistant subline (GLC4/CDDP). Since reduced cellular drug accumulation has been shown to be the main mechanism responsible for resistance in the GLC4/CDDP subline, we evaluated the ability of this new delivery system to improve cellular uptake. The liposomes were composed of dioleoylphosphatidylethanolamine (DOPE), cholesteryl hemisuccinate (CHEMS), and distearoylphosphatidylethanolamine-polyethyleneglycol 2000 (DSPE-PEG_{2000}) and were characterized by determining the encapsulation percentage as a function of lipid concentration. Among the different formulations, DOPE/CHEMS/DSPE-PEG liposomes (lipid concentration equal to 40 mM) encapsulated cisplatin more efficiently than other concentrations of liposomes (about 20.0%, mean diameter of 174 nm). These liposomes presented good stability in mouse plasma which was obtained using a 0.24-M EDTA solution (70% cisplatin was retained inside the liposomes after 30 min of incubation). Concerning cytotoxic effects, they are more effective (1.34-fold) than free cisplatin for growth inhibition of the human lung cancer cell line A549. The study of cytotoxicity to GLC4 and GLC4/CDDP cell lines showed similar IC_{50} values (approximately 1.4 μM), i.e., cisplatin-resistant cells were sensitive to this cisplatin formulation. Platinum accumulation in both sensitive and resistant cell lines followed the same pattern, i.e., approximately the same intracellular platinum concentration (4.0×10^{-17} mol/cell) yielded the same cytotoxic effect. These results indicate that long-circulating pH-sensitive liposomes, also termed as stealth pH-sensitive liposomes, may present a promising delivery system for cisplatin-based cancer treatment. This liposome system proved to be able to circumvent the cisplatin resistance, whereas it was not observed when using non-long-circulating liposomes composed of phosphatidylcholine, phosphatidylserine, and cholesterol.

Correspondence
M.C. De Oliveira
Departamento de Produtos Farmacêuticos
Faculdade de Farmácia
UFMG
Av. Antônio Carlos, 6627
31270-901 Belo Horizonte, MG
Brasil
Fax: +55-31-3499-6935
E-mail: monicacristina@ufmg.br

Research supported by FAPEMIG and CNPq. A.D. Carvalho Júnior was the recipient of a CAPES fellowship.

Received April 10, 2006
Accepted March 26, 2007

Key words
- Cisplatin
- Liposomes
- Encapsulation
- Cytotoxicity

Introduction

cis-Diamminedichloroplatinum (II) (CDDP) or cisplatin is one of the most effective chemotherapeutic agents used for the treatment of ovary, lung, testicle, head, and neck carcinoma (1-5). However, its use presents some inconveniences, such as development of resistance in human ovarian cell line A2780, cervical cancer cell line ME180 and colon carcinoma cell line LoVo; side effects, principally nephrotoxicity, and chemical incompatibility with other drugs used simultaneously in polychemotherapy, such as etoposide and thiotepa (6,7). The appearance of resistance during therapy is an important limitation to the use of CDDP, leading to treatment failure (8-11). The use of higher doses of CDDP is not desirable due to the toxicity of the drug to multiple organs, such as damage to the kidneys and bone marrow, intractable vomiting, peripheral neuropathy, deafness, seizures, and blindness (12-14). The reasons for resistance to cisplatin have been reported to be multifactorial. Four main events accompany it in most cases: i) decreased accumulation of drug concentration (to below that necessary for cytotoxic activity), ii) increased levels of sulfur-containing molecules such as glutathione or metallothionein (which could play a role in metal detoxification), iii) enhanced repair of DNA damage caused by CDDP-DNA adducts by nucleotide excision repair proteins such as ERCC1, XPA, and XPB which can remove DNA adducts produced by CDDP, and iv) increased tolerance to CDDP-DNA adducts as a consequence of deficiencies in the mismatch repair system and enhanced replication bypass (15-18). Among the various resistance mechanisms involved, decreased cellular accumulation of CDDP has been demonstrated in most cases (19-24). Reduced intracellular CDDP concentration results in decreased DNA platination, which leads to CDDP resistance. The mechanism by which CDDP enters cells is not known. It has been postulated that cellular uptake of CDDP occurs by passive diffusion; however, some reports support a protein-mediated transport (21,24-26).

Thus, the employment of new delivery systems of CDDP such as stealth pH-sensitive liposomes can be a strategy to overcome these limitations. The encapsulation of CDDP into pH-sensitive liposomes can improve its entry into cells, can lead to an another pharmacokinetics profile, reducing or eliminating the side effects, and can allow the association with other drugs without the appearance of degradation products. These liposomes are generally taken up by the cells through an endocytosis process. The release of CDDP into the cytoplasm results from the ability of these liposomes to cross the endosomal membrane. Inside endosomes, the stealth pH-sensitive liposomes are exposed to an acidic medium, pH 5.5-6.5, which provokes their fusion with and the destabilization of the endosome membrane. Then, the encapsulated content is delivered into the cytoplasm (27,28). Therefore, in the present study, we investigated the encapsulation of CDDP into stealth pH-sensitive liposomes, the cytotoxic activity of the preparation, and its ability to circumvent CDDP resistance using A549, A431, BHK-21, and GLC4, GLC4/CDDP cell lines, respectively.

Material and Methods

Material

Cisplatin was supplied by Quiral Química do Brasil S.A. (Juiz de Fora, MG, Brazil). Distearoylphosphatidylethanolamine-polyethyleneglycol (DSPE-PEG) and dioleoylphosphatidylethanolamine (DOPE) were supplied by Lipoid GmBh (Ludwigshafen, Germany). Cholesteryl hemisuccinate (CHEMS) was purchased from Sigma (St. Louis, MO, USA), and sodium chloride was purchased from Merck (Rio de Janeiro, RJ, Brazil).

Preparation of liposomes

Initially, DOPE, CHEMS, and DSPE-PEG_{2000} were dissolved in chloroform (lipid concentration 20, 30, and 40 mM; molar ratio 5.7:3.8:0.5) and were transferred to a round bottom flask and submitted to evaporation. The lipid film obtained was dissolved in ethyl ether and then added to the 2 mg/mL CDDP solution prepared in 0.9% NaCl. The ratio of the aqueous to ether phase was 1:3. The resulting mixture was submitted to fast vortex agitation to produce a type of water/oil emulsion. Next, ethyl ether was evaporated, with the resulting formation of liposomes. These liposomes were submitted or not to filtration through 0.4-µm and 0.2-µm polycarbonate membranes (5 cycles each) and the unencapsulated CDDP was eliminated by ultracentrifugation with a Sorvall Ultra 80 ultracentrifuge (Albertville, MN, USA) at 150,000 *g* at 10ºC for 60 min.

Characterization of liposomes

The liposomes were characterized on the basis of their encapsulation percentage, size and zeta potential. The encapsulation percentage of CDDP into liposomes was determined by high-performance liquid chromatography. The chromatographic apparatus consisted of a Model 515 pump (Waters Instruments, Milford, MA, USA), a Model 717 Plus auto-injector (Waters Instruments) and a Model 2487 variable wavelength UV detector (Waters Instruments) connected to the Millennium software. Separations were done using Lichrospher® 100 NH2 guard column, 4 x 4 mm, 5 µm (Merck, Darmstadt, Germany) connected to a 25 cm x 4 mm Lichrospher® 100 NH2 column, 10-µm particles (Merck). The eluent system was composed of methanol/ethyl acetate/N,N-dimethylformamide/water, 4:4:1:1, and the flow rate was 1.0 mL/min. Samples (20 µL) were injected and the eluate absorbance was monitored at 310 nm. The amount of CDDP was determined in the stock solution employed for the preparation of liposomes and in the supernatant. The encapsulation percentage (EP) was calculated as:

$$EP = \frac{[CDDP]_{\text{liposomes before ultracentrifugation}} \text{ minus } [CDDP]_{\text{supernatant}} \times 100}{[CDDP]_{\text{liposomes before ultracentrifugation}}}$$

The loading capacity was assessed by measuring inorganic phosphorus (29). The mean diameter of the liposomes-containing CDDP was determined by the quasi-elastic light scattering, at 25ºC and at an angle of 90º. The zeta potential was evaluated by the determination of electrophoretic mobility at the 90º angle. The measurements were performed in triplicate using the 3000 HS Zetasizer equipment (Malvern Instruments, Worcestershire, England). The samples were diluted with a 0.9% NaCl.

Liposome stability

Stealth pH-sensitive liposomes containing CDDP were diluted 10-fold in 0.9% NaCl, pH 6.5, or mouse plasma, pH 7.4, and incubated at 37ºC for 30 min. The platinum released from liposomes containing CDDP was separated and determined by ultracentrifugation at 150,000 *g*, 10ºC, for 60 min followed by graphite furnace atomic absorption spectrometry (Springvale, Victoria, Australia).

Cytotoxicity assay

The human lung cancer cell line A549 and human cervix squamous carcinoma cell line A431 were cultured in modified DEMEN medium supplemented with 10% fetal bovine serum. The Baby Hamster Kidney cell line (BHK-21) was grown in RPMI 1640 medium supplemented with 10% fetal bovine serum. All cell lines were maintained at 36.5ºC in a humidified 2.5% CO_2 atmosphere. An aliquot containing 4 x 10^3 BHK

cells, 5 x 10^3 A549 or A431 cells was distributed in 96-well plates. After 24 h of growth, the cells were submitted to treatment with free CDDP, stealth pH-sensitive liposomes containing CDDP and empty stealth pH-sensitive liposomes. The CDDP concentration employed was 79.4 nM, 3.7 and 0.46 µM for the A431, A549 and BHK cells, respectively. These concentrations correspond to the IC_{50} of CDDP for each cell line. The treatment was performed on three consecutive days, with a change of the culture medium for each new treatment. Seventy-two hours after the initial treatment, cell viability was assessed by 3-[4,5-dimethylthiazol-2yl]-diphenyltetrazolium bromide (MTT) reduction. First, 10 µL of a 5-mg/mL tetrazolium salt solution was added to each well of the plate. After 4 h, MTT crystals were solubilized in 150 µL dimethylsulfoxide. Absorbance readings were performed at 600 nm using a Stat Fax 2100 spectrophotometer (Awareness Technology, Inc., Palm City, FL, USA). Data were analyzed by two-way ANOVA and the means were compared by applying the Bonferroni test ($P \leq 0.05$) using the GraphPad Prism, version 4.0, software.

Evaluation of resistance of cisplatin

The GLC4 cell line was derived from the pleural effusion of a patient with small cell lung carcinoma in the laboratories of Prof. E.G.E. de Vries (Department of Internal Medicine, University Hospital, Groningen, The Netherlands). The GLC4/CDDP subline was obtained by continuous exposure to CDDP. The cell lines were cultured in RPMI 1640 medium supplemented with 10% fetal calf serum at 37ºC in a humidified 5% CO_2 atmosphere. Cultures were initiated at 10^5 cells/mL and grew exponentially to about 10^6 cells/mL within three days. Cell viability was checked by Trypan blue exclusion. The number of cells was determined by Coulter counter analysis. For the long-term growth inhibition 1 x 10^5 cells/mL were cultured for 72 h in the presence and absence of different concentrations of CDDP encapsulated or not into stealth pH-sensitive liposomes. The sensitivity to the drug was evaluated by the IC_{50}, i.e., the drug concentration needed to inhibit cell growth by 50%. A resistance factor (RF) was obtained by dividing the IC_{50} of resistant cells by the IC_{50} of sensitive cells. RF is equal to 6.3 for CDDP and CDDP resistance is stable for at least 8 months (24).

Determination of cellular platinum concentrations

Cells were incubated with different concentrations of CDDP or CDDP containing stealth pH-sensitive liposomes for 3 days. After incubation, an aliquot was taken and washed twice with ice-cold PBS and the pellet was resuspended in 65% HNO_3. Platinum concentration was determined by atomic absorption spectroscopy using a Varian model Zeeman 220 spectrophotometer (Mulgrave, Victoria, Australia) equipped with a graphite tube atomizer and an autosampler.

Results and Discussion

Preparation of stealth pH-sensitive liposomes containing CDDP

Formulation studies showed that the encapsulation of CDDP was significantly improved by increasing the amount of lipids used. Percent CDDP entrapment ranged from 6.6 to 18.6% depending on the lipid concentration (Table 1). The loading capacity of liposomes also increased when the lipid concentration varied only from 30 to 40 mM (Table 1). However, these liposomes showed a heterogeneous size distribution (444.5 nm, polydispersity index equal to 0.6) that could induce the destabilization of the vesicles, provoking the release of CDDP. Thus, these liposomes were submitted to extrusion

against 0.4 and 0.2 µm polycarbonate membranes before purification by ultracentrifugation. However, the size reduction did not alter the entrapment percentage (20.0%), but produced a vesicle suspension of homogeneous diameter (174 nm, polydispersity index equal to 0.03) and a zeta potential equal to 1.6 mV. The liposomes containing the largest amount of CDDP were chosen for the evaluation of cytotoxicity and resistance.

Liposome stability

Stealth pH-sensitive liposomes containing CDDP showed good stability in protein-rich medium such as mouse plasma. Approximately 70% CDDP remained inside the liposomes after their incubation in this medium. The leakage of CDDP from the liposomes exposed to 0.9% NaCl was similar, with no significant difference ($P < 0.05$). Probably, the release of CDDP from liposomes was due to heating (37ºC) and not to the destabilization provoked by interactions with plasma proteins.

Cytotoxicity

Figure 1 illustrates the cytotoxic effects of CDDP encapsulated or not into stealth pH-sensitive liposomes on normal and tumor cell lines. The cytotoxic activity of stealth pH-sensitive liposomes containing CDDP was higher than that of free CDDP against the A549 cell line ($P < 0.05$). However, these liposomes did not prove to be more effective against the A431 cell line. Cell growth inhibition was lower with the encapsulation of CDDP into stealth pH-sensitive liposomes. The same effect was observed for the GLC4 cell line (Table 2). The cellular sensitivity to CDDP encapsulated into stealth pH-sensitive liposomes was lower than for free CDDP, as revealed by the determination of the IC_{50}. These findings suggest that the cytotoxic activity of these liposomes containing CDDP is dependent on the cell line type. Statistical analysis indicated the influence of cell type on the response to treatment with free CDDP or with stealth pH-sensitive liposomes containing CDDP. The A549 cells showed higher sensitivity to treatment with stealth pH-sensitive liposomes containing CDDP than A431 cells ($P = 0.0006$). Perhaps, the cell line-associated differences in the efficacy of stealth pH-sensitive liposomes containing CDDP are related to the uptake mechanisms

Table 1. Effect of lipid concentration on the encapsulation of CDDP into stealth pH-sensitive liposomes.

Lipid concentration during preparation of liposomes	Entrapment (%)	Loading capacity (mg CDDP/nmol lipid)
20 mM	6.95 ± 0.32	10.96 ± 0.35
30 mM	8.80 ± 0.29	10.20 ± 0.92
40 mM	18.60 ± 1.26	14.32 ± 0.81

Data are reported as means ± SD for three determinations. CDDP = cis-diamminedichloroplatinum (II) (cisplatin).

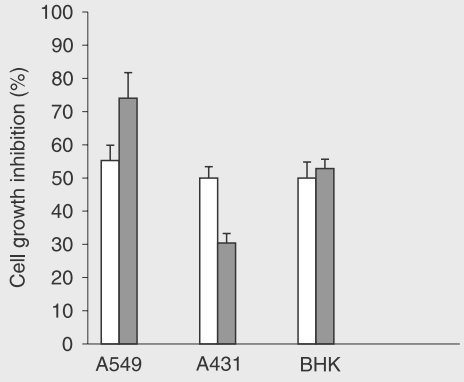

Figure 1. Cytotoxic activity of free CDDP (open bars) and of stealth pH-sensitive liposomes containing CDDP (filled bars). Data are reported as means ± SD and were obtained from six experiments. CDDP = cis-diamminedichloroplatinum (II) (cisplatin); A549 = human lung cancer cell line; A431 = human cervix squamous carcinoma cell line; BHK-21 = Baby Hamster Kidney cell line.

Table 2. IC_{50}, resistance factor (RF) and intracellular platinum concentrations after 3 days of incubation with CDDP or liposomal CDDP.

Compound	Cell line	IC_{50} (µM)	RF	$[Pt]_i \times 10^{17}$ (mol/cell)
CDDP	GLC4	0.40 ± 0.05		9.8
CDDP	GLC4/CDDP	2.50 ± 0.20	6.3	10.7
Liposomal CDDP	GLC4	1.32 ± 0.10		4.0
Liposomal CDDP	GLC4/CDDP	1.45 ± 0.15	1.1	4.0

IC_{50} is the CDDP concentration required to inhibit cell growth by 50%. The resistance factor (RF) is the IC_{50} of the resistant cells divided by the IC_{50} of the sensitive cells. $[Pt]_i$ is the intracellular platinum concentration. Data are reported as the mean ± SD of triplicate determinations. CDDP = cis-diamminedichloroplatinum (II) (cisplatin).

involved in each cell line. Lim et al. (30) demonstrated different levels of liposomal mitoxantrone accumulation in LS180 human colon carcinoma tumors compared to A431 tumors. This finding has been attributed to the more rapid liposome uptake in the LS180 cell line. The cytotoxicity of free or liposome-encapsulated CDDP on the BHK cell line was identical. This cell line was chosen for the assay due to the renal toxicity induced by the use of CDDP. In spite of this finding, it should be pointed out that the biodistribution behavior of the free drug and of the drug encapsulated into nanostructured systems is not the same. Júnior et al. (31) and Newman et al. (32) obtained different pharmacokinetics profiles from administration of liposomal formulations containing CDDP in comparison with free CDDP. In both studies, a lower renal accumulation of CDDP from liposomal CDDP treatment was observed than that from free CDDP. Thus, the *in vivo* toxicologic response to stealth pH-sensitive liposomes containing CDDP can be modified, avoiding the occurrence of kidney failure. No cell growth inhibition was observed with empty stealth pH-sensitive liposomes.

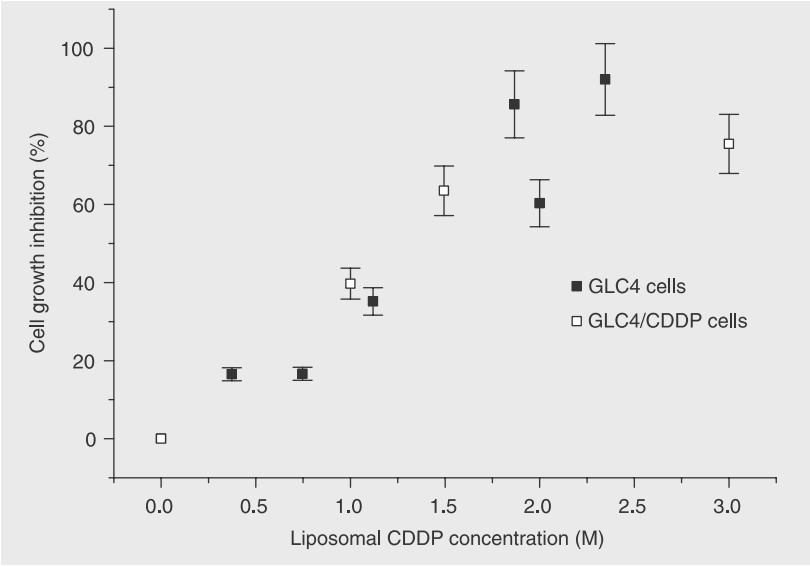

Figure 2. Dose-response curves of GLC4 and GLC4/CDDP cells for stealth pH-sensitive liposomes of CDDP obtained after 3 days of incubation. Data are reported as means ± SD for three experiments. GLC4 = human small-cell lung carcinoma cell line; CDDP = cis-diamminedichloroplatinum (II) (cisplatin).

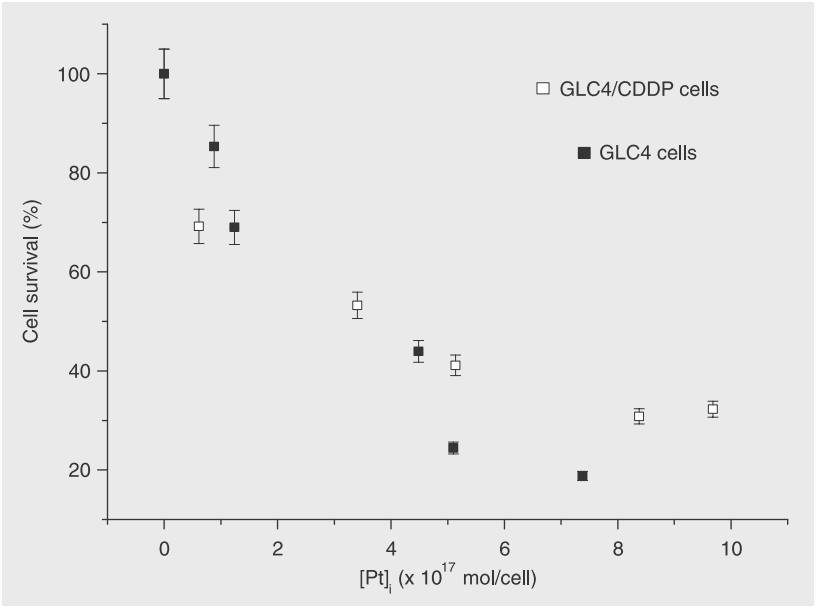

Figure 3. Cell survival as a function of intracellular platinum concentration after equitoxic drug exposure for 3 days. Data are reported as means ± SD for three independent experiments. GLC4 = human small-cell lung carcinoma cell line; CDDP = cis-diamminedichloroplatinum (II) (cisplatin).

Drug sensitivity

The effect of stealth pH-sensitive liposomes containing CDDP on the growth of the GLC4 and GLC4/CDDP cell lines is shown in Figure 2. One can observe that the response of both cell lines to a given dose of this new cisplatin formulation was comparable. Table 2 shows the drug concentration that inhibits cell growth by 50% and the RF obtained. For the sake of comparison, CDDP data are also shown. Intriguingly, the cytotoxic activity of stealth pH-sensitive liposomes containing CDDP on the sensitive cell line was inferior to that of free CDDP. This fact is probably related to different uptake mechanisms of the free and the encapsulated CDDP.

Drug accumulation after equitoxic exposure

The percentage of growth inhibition ver-

sus the content of platinum within the cell determined in GLC4 and in GLC4/CDDP is plotted in Figure 3. Comparing platinum accumulation in the two cell lines, one notices that almost the same levels of platinum are necessary to produce a certain cytotoxic effect. For example, incubation of CDDP with stealth pH-sensitive liposomes at IC_{50} doses yielded a comparable $[Pt]_i$ for both sensitive and resistant cells of about 4 x 10^{-17} mol/cell. We have previously shown that the accumulation of CDDP in both GLC4 and GLC4/CDDP cell lines follows the same pattern, i.e., incubation with equitoxic doses yields practically the same intracellular platinum levels. For example, incubation with CDDP at IC_{50} doses (glc4 = 0.4 µmol/L and GLC4/CDDP = 2.5 µmol/L) yielded comparable $[Pt]_i$ of 10 x 10^{-17} mol/cell for both sensitive and resistant cells. These results show the importance of transport as a mechanism of resistance to CDDP exhibited by GLC4/CDDP cells. In the case of free CDDP, it was necessary to use a higher dose to force its uptake by GLC4/CDDP cells, a fact that was not observed with the use of stealth pH-sensitive liposomes containing CDDP. CDDP encapsulated into stealth pH-sensitive liposomes enters sensitive cells as easily as resistant cells. The liposomal formulation exhibited the same efficacy against CDDP-sensitive and CDDP-resistant cells, with an RF equal to 1.1 (Table 2). This factor is much lower than that for non-encapsulated CDDP, which is equal to 6.3 (24). Thus, these liposomes were able to overcome the resistance mechanisms. In addition, the lower intracellular platinum concentration detected when the cells were incubated with an equitoxic CDDP concentration (IC_{50}) suggests the occurrence of a different transport mechanism for stealth pH-sensitive liposomes. Aqueous formulations of CDDP are solutions of the native and hydrated forms of the drug in equilibrium, which is dependent on the pH and Cl^- concentrations. Chloride ions can be replaced with water molecules, which in turn can be hydrolyzed, yielding hydroxy species. The most important product, the monohydrated species, $[Pt(NH_3)_2(OH_2)Cl]^+$, is formed by the following reaction:

$$cis\text{-}[Pt(NH_3)_2Cl_2] + H_2O \leftrightarrows cis\text{-}[Pt(NH_3)_2(OH_2)Cl]^+ + Cl^-$$

We have previously proposed that CDDP uptake by sensitive GLC4 cells is the sum of two components: an energy-dependent pathway and passive diffusion. The active component is deficient in the GLC4/CDDP subline. The actively transported species is hydro-derivative, probably $[Pt(NH_3)_2(H_2O)OH]^+$ or $[Pt(NH_3)_2(H_2O)Cl]^+$ (24). Cationic aquated species are more reactive with DNA, producing intra- and inter-strand adducts and, consequently, the cytotoxic effects. Therefore, one can speculate that the CDDP delivery by stealth pH-sensitive liposomes favors the formation of hydrated species. It is known that CDDP is almost completely converted to the monohydro species at pH 6.0 (80%) (33). As the stealth pH-sensitive liposomes enter the cells by endocytosis, the release of CDDP might occur as a consequence of the acidification process inside the endosomes, as explained above. Inside late endosomes the pH ranges from 5.5 to 6.0, and consequently, the main species present is the aquohydroxy-derivative. This could explain the achievement of a similar cytotoxicity level with the presence of a lower intracellular platinum concentration.

Finally, it is noteworthy that the stealth pH-sensitive liposomes might offer advantages over conventional liposomes due to their ability to deliver their contents into the cytoplasm. These liposomes can be an alternative to solve the clinical failure observed with the use of stealth liposomes in the treatment of neck and head carcinoma (34). The authors believe that the clinical inefficacy results from the low release of CDDP. To solve this problem would be appropriate to improve liposome composition. Thus, the

present study allowed us to determine more adequate conditions for the encapsulation of CDDP into stealth pH-sensitive liposomes. These stealth pH-sensitive liposomes are stable in plasma and this finding is important to the *in vivo* evaluation of their antitumoral efficacy and pharmacokinetics. Moreover, these liposomes proved to be active against a type of lung tumor cell line (A549) and to provide an excellent strategy to circumvent the pre-clinical resistance to treatment with CDDP. These carriers were able to introduce the same level of CDDP into resistant and sensitive cells after incubation with equal CDDP concentrations.

Acknowledgments

The authors gratefully acknowledge Lipoid GmBh and Quiral Química do Brasil S.A. for providing materials. We are also grateful to Prof. Elzíria Aguiar Nunan for help with the statistical analysis.

References

1. Kondagunta GV, Bacik J, Donadio A, Bajorin D, Marion S, Sheinfeld J, et al. Combination of paclitaxel, ifosfamide, and cisplatin is an effective second-line therapy for patients with relapsed testicular germ cell tumors. *J Clin Oncol* 2005; 23: 6549-6555.
2. Guillot T, Spielmann M, Kac J, Luboinski B, Tellez-Bernal E, Munck JN, et al. Neoadjuvant chemotherapy in multiple synchronous head and neck and esophagus squamous cell carcinomas. *Laryngoscope* 1992; 102: 311-319.
3. Le Chevalier T, Brisgand D, Douillard JY, Pujol JL, Alberola V, Monnier A, et al. Randomized study of vinorelbine and cisplatin versus vindesine and cisplatin versus vinorelbine alone in advanced non-small-cell lung cancer: results of a European multicenter trial including 612 patients. *J Clin Oncol* 1994; 12: 360-367.
4. Shirazi FH, Molepo JM, Stewart DJ, Ng CE, Raaphorst GP, Goel R. Cytotoxicity, accumulation, and efflux of cisplatin and its metabolites in human ovarian carcinoma cells. *Toxicol Appl Pharmacol* 1996; 140: 211-218.
5. Muggia FM, Fojo T. Platinums: extending their therapeutic spectrum. *J Chemother* 2004; 16 (Suppl 4): 77-82.
6. Stewart CF, Hampton EM. Stability of cisplatin and etoposide in intravenous admixtures. *Am J Hosp Pharm* 1989; 46: 1400-1404.
7. Trissel LA, Martinez JF. Compatibility of thiotepa (lyophilized) with selected drugs during simulated Y-site administration. *Am J Health Syst Pharm* 1996; 53: 1041-1045.
8. Hospers GA, Mulder NH, de Jong B, de Ley L, Uges DR, Fichtinger-Schepman AM, et al. Characterization of a human small cell lung carcinoma cell line with acquired resistance to cis-diamminedichloroplatinum (II) *in vitro*. *Cancer Res* 1988; 48: 6803-6807.
9. Muggia FM, Los G. Platinum resistance: laboratory findings and clinical implications. *Stem Cells* 1993; 11: 182-193.
10. Siddik ZH. Cisplatin: mode of cytotoxic action and molecular basis of resistance. *Oncogene* 2003; 22: 7265-7279.
11. Wernyj RP, Morin PJ. Molecular mechanisms of platinum resistance: still searching for the Achilles' heel. *Drug Resist Updat* 2004; 7: 227-232.
12. Chu G. Cellular responses to cisplatin. The roles of DNA-binding proteins and DNA repair. *J Biol Chem* 1994; 269: 787-790.
13. Conti M, De Giorgi U, Tazzari V, Bezzi F, Baccini C. Clinical pharmacology of intraperitoneal cisplatin-based chemotherapy. *J Chemother* 2004; 16 (Suppl 5): 23-25.
14. Ekborn A, Hansson J, Ehrsson H, Eksborg S, Wallin I, Wagenius G, et al. High-dose cisplatin with amifostine: ototoxicity and pharmacokinetics. *Laryngoscope* 2004; 114: 1660-1667.
15. Kelland LR. Preclinical perspectives on platinum resistance. *Drugs* 2000; 59 (Suppl 4): 1-8.
16. Oldenburg J, Begg AC, van Vugt MJ, Ruevekamp M, Schornagel JH, Pinedo HM, et al. Characterization of resistance mechanisms to cis-diamminedichloroplatinum (II) in three sublines of the CC531 colon adenocarcinoma cell line *in vitro*. *Cancer Res* 1994; 54: 487-493.
17. Santarpia M, Altavilla G, Salazar F, Taron M, Rosell R. From the bench to the bed: individualizing treatment in non-small-cell lung cancer. *Clin Transl Oncol* 2006; 8: 71-76.
18. Jakupec MA, Galanski M, Keppler BK. Tumour-inhibiting platinum complexes - state of the art and future perspectives. *Rev Physiol Biochem Pharmacol* 2003; 146: 1-54.
19. Dzamitika S, Salerno M, Pereira-Maia E, Le Moyec L, Garnier-Suillerot A. Preferential energy- and potential-dependent accumulation of cisplatin-glutathione complexes in human cancer cell lines (GLC4 and K562): A likely role of mitochondria. *J Bioenerg Biomembr* 2006; 38: 11-21.
20. Schmidt W, Chaney SG. Role of carrier ligand in platinum resistance of human carcinoma cell lines. *Cancer Res* 1993; 53: 799-805.
21. Gately DP, Howell SB. Cellular accumulation of the anticancer agent cisplatin: a review. *Br J Cancer* 1993; 67: 1171-1176.
22. Lanzi C, Perego P, Supino R, Romanelli S, Pensa T, Carenini N, et al. Decreased drug accumulation and increased tolerance to DNA damage in tumor cells with a low level of cisplatin resistance. *Biochem Pharmacol* 1998; 55: 1247-1254.
23. Cesar ET, de Almeida MV, Fontes AP, Pereira Maia EC, Garnier-Suillerot A, Rubia Costa CM, et al. Synthesis, characterization, cytotoxic activity, and cellular accumulation of dinuclear platinum complexes derived from N,N'-di-(2-aminoethyl)-1,3-diamino-2-propanol, aryl substituted N-benzyl-1,4-butanediamines, and N-benzyl-1,6-hexanediamines. *J Inorg Biochem* 2003; 95: 297-305.
24. Pereira-Maia E, Garnier-Suillerot A. Impaired hydrolysis of cisplatin derivatives to aquated species prevents energy-dependent uptake in GLC4 cells resistant to cisplatin. *J Biol Inorg Chem* 2003; 8: 626-634.
25. Andrews PA, Mann SC, Huynh HH, Albright KD. Role of the Na+,

K(+)-adenosine triphosphatase in the accumulation of cis-diamminedichloroplatinum (II) in human ovarian carcinoma cells. *Cancer Res* 1991; 51: 3677-3681.
26. Beretta GL, Gatti L, Tinelli S, Corna E, Colangelo D, Zunino F, et al. Cellular pharmacology of cisplatin in relation to the expression of human copper transporter CTR1 in different pairs of cisplatin-sensitive and -resistant cells. *Biochem Pharmacol* 2004; 68: 283-291.
27. Collins D. pH-sensitive liposomes as tools for cytoplasmic delivery. In: Philippot R, Schuber F (Editors), *Liposomes as tools in basic research and industry*. Boca Raton: CRC Press; 1995. p 201-214.
28. De Oliveira MC, Boutet V, Fattal E, Boquet D, Grognet JM, Couvreur P, et al. Improvement of *in vivo* stability of phosphodiester oligonucleotide using anionic liposomes in mice. *Life Sci* 2000; 67: 1625-1637.
29. New RRC. Characterization of liposomes. In: New RRC (Editor), *Liposomes a pratical approach*. New York: Oxford University Press; 2000. p 105-161.
30. Lim HJ, Masin D, McIntosh NL, Madden TD, Bally MB. Role of drug release and liposome-mediated drug delivery in governing the therapeutic activity of liposomal mitoxantrone used to treat human A431 and LS180 solid tumors. *J Pharmacol Exp Ther* 2000; 292: 337-345.
31. Júnior AD, Mota LG, Nunan EA, Wainstein AJ, Wainstein AP, Leal AS, et al. Tissue distribution evaluation of stealth pH-sensitive liposomal cisplatin versus free cisplatin in Ehrlich tumor-bearing mice. *Life Sci* 2007; 80: 659-664.
32. Newman MS, Colbern GT, Working PK, Engbers C, Amantea MA. Comparative pharmacokinetics, tissue distribution, and therapeutic effectiveness of cisplatin encapsulated in long-circulating, pegylated liposomes (SPI-077) in tumor-bearing mice. *Cancer Chemother Pharmacol* 1999; 43: 1-7.
33. Yachnin JR, Wallin I, Lewensohn R, Sirzen F, Ehrsson H. The kinetics and cytotoxicity of cisplatin and its monohydrated complex. *Cancer Lett* 1998; 132: 175-180.
34. Harrington KJ, Lewanski CR, Northcote AD, Whittaker J, Wellbank H, Vile RG, et al. Phase I-II study of pegylated liposomal cisplatin (SPI-077) in patients with inoperable head and neck cancer. *Ann Oncol* 2001; 12: 493-496.

International Journal of Pharmaceutics 420 (2011) 319–332

Contents lists available at SciVerse ScienceDirect

International Journal of Pharmaceutics

journal homepage: www.elsevier.com/locate/ijpharm

Pharmaceutical Nanotechnology

Nuclear delivery of a therapeutic peptide by long circulating pH-sensitive liposomes: Benefits over classical vesicles

E. Ducat[a], J. Deprez[b], A. Gillet[a], A. Noël[b], B. Evrard[a], O. Peulen[c,1], G. Piel[a,*,1]

[a] Laboratory of Pharmaceutical Technology, CIRM, Department of Pharmacy, University of Liege, B36, Tour 4, Level 2, Avenue de l'hôpital, 1, B-4000 Liege, Belgium
[b] Laboratory of Tumor and Development Biology, GIGA-Cancer, University of Liege, Pathology Building, B23, Level 4, B-4000 Liege, Belgium
[c] Metastasis Research Laboratory, GIGA-Cancer, University of Liege, Pathology Building, B23, Level 4, B-4000 Liege, Belgium

ARTICLE INFO

Article history:
Received 1 June 2011
Received in revised form 16 August 2011
Accepted 17 August 2011
Available online 25 August 2011

Keywords:
Peptide
pH-sensitive liposomes
Drug delivery
PEG
Cellular uptake

ABSTRACT

The purpose of this study is to propose a suitable vector combining increased circulation lifetime and intracellular delivery capacities for a therapeutic peptide. Long circulating classical liposomes [SPC:CHOL:PEG-750-DSPE (47:47:6 molar% ratio)] or pH-sensitive stealth liposomes [DOPE:CHEMS:CHOL:PEG_{750}-DSPE (43:21:30:6 molar% ratio)] were used to deliver a therapeutic peptide to its nuclear site of action. The benefit of using stealth pH-sensitive liposomes was investigated and formulations were compared to classical liposomes in terms of size, shape, charge, encapsulation efficiency, stability and, most importantly, in terms of cellular uptake. Confocal microscopy and flow cytometry were used to evaluate the intracellular fate of liposomes themselves and of their hydrophilic encapsulated material. Cellular uptake of peptide-loaded liposomes was also investigated in three cell lines: Hs578t human epithelial cells from breast carcinoma, MDA-MB-231 human breast carcinoma cells and WI-26 human diploid lung fibroblast cells. The difference between formulations in terms of peptide delivery from the endosome to the cytoplasm and even to the nucleus was investigated as a function of time. Characterization studies showed that both formulations possess acceptable size, shape and encapsulation efficiency but cellular uptake studies showed the important benefit of the pH-sensitive formulation over the classical one, in spite of liposome PEGylation. Indeed, stealth pH-sensitive liposomes were able to deliver hydrophilic materials strongly to the cytoplasm. Most importantly, when encapsulated in pH-sensitive stealth liposomes, the peptide was able to reach the nucleus of tumorigenic and non tumorigenic breast cancer cells.

1. Introduction

Print3G is a putative antagonist of an oncoprotein involved in breast cancer growth and invasion. Until now, only a few biologically active peptides have been successfully used in clinical medicine. Indeed, administration of peptidic drugs presents several disadvantages, related to their rapid elimination from the blood circulation by the lymphatic system, their enzymatic degradation, their uptake by the reticulo-endothelial system (RES) and their non-selective accumulation (Banga and Chien, 1988; Zhou and Li Wan Po, 1991; Torchilin, 2006; Katanasaka et al., 2008).

The necessity for intravenous administration of Print3G has led to the development of PEGylated liposomes as drug carriers. Recently, several studies successfully explored the path of liposomes for the administration of several peptides (Katanasaka et al., 2008; Hanato et al., 2009; Petrikovics et al., 2009). Liposomes, spherical structures composed of one or several phospholipid bilayers, possess many attractive characteristics for stabilizing peptidic drugs and for improving their pharmacological properties. Being biocompatible and biodegradable, liposomes cause no or very mild antigenic, pyrogenic, allergic or toxic reactions. They can entrap hydrophilic drugs within their aqueous compartment, lipophilic compounds in their membrane or amphipathic drugs. First generation liposomes have been shown to be easily eliminated from the bloodstream and to accumulate in the Kupfer cells in the liver and in spleen macrophages (Klibanov et al., 2003). Therefore, the strategy has been to graft polymers onto nanoparticles and particularly onto liposomal phospholipids with polyethylene glycol (PEG). PEGs are synthetic, inert and biocompatible polymers, allowing the formation of a protective layer on the particle surface and providing protection against opsonization and capture by the RES (Torchilin, 2009). The increase in circulation lifetime by PEGs was demonstrated by Dos Santos et al., who showed an increase in vascular remanence for the surface-grafted PEG liposomes, preventing

* Corresponding author. Tel.: +32 4 366 43 08; fax: +32 4 3664302.
E-mail addresses: Emilie.Ducat@ulg.ac.be (E. Ducat), geraldine.piel@ulg.ac.be (G. Piel).
[1] These authors contributed equally to this research.

0378-5173/$ – see front matter © 2011 Elsevier B.V. All rights reserved.
doi:10.1016/j.ijpharm.2011.08.034

aggregation and building a steric barrier around the liposome, in comparison with non-grafted vectors (Dos Santos et al., 2007). These two properties, namely the increase in circulation time and the decrease in capture by the RES, explain the Enhanced Permeability and Retention (EPR) effect, applicable to almost all rapidly growing solid tumors (Maeda et al., 2008). The enhanced extravasations of macromolecules from blood vessels to tumor and their retention within these tissues, due to the anatomical and permeability particularities of tumors, represent a phenomenon not observed in normal tissue, leading to a passive targeting towards affected tissues.

Print3G is a hydrophilic peptide composed of 25 natural amino acids (M.W. = 3000, p*I* = 11.1), freely soluble in water, as such it is encapsulated in the inner aqueous cavity of liposomes. The first formulation of PEGylated liposomes developed as Print3G vector (Ducat et al., 2010) was made of soybean phosphatidylcholine (SPC), methoxypolyethyleneglycol grafted onto distearoylphosphoethanolamine (PEG_{750}-DSPE) and cholesterol (CHOL), added because of their stabilizing properties (Kirby et al., 1980a,b; Dos Santos et al., 2007). In order to improve the introduction of encapsulated material into the cytoplasm, a second formulation was developed, replacing SPC with a combination of dioleylphosphoethanolamine (DOPE) and cholesterylhemisuccinate (CHEMS) (Simoes et al., 2004). DOPE exhibits a conical shape because of its small and minimally hydrated headgroup, compared to its lipophilic tail. DOPE is associated with a compound used as a stabilizer of the liposomal membrane: CHEMS. This molecule possesses an inverted cone shape at physiological pH, but, under acidic conditions, the carboxylic acid group becomes protonated and loses this particular shape. During endocytosis, the pH decreases within the endosome, resulting in a destabilization of the liposomal membrane transiting from a lamellar to a hexagonal phase. Some publications have described the mechanism of action of pH-sensitive liposomes containing a derivative of PE associated with a compound containing an acidic group as stabilizer (Straubinger et al., 1985; Skalko et al., 1998; Peschka-Suss and Schubert, 2003; Huth et al., 2006). PEG and cholesterol added into formulations decrease the membrane fluidity of fluid liposomes and can hamper their penetration capacity/potency and their pH-sensitivity (Bellavance et al., 2010; Liu and Huang, 1989). Cholesterol indeed is able to increase the fluidity of solid membranes. The use of PEG_{750}, characterized by a lower molecular weight than PEG often used to obtain long circulating liposomes, could allow finding a compromise between the improvement of vascular remanence and intracellular delivery. Maintenance of liposomes pH-sensitivity using DSPE-PEG_{750} will be studied and discussed in this publication. Moreover, few publications have described formulations of long circulating pH-sensitive liposomes (Junior et al., 2007; Momekova et al., 2007; Obata et al., 2009), none has investigated the difference in terms of cellular uptake between classical and pH-sensitive liposomes and no study has proposed a suitable vector for the delivery of nuclear peptides.

The purpose of this study is to propose a suitable vector for the intracellular delivery of a therapeutic peptide called Print3G, while keeping the formulation properties of long-circulating liposomes to effectively deliver the peptide to its site of action. To investigate the benefit of developing a formulation of long circulating pH-sensitive liposomes beside a classical formulation of stealth liposomes, these two formulations were compared in terms of size, shape, charge, encapsulation efficiency, stability and cellular uptake. Confocal laser scanning microscopy (CLSM) and fluorescence-activated cell sorting (FACS) were used to evaluate the intracellular fate of liposomes themselves and of their encapsulated material as a function of time. In order to demonstrate the benefit of the vector, research was expanded to various cell lines: Hs578t human epithelial cells from breast carcinoma, MDA-MB-231 human breast carcinoma cells and WI-26 human diploid lung fibroblast cells.

Firstly, we studied the cellular uptake of liposomes themselves, using NBD-CHOL as a fluorescent marker of the phospholipids bilayer.

Secondly, the delivery of a model molecule, calcein, was investigated. Calcein was chosen as a model molecule for two reasons: (1) its localization in the aqueous compartment of liposomes because of its hydrophilicity similar to Print3G and (2) its self-quenching behavior, often used to study the endosomal escape triggered by pH-sensitive liposomes (Kono et al., 1997; Shi et al., 2002; Hong et al., 2010).

Finally, we studied the intracellular outcome of Print3G, which has to reach the nucleus for its therapeutic action. This helped us to discern the difference between the two formulations in terms of delivery of the entrapped peptide from the endosome to the cytoplasm and even to the nucleus.

2. Materials and methods

2.1. Materials

Soybean phosphatidylcholine (SPC, purity: 98%) was provided by Lipoid (Ludwigshafen, Germany). N-(Carbonyl-methoxypolyethylenglycol-750)-1,2-distearoyl-sn-glycero-3-phosphoethanolamine sodium salt (PEG-750-DSPE, purity 100%) and 1,2-dioleoyl-sn-glycero-3-phosphoethanolamine (DOPE) were purchased from Genzyme Pharmaceuticals (Liestal, Switzerland). Cholesterol (CHOL, purity > 99%), cholesteryl-hemisuccinate (CHEMS) and calcein were purchased from Sigma–Aldrich (Bornem, Belgium). Print3G (purity: 95.39%) biotinylated peptide called Print3G (purity: 98.44%) was acquired from GL Biochem (Shanghai, China). 25-[N-[(7-nitro-2-1,3-benzoxadiazol-4-yl)methyl]amino]-27-norcholesterol (25-NBD-CHOL) was purchased from Avanti Polar Lipids (Pelham, USA). Water was deionized using the Millipore system (18.2 MΩ/cm resistivity) and was filtered through a 0.22 μm Millipore Millipak®-40 disposable filter unit (Millipore Corporation, USA). Dulbecco's Modified Eagle's Medium (DMEM), Foetal Bovine Serum (FBS), penicillin–streptomycin, L-glutamine and streptavidin conjugate Alexa Fluor 555 were purchased from Gibco-Life Technologies (Invitrogen Corporation, Paisley, UK). Paraformaldehyde and polysorbate 20 were provided by Merck (Schuchardt and Darmstadt, respectively, Germany). Vectashield mounting medium with DAPI was purchased from Vector Laboratories (Burlingame, CA, USA). All other reagents and solvents were of analytical grade.

2.2. Liposome characterization

Liposome characterization was performed by photon correlation spectroscopy (PCS), zeta potential measures and freeze-fracture electron microscopy to ensure that the selected formulations possessed the required properties of shape and size for *in vitro* studies and further intravenous administration of the encapsulated peptide.

2.2.1. Blank liposomes

Blank unilamellar vesicles, made of SPC:CHOL:PEG-750-DSPE (47:47:6 molar% ratio) for classical stealth liposomes or made of DOPE:CHEMS:CHOL:PEG_{750}-DSPE (43:21:30:6 molar% ratio) for pH-sensitive long circulating liposomes, were prepared by the hydration of lipid film method. Briefly, required amounts of lipids were dissolved in chloroform and evaporated under reduced pressure in a round-bottomed flask to form a thin lipid film. The film was hydrated using a vortex mixer with HEPES-buffered

Table 1
Z-average sizes and zeta potentials of classical and pH-sensitive stealth liposomes ($n > 3$).

	Classical stealth liposomes		pH-sensitive stealth liposomes	
	Z-average size	Zeta potential	*Z*-average size	Zeta potential
Empty liposomes	172.6 ± 14.7 nm	−8.0 ± 3.9 mV	150.4 ± 14.1 nm	−16.3 ± 5.1 mV
Liposomes containing calcein	162.6 ± 4.3 nm	−11.5 ± 3.4 mV	176.2 ± 21.3 nm	−16.6 ± 3.4 mV
Liposomes containing Print3G	163.8 ± 7.2 nm	−6.8 ± 2.8 mV	165.2 ± 1.4 nm	−14.0 ± 3.4 mV

saline, containing 67 mM NaCl and adjusted to pH 7.4 with 0.1 N NaOH solution. The resulting suspension was extruded 5 times through a 0.2 μm Nucleopore polycarbonate membrane (Whatman International Ltd., Maidstone, UK). Final concentrations of lipids were as follows: SPC/CHOL/PEG_{750}-DSPE (36.1:36.1:4, mM) and DOPE/CHEMS/CHOL/PEG_{750}-DSPE (33:16:23:4.5, mM).

2.2.2. Photon correlation spectroscopy (PCS)

Liposome dispersions were diluted 10 times in isotonic HEPES buffer for PCS measurements (HPPS, Malvern Instruments, UK). Measurements were made at 25 °C with a fixed angle of 90°. Quoted sizes represented the average mean for the liposomal hydrodynamic diameter (nm). The polydispersity index (PDI) expressed the size distribution width.

2.2.3. Zeta potential

The zeta potential of liposome formulations was measured with a Zetasizer 2000 DTS52013 (Malvern Instruments, UK) at pH 7.4. Liposome suspensions were diluted 100 times in HEPES buffer pH 7.4, then loaded into a capillary cell mounted on the apparatus and measured 5 times at 37 °C.

2.2.4. Freeze-fracture electron microscopy

Freeze-fracture replicas of blank liposome suspensions were analysed under transmission electron microscopy. In practice, a drop of liposome suspension containing 20% (v/v) glycerol as a cryoprotectant was deposited into a small gold cup and rapidly frozen in liquid nitrogen. Fracturing, freeze etching and shadowing with Pt-C were performed at −100 °C in shadowing equipment (Balzers® BAF-400) fitted with a freeze-fracture and etching unit. The replicas were examined with a JEOL (JEM-100SX) transmission electron microscope, operating at 80 kV accelerating voltage.

2.3. Determination of Print3G encapsulation efficiency

2.3.1. Print3G encapsulation

The encapsulation of Print3G into the classical formulation of liposomes was made using the freeze-thawing method. Blank liposomes (see Section 2.2.1) were mixed with a 400 μM Print3G solution in HEPES buffer, frozen for 1 min at −196 °C in liquid nitrogen and thawed for 5 min at 30 °C in a water bath. 11 cycles were performed to promote the entry of Print3G into vesicles. Between each cycle, the suspension was mixed for 10 s using a vortex mixer (Ducat et al., 2010).

Concerning the classical formulation, the freeze-thawing method was found to give the best results because it avoids adsorption of Print3G on materials during manufacture. Encapsulation efficiencies were significantly increased in comparison to the hydration of lipid film technique. A design of experiments was built to obtain the best encapsulation efficiency for this formulation and was plainly described by Ducat et al. (2010).

On the contrary, this method could not be used to encapsulate Print3G into pH-sensitive PEGylated liposomes because liposome destruction after freeze-thawing cycles was observed by PCS measurements. High encapsulation efficiency for pH-sensitive liposomes was obtained using the hydration of lipid film method associated with pre-saturation of the extruder by a Print3G solution.

Liposomes were prepared by the hydration of lipid film method described in Section 2.2.1, the hydration of the lipid film was made with a 200 μM Print3G solution in HEPES buffer. Before extrusion, the extruder was saturated with the same solution to avoid any adsorption of the peptide onto extrusion materials. The resulting suspension was extruded five times through a 0.2 μm polycarbonate membrane.

Finally, the obtained suspensions underwent two ultracentrifugation cycles at 35,000 rpm for 3 h and 30 min at 4 °C using the Beckman SW60 rotor (86,496 × *g*) in order to remove free Print3G.

2.3.2. Print3G determination

An HPLC method with UV/visible diode array detector (DAD) was developed and validated for the determination of Print3G using a Hewlett-Packard 1100 series equipment (Agilent Technologies, USA). This method was detailed in our previous study [11]. Ten-μl samples were injected into a Zorbax 300 SB-C18 (3.5 μm, 150 mm × 4.6 mm I.D., Agilent Technologies, USA) in an oven set at 35 °C with a mobile phase containing water and acetonitrile (ACN). Both solvents were acidified with 0.1% of trifluoroacetic acid (TFA). The applied gradient was as follows: 18–22.8% ACN from 0 to 20 min, 100% ACN at 25 min and 18% at 25.2 min. Detection was achieved at absorbance wavelengths of 220 nm and 275 nm.

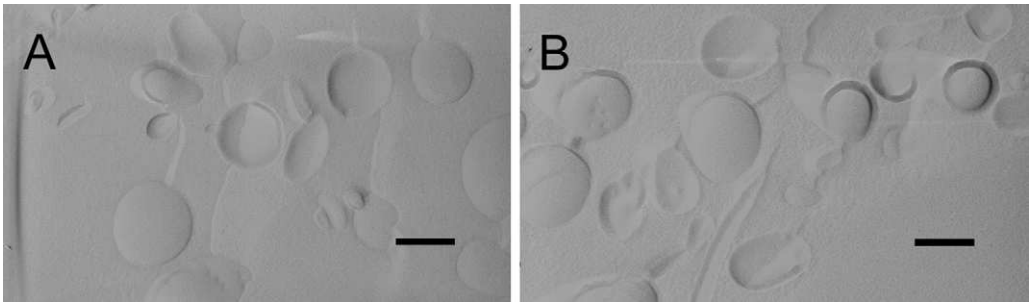

Fig. 1. Micrographs of (A) classical or (B) pH-sensitive PEGylated liposomes as observed on freeze-fracture replicas in transmission electron microscopy. Bars represent 0.125 μm.

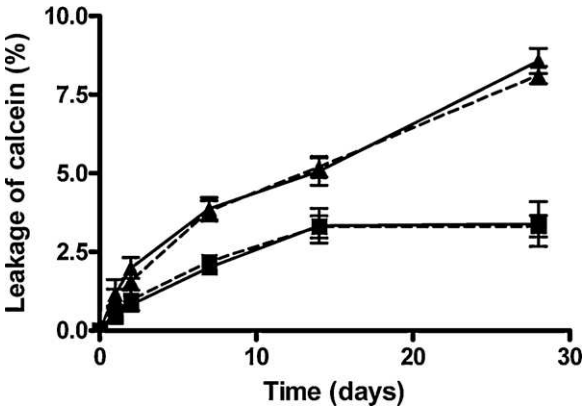

Fig. 2. Leakage of calcein from pH-sensitive liposomes (dotted lines) or standard liposomes (plain lines) as a function of time at 37 °C (full triangles) and 4 °C (full squares) in isotonic HEPES buffer. Data points represent mean values (±S.D.) of three independent experiments.

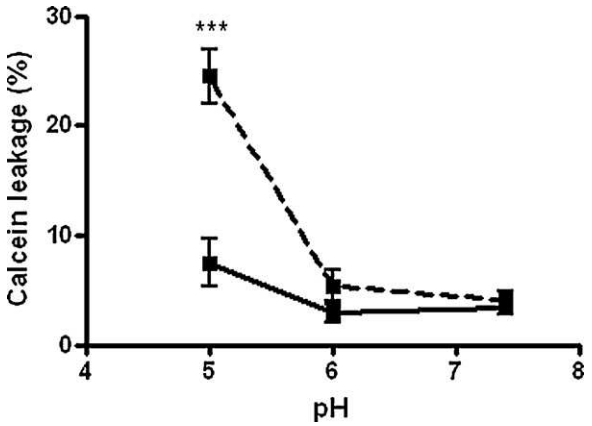

Fig. 3. Leakage of calcein from pH-sensitive liposomes (dotted lines) or standard liposomes (plain lines) as a function of the pH. Data points represent mean values (±S.D.) of three independent experiments.

2.3.3. Encapsulation efficiency

Encapsulation efficiency was expressed in terms of the quantity of peptide loaded into liposomes as a function of the quantity operated. This encapsulation efficiency (EE) was calculated by the following equation (Eq. (1)).

$$\text{EE}\ \ (\%) = \frac{\text{Amount of encapsulated Print3G}}{\text{Total amount of Print3G}} \times 100 \qquad (1)$$

where the "amount of encapsulated Print3G" is the amount of Print3G (in μg) loaded into liposomes and the "total amount of Print3G" is the amount of Print3G (in μg) implemented.

2.4. Stability

Calcein was encapsulated into vesicles in order to study the leakage of a hydrophilic encapsulated material. A 60 mM calcein isotonic solution was used to hydrate the lipid film (see Section 2.2.1) in order to detect a leakage-induced effect. After extrusion, external calcein was removed by 6 ultracentrifugation cycles at 35,000 rpm for 60–45–30–30–30–30 min at 4 °C using the Beckman SW60 rotor (86,496 × *g*).

Encapsulated calcein shows minimal fluorescence, owing to the formation of ground state dimers. Any fluorescence measured will be due to the leakage of calcein out of vesicles and dilution in the exterior aqueous media (Chen and Knutson, 1988). Fluorescence was measured after 0, 1, 2, 7, 14 and 28 days of storage at 4 °C and 37 °C. For the pH sensitivity study, the leakage of calcein as a function of the pH was measured after 6 h under stirring in phosphate buffers at pH 5, pH 6 and pH 7.4. In practice, 100 μl liposome suspension was added to 100 μl HEPES buffered solution or 100 μl of a 4% Triton X-100 solution, for complete liposome destruction, in a 96-well plate. Calcein release from liposomes was measured fluorometrically (SpectraMax Gemini XS); excitation and emission wavelengths were 490 and 520 nm, respectively. The amount of calcein released was calculated using the following equation (Eq. (2)):

$$\%\,\text{calcein released} = \frac{I}{I_t} \times 100 \qquad (2)$$

where I is the fluorescence intensity at 520 nm and I_t is the fluorescence intensity at 520 nm after complete destruction of the liposomes by Triton X-100.

2.5. Cellular uptake of liposomes and of their encapsulated material

2.5.1. Liposomes

In order to follow the intracellular delivery of the encapsulated material, calcein was used as hydrophilic fluorescent marker. These liposomes were prepared as described in Section 2.4, using a 40 mM isotonic solution of calcein. Intracellular penetration of the liposomes themselves was studied using 25-NBD-CHOL incorporated into the bilayer. These vesicles were prepared using the hydration of lipid film method. 300 μM of 25-NBD-CHOL in chloroform was added before evaporation under reduced pressure. Intracellular penetration of Print3G was studied using a biotinylated derivative of Print3G, which was incorporated into liposomes using the same methods as described in Section 2.3.1.

Final concentrations of lipids were 5 times lower than those used for blank liposomes (see Section 2.2.1).

2.5.2. Cell culture

The human cell lines used in this study were obtained from the American Type Culture Collection (Manassas, VA, USA). Hs578t and MDA-MB-231 were chosen as breast carcinoma cell lines, respectively non-tumorigenic and tumorigenic. The last cell line chosen, WI-26, is an SV-40 immortalized lung fibroblast cell line.

Cells were cultured in DMEM supplemented with 10% heat-inactivated FBS, 4.5 g/l glucose, 2 mM L-glutamine, 100 U/ml of penicillin and 100 μg/ml of streptomycin at 37 °C in a humidified 5% CO_2 atmosphere. The three cell lines were seeded on glass coverslips in 24-well plates for CLSM analysis. For FACS studies, Hs578t cells and MDA-MB-231 cells were seeded respectively in 6-well and in 19-well plates.

After 24 h incubation, cells were grown to 70% confluence. The medium was removed before adding liposomes resuspended in serum-free DMEM.

2.5.3. Confocal microscopy analysis

Cells were treated with fluorescently labelled liposomes for various lengths of time (15 min, 2.5 h, 5 h or 15 h) at 37 °C in a humidified 5% CO_2 atmosphere. This step was followed by several washes with phosphate-buffered saline (PBS). Cells were then fixed in 4% paraformaldehyde in PBS for 15 min at 4 °C and rinsed in PBS. Streptavidin conjugate Alexa Fluor 555 was used as binding pair to link and reveal the biotinylated peptide. In practice, cells were permeabilized with 0.2% polysorbate 20 in PBS for 30 min at room temperature, incubated with streptavidin conjugate Alexa Fluor 555 at a dilution of 1:500 (v/v) for 30 min at room temperature

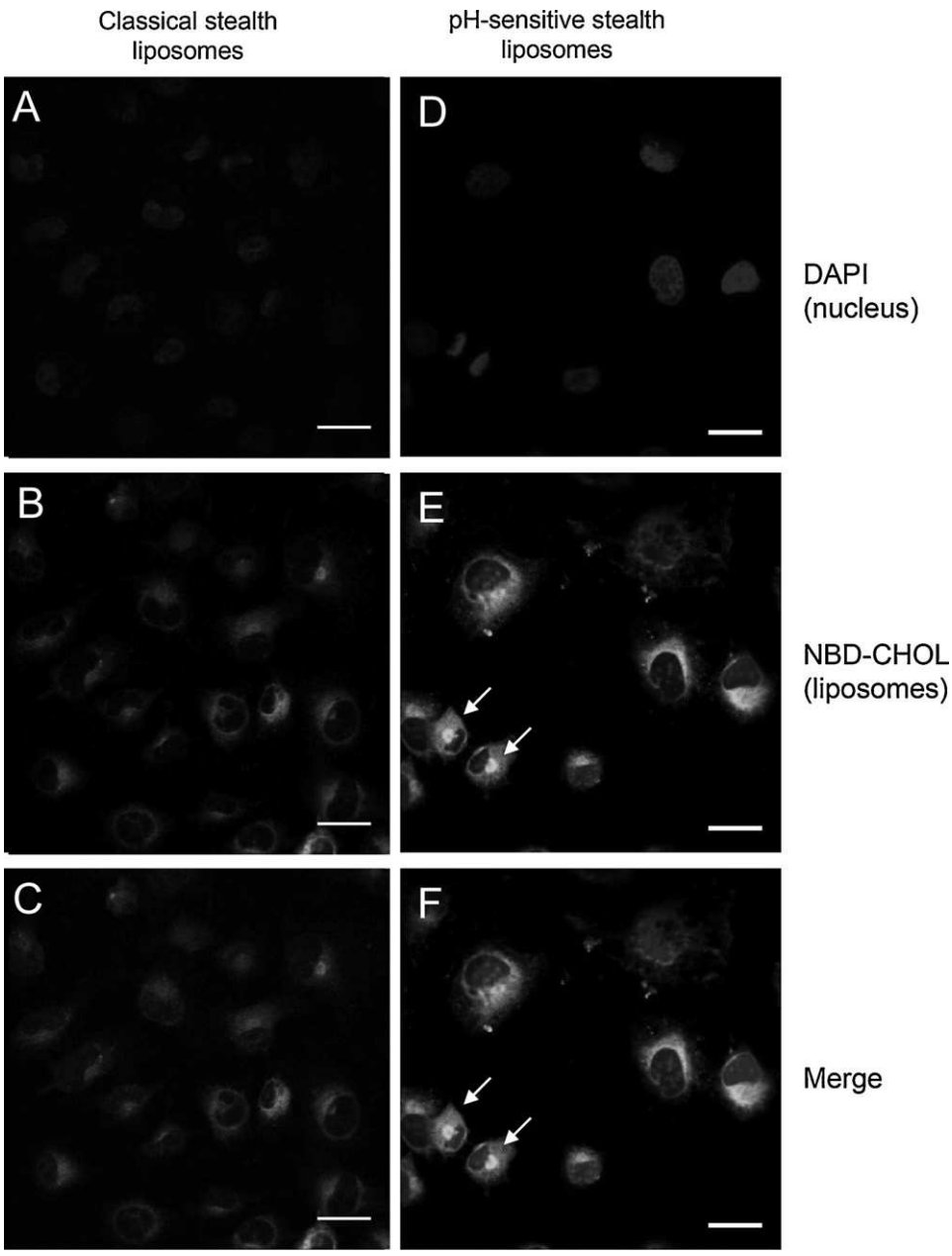

Fig. 4. Confocal laser microscopy analysis of Hs578t cells treated for 2.5 h with classical stealth liposomes incorporating NBD-CHOL (A–C) or with pH-sensitive stealth liposomes incorporating NBD-CHOL (D–F). (A and D) Nuclei blue staining with DAPI; (B and E) green staining of liposomes incorporating NBD-CHOL; (C and F) merge of DAPI and NBD-CHOL channels. Bars represent 30 μm. (For interpretation of the references to colour in this figure legend, the reader is referred to the web version of the article.)

and washed with PBS. The coverslips were finally mounted with Vectashield medium with DAPI onto glass slides for microscopic observations.

The location of intracellular fluorescence was validated using confocal laser scanning microscope (Olympus FluoView FV100). Several fluorescent molecules were used and observed at several excitation wavelengths: DAPI at 405 nm, calcein and 25-NBD-CHOL at 488 nm, Alexa Fluor 555 at 561 nm.

All optical sections were recorded with the same settings (in particular the laser power and the photomultiplier voltage) for each colour detected. Kalman collection filter 3-frame was used for each acquired image and for each colour.

2.5.4. Flow cytometry analysis

Flow cytometry analysis was conducted on liposomes containing calcein or NBD-CHOL and on empty liposomes without any fluorescent markers (negative controls). Fluorescence intensities and lipid content determination were used as liposome quality control before application on cells. Fluorescence intensities were measured using the SpectraMax Gemini XS; excitation and emission wavelengths were 490 and 520 nm, respectively. Lipid concentration was measured using the phospholipids *C* test (Wako Chemicals, LabAssay Phospholipid, choline oxidase—DAOS method, Wako Chemicals, Neuss, Germany) or the Cholesterol FS test (Dyasis Diagnostic Systems, Holzheim, Germany). Difference between pH-sensitive and classical formulations was less than 10% in terms of fluorescence and lipid concentration.

Cells were treated for 2.5 h with blank liposomes, liposomes containing NBD-CHOL or liposomes encapsulating calcein. After incubation at 37 °C, cells were washed twice with PBS and dissociated with 0.05% trypsin/EDTA. After a centrifugation step at

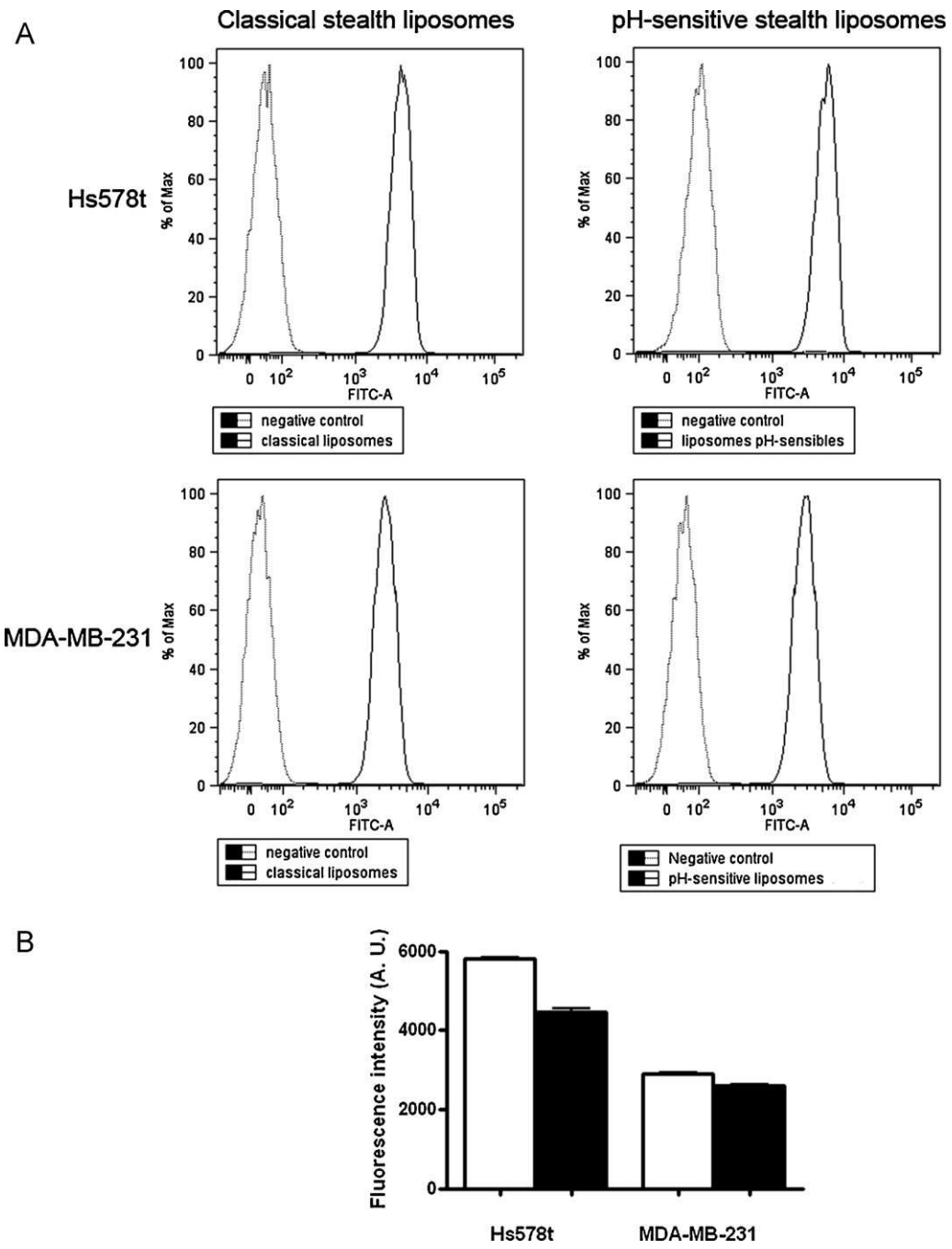

Fig. 5. Flow cytometry analysis of Hs578t or MDA-MB-231 cells treated for 2.5 h with classical or pH-sensitive PEGylated liposomes incorporating NBD-CHOL. (A) Representative FACS normalized histogram of liposomes without NBD-CHOL (doted lines) or NBD-CHOL-incorporating liposomes (plain lines). (B) NBD-CHOL-associated fluorescence (arbitrary unit) in Hs578t cells or MDA-MB-231 cells treated with classical (black) or pH-sensitive (white) liposomes incorporating NBD-CHOL.

1200 rpm for 5 min at 4 °C, supernatants were discarded and cell pellets were washed with cold PBS. Cells were then fixed in paraformaldehyde (4%, v/v) at 4 °C for 10 min and washed twice with cold PBS. Finally, cells were resuspended in 250 μl of cold PBS and kept on ice in the dark.

Analyses were performed using the flow cytometer FACS Canto II (Becton Dickinson, San Jose, CA, USA). The autofluorescence of each cell line was determined with non fluorescent blank liposomes. For calcein-loaded liposomes experiments ($n = 3$), a total of 10,000 events were recorded. For pH-sensitive ($n = 3$) and classical ($n = 2$) formulations of liposomes incorporating NBD-CHOL, a total of respectively 10,000 and 5000 events were recorded. Cell-associated calcein or NBD-CHOL was excited with 488-nm solid state laser (20 mW) and fluorescence was detected using 502LP and 530/30 filters. Data were analysed using FACSDiva and FlowJo software programs.

2.6. Statistical analysis

Assuming Gaussian distribution and homoscedasticity, the statistical significance of the results in the liposome integrity section was tested using the student's *t*-test. Values are presented as mean ± standard deviation. For the measurements of calcein leakage in the stability study, multiple comparisons were performed

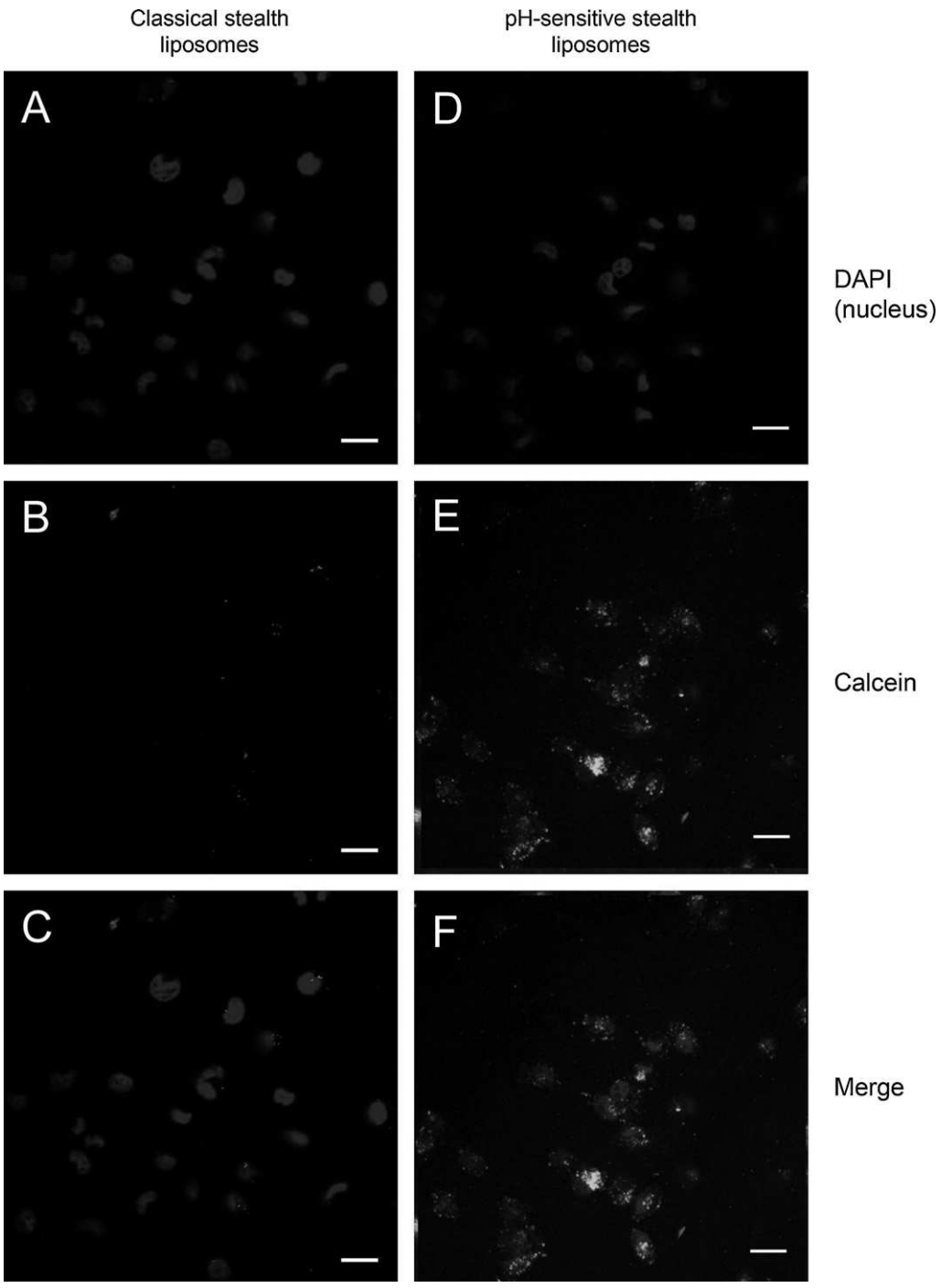

Fig. 6. Confocal laser microscopy analysis of Hs578t cells treated for 2.5 h with classical stealth liposomes (A–C) or with pH-sensitive stealth liposomes (D–F) encapsulating calcein. (A and D) Nuclei blue staining with DAPI; (B and E) green staining of liposomes containing calcein; (C and F) merge of DAPI and calcein channels. Bars represent 30 μm. (For interpretation of the references to colour in this figure legend, the reader is referred to the web version of the article.)

using a one-way ANOVA. A p value of less than 0.05 was considered to be statistically significant.

3. Results and discussion

3.1. Liposome characterization

Unilamellar liposomes were first characterized using the PCS technique. Data on size and zeta potentials of both formulations of empty liposomes, liposomes loaded with calcein and liposomes encapsulating Print3G are presented in Table 1. Sizes of 172.6 ± 14.7 nm were obtained for blank liposomes of classical composition while pH-sensitive liposomes gave sizes around 150.4 ± 14.1 nm, with a PDI always lower than 0.2 (Table 1). Blank stealth pH-sensitive liposomes are significantly smaller than the classical formulation ($p < 0.01$). Loaded-liposomes were comparable in size regardless of the type of formulation ($p > 0.05$). These sizes were acceptable for the following experiments and were consistent with the concept of passive accumulation in tumor tissues by the EPR effect. Zeta potentials of -8.0 ± 3.9 mV and of -16.3 ± 5.1 mV were respectively obtained for blank classical and

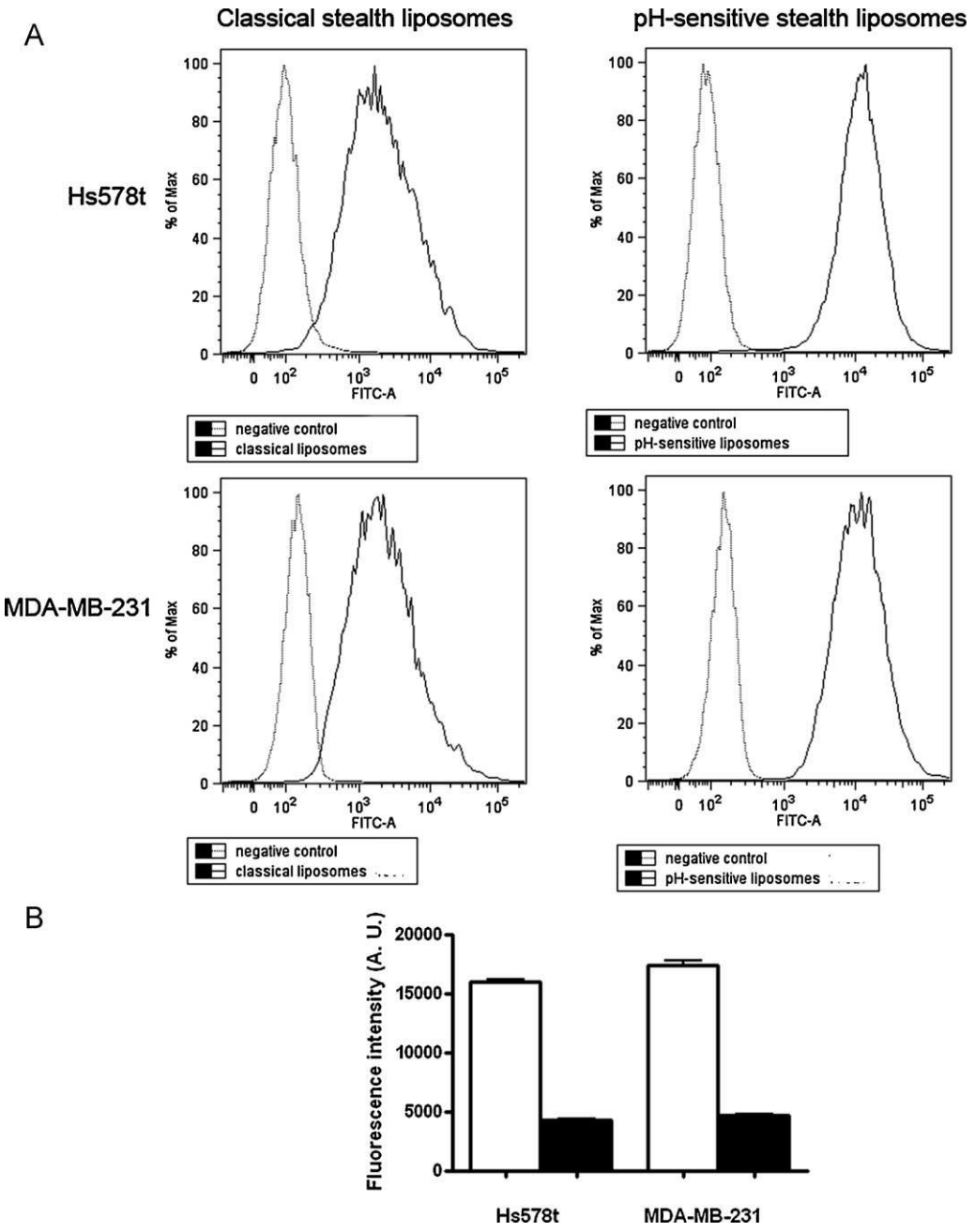

Fig. 7. Flow cytometry analysis of Hs578t or MDA-MB-231 cells treated for 2.5 h with classical or pH-sensitive stealth liposomes encapsulating calcein. (A) Representative FACS normalized histograms of empty (dotted line) or calcein-loaded (plain line) liposome-treated cells. (B) Calcein-associated fluorescence (arbitrary unit) in Hs578t or MDA-MB-231 cells treated with classical (black) or pH-sensitive (white) calcein-loaded liposomes. Results represent mean values (±S.D.) of 3 independent experiments.

blank pH-sensitive stealth liposomes. Liposomes containing calcein or Print3G follow the same tendency. The relatively negative net charge obtained for pH-sensitive liposomes is conferred by the amphiphilic stabilizer (CHEMS), not completely masked by the protective layer constituted by PEGs.

Freeze-fracture electron microscopy allowed the visualization of the shape of the two types of liposomes. Unilamellar vesicles of classical or pH-sensitive stealth liposomes are shown in Fig. 1.

These experiments allowed the visualization of the round shape of vesicles, sometimes elongated, their relatively close size distribution width and their size, close to 130 μm in diameter. PCS gives hydrodynamic diameters, resulting in higher sizes than those given by freeze-fracture electron microscopy.

3.2. Encapsulation efficiency

Print3G is a hydrophilic peptide freely soluble in water, as such it is encapsulated in the inner aqueous cavity of liposomes. In order to encapsulate Print3G into the formulation of classical stealth liposomes, blank liposomes were mixed with a Print3G solution, then freeze-thawed to promote the entry of the peptide into the vesicles. The encapsulation efficiency with this first formulation amounted to $62.68 \pm 2.93\%$ ($n = 3$). This encapsulation technique had been described in a previous study by Ducat et al. (2010), using the experimental design to improve peptide entrapment.

This method could not be used to encapsulate Print3G into pH-sensitive PEGylated liposomes because liposome destruction after

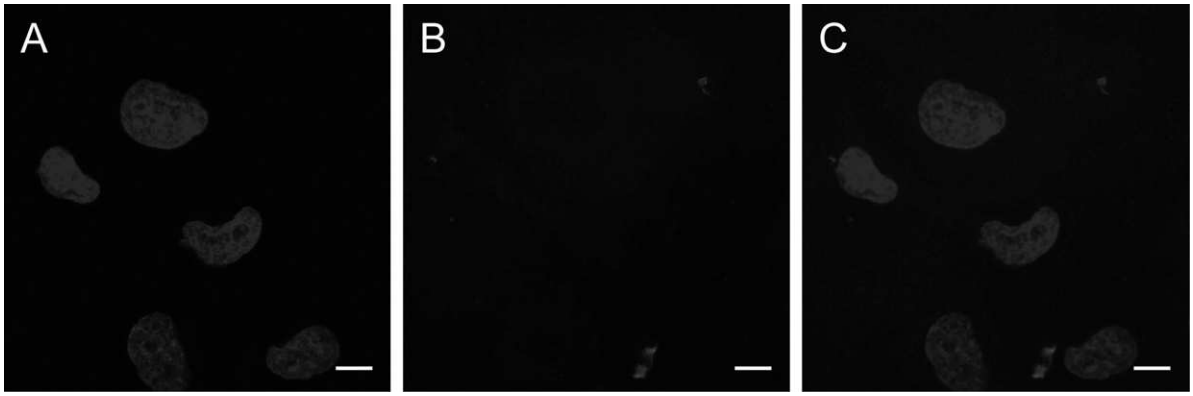

Fig. 8. Confocal laser microscopy analysis of Hs578t cells treated for 5 h with free biotinylated Print3G. (A) Nuclei blue staining with DAPI; (B) free biotinylated Print3G red staining; (C) merge of blue and red channels. Bars represent 10 μm. (For interpretation of the references to colour in this figure legend, the reader is referred to the web version of the article.)

freeze-thawing cycles was observed by PCS measurements. High encapsulation efficiency for pH-sensitive liposomes was obtained using the hydration of lipid film method associated with presaturation of the extruder by a Print3G solution. The encapsulation efficiency amounted to 90.69 ± 5.65% ($n = 4$). Both formulations possess comparable sizes and shapes and good encapsulation efficiencies of Print3G. Even if two protocols are used, the final formulations are similar. The encapsulation efficiency of Print3G in the pH-sensitive formulation was found to be significantly better than in the classical one ($p < 0.05$). This could be explained by the presence of more negative charges in pH-sensitive liposomes, which could promote the entrapment of Print3G, presenting a theoretical positive charge of +6.1.

3.3. Stability

A one month stability following the leakage of calcein from the two types of liposomes was conducted at physiological temperature and at 4 °C. As shown in Fig. 2, a significantly higher leakage of the encapsulated material was observed at 37 °C than at 4 °C after 30 days ($p < 0.05$). No significant difference was observed between the two formulations. The leakage of calcein did not exceed 3% after one month at 4 °C.

For the study of the influence of pH on stability (Fig. 3), liposomes containing pH-sensitive lipids showed a leakage of calcein significantly higher at pH 5 (ANOVA-1, $p < 0.05$).

However, there was no significant difference between results at pH 6 and pH 7 ($p > 0.05$). Moreover, compared to classical liposomes, the leakage of calcein after 6 h at pH 5 was significantly higher ($p < 0.05$). These results are linked to the composition of liposomes. Long circulating pH-sensitive liposomes contain DOPE which exhibits a conical shape and which is associated with a compound used as a stabilizer of the liposomal membrane: CHEMS. This molecule possesses an inverted cone shape at physiological pH, but, under acidic conditions, the carboxylic acid group becomes protonated and loses this particular shape. The pH decrease destabilizes the liposomal membrane, transiting from a lamellar to a hexagonal phase. The actual data could not be compared with the results found in other studies in the literature because various protocols were followed in those cases to evaluate the pH sensitivity of liposomes. Nevertheless, our results are consistent with those reported by Simoes et al. (2001). We can hypothesize that the pH-sensitivity of this formulation is partially hampered because pH-sensitive liposomes made of only DOPE and CHEMS release almost 85% of their calcein content at pH 5 (Simoes et al., 2001, 2004). Johnsson and Edwards (2001) showed in their studies that adding PEG-lipids to a system made of DOPE alone, could stabilize the lamellar phase. Despite these observations, we measured a significant increase of calcein release by pH-sensitive formulation compared to the classical one. The use of PEG of lower molecular weight than those usually used to obtain long circulating pH-sensitive liposomes, such as PEG_{2000}, could explain why pH-sensitive liposomes containing DSPE-PEG_{750} keep a significant sensitivity at low pH.

So as a compromise must be found between intracellular delivery and protection against opsonization, this pH-sensitivity study allows us expecting a better efficacy of transfection for pH-sensitive formulation than for the classical one, enabling a leakage of the drug into the cytoplasm and avoiding enzymatic degradation.

3.4. Cellular uptake of liposomes and of their encapsulated material

The confocal laser scanning microscopy (CLSM) study allowed evaluating the intracellular fate of liposomes themselves and of their encapsulated material as a function of time and in various cell lines. CLSM offers the major benefit of optically sectioning the cell. Simple fluorescence microscopy can distort the reality and possibly confuse fluorescent compounds in the cytoplasm/nucleus with those adsorbed on the cellular surface. CLSM ensures that liposomes and/or their content have actually penetrated the cell (Mady et al., 2009). Note that all the pictures used to compare formulations were acquired at the same settings (PMT and %laser).

CLSM is frequently associated with Fluorescence Activated Cell Sorting (FACS) to provide quantitative results related to the transfection of vectors in cells. FACS produces simultaneously multiple optical measurements on individual cells at high rates, allowing sorting of cells that meet specific criteria. Herein, FACS study was conducted on Hs578t and MDA-MB-231 cell lines to compare the internalization of classical and pH-sensitive stealth liposomes.

3.4.1. Liposomes containing NBD-CHOL

The penetration of liposomes themselves was studied using NBD-CHOL as a fluorescent marker of the phospholipid membrane. Indeed, cholesterol is the only common compound of both formulations that is inserted in the phospholipids bilayer of classical and pH-sensitive liposomes. NBD-CHOL was added at the same molar ratio in the two formulations. Therefore, it was a suitable compound to label fluorescently the phospholipids membrane of liposomes in order to follow their intracellular fate.

Results obtained using CLSM to evaluate the cellular uptake of NBD-CHOL liposomes by Hs578t cells are presented in Fig. 4. Fig. 4E shows a strong green fluorescence in the cytoplasm of Hs578t cells with a brighter area near the nucleus, following the application of stealth pH-sensitive liposomes. When cells were treated

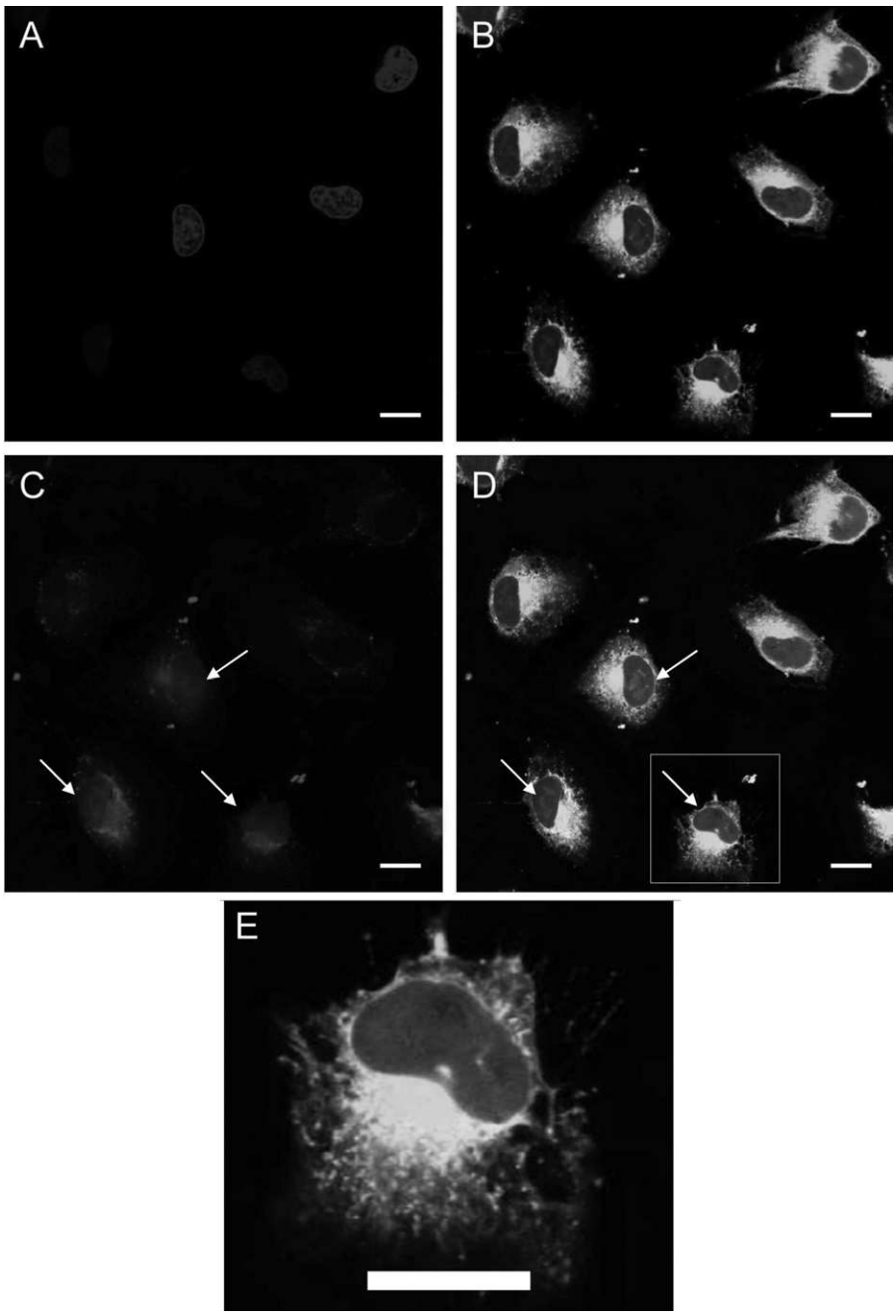

Fig. 9. Confocal laser microscopy analysis of Hs578t cells treated for 2.5 h with long circulating pH-sensitive NBD-CHOL liposomes containing biotinylated Print3G. (A) Nuclei blue staining with DAPI; (B) NBD-CHOL green staining of liposomes; (C) biotinylated Print3G red staining; (D) merge of blue, green and red channels. Bars represent 20 μm. (For interpretation of the references to colour in this figure legend, the reader is referred to the web version of the article.)

with the classical formulation of stealth liposomes (Fig. 4B), the cytoplasmic fluorescence was weaker and no brighter area was observed near the nucleus. Results obtained for penetration of fluorescent-labelled liposomes within WI-26 cells were similar to those obtained with Hs578t cells while difference between the two formulations was not discernible in MDA-MB-231 cells (data not shown).

To support these CLSM results, FACS study was carried out on Hs578t cells and MDA-MB-231 cells (Fig. 5). Results obtained with Hs578t cells showed that long circulating pH-sensitive liposomes gave fluorescence intensities of 5804 ± 73, higher than those obtained for classical stealth liposomes (4705 ± 109). When liposomes were applied on MDA-MB-231 cells, fluorescence intensities of 2966 ± 12 were obtained using long circulating pH-sensitive liposomes and of 2496 ± 45 for the classical formulation of stealth liposomes. These results confirmed those obtained by confocal microscopy. CLSM and FACS results indicate that long circulating pH-sensitive liposomes penetrate in a higher quantity in Hs578t cells.

This difference could be explained by the fact that the lipids employed in this formulation should allow a better interaction with the cellular membrane (Huth et al., 2006). DOPE is a non bilayer, fusion-promoting lipid, because it can adopt inverted lipid phases and then promote the fusion of lipid bilayers while the presence of PEG could decrease this DOPE capacity (Hafez and Cullis, 2001). Indeed, such a fusion process requires a very close contact between the two membrane structures (cell and liposome). Dos Santos et al. explained that PEG_{750} do not cover completely the

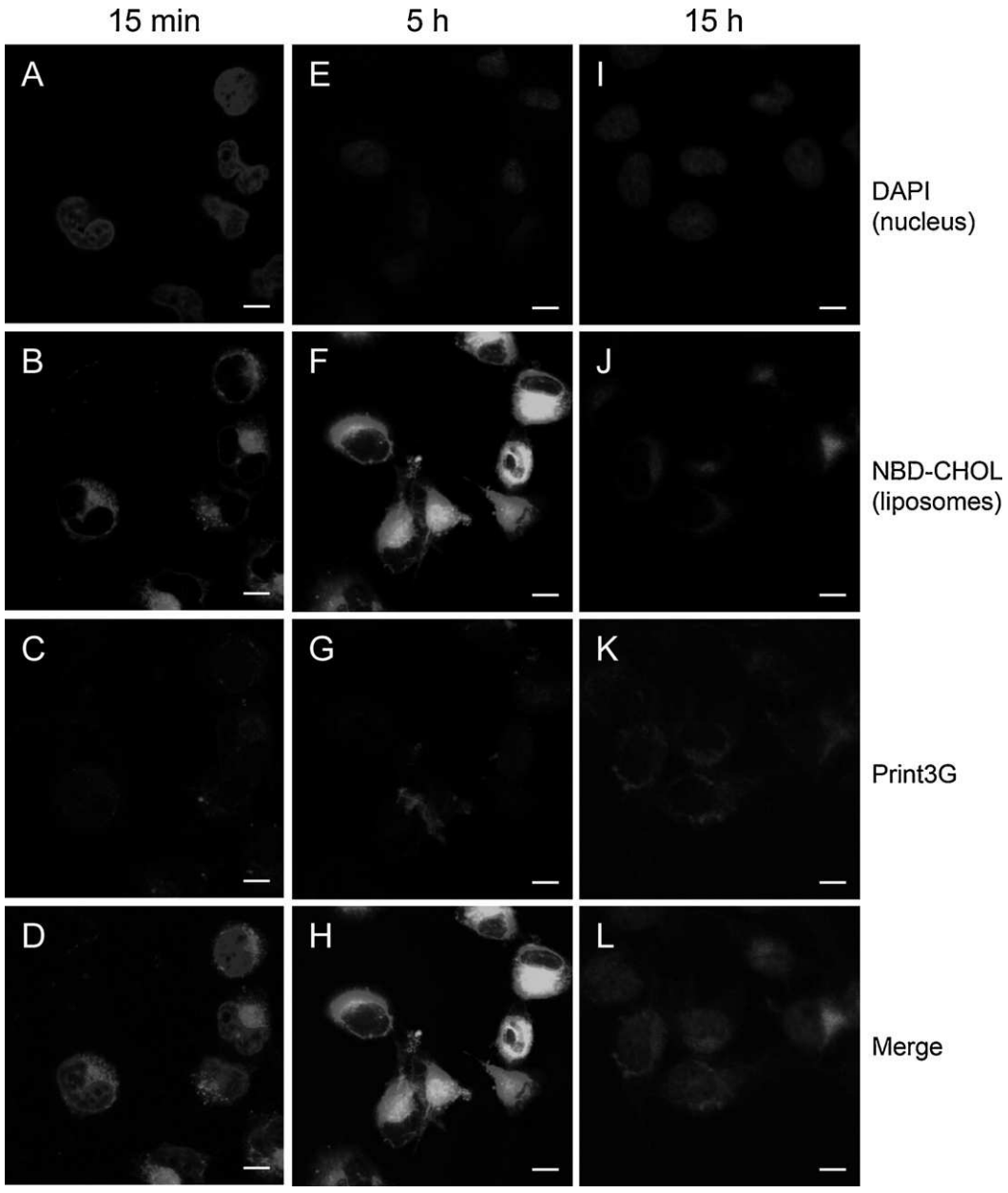

Fig. 10. Confocal laser microscopy analysis of Hs578t cells treated for 15 min (A–D), 5 h (E–H) and 15 h (I–L) with classical stealth liposomes incorporating NBD-CHOL and encapsulating the biotinylated Print3G. (A, E, and I) Nuclei blue staining with DAPI; (B, F, and J) NBD-CHOL green staining of liposomes; (C, G, and K) biotinylated Print3G red staining; (D, H, and L) merge of blue, green and red channels. Bars represent 10 μm. (For interpretation of the references to colour in this figure legend, the reader is referred to the web version of the article.)

liposome surface, in opposition to PEG_{2000} (Dos Santos et al., 2007). Moreover, their results suggest that a complete surface coverage is not required for PEG to cause increased circulation time. If PEG_{750} does not cover totally the surface of pH-sensitive liposomes, it could remain some regions of interactions between DOPE and cellular/endosomal membrane, but also a significant pH-sensitivity. The use of DSPE-PEG_{750}, of lower molecular weight, could allow keeping an effective interaction of DOPE with the cellular membrane, explaining the better internalization of the pH-sensitive formulation.

3.4.2. Calcein-loaded liposomes

The penetration of calcein-loaded liposomes was studied in order to better understand the intracellular delivery mechanism of an encapsulated material in classical or pH-sensitive stealth liposomes. Hydrophilic model molecule calcein (M.W. = 376; log *P* = −5.219; 492/517 nm) was entrapped at a self-quenched concentration within the two formulations. The use of calcein as a model molecule could be justified by two ways. Firstly, calcein is encapsulated in the inner cavity of liposomes because of its hydrophilicity. Print3G, which is also water-soluble, is entrapped in the same liposome compartment. Secondly, calcein is a self-quenching fluorescent dye, often used to study the endosomal escape of hydrophilic compounds triggered by pH-sensitive liposomes. Concentration quenching of calcein is a complex phenomenon, based on dimerization and energy transfer to dimer (Chen and Knutson, 1988; Weinstein et al., 1977; Duzgunes et al., 2003). Calcein, encapsulated at high concentration, is virtually non-fluorescent, owing to the formation of ground state dimers. Any fluorescence measured will be due to the leakage of calcein out

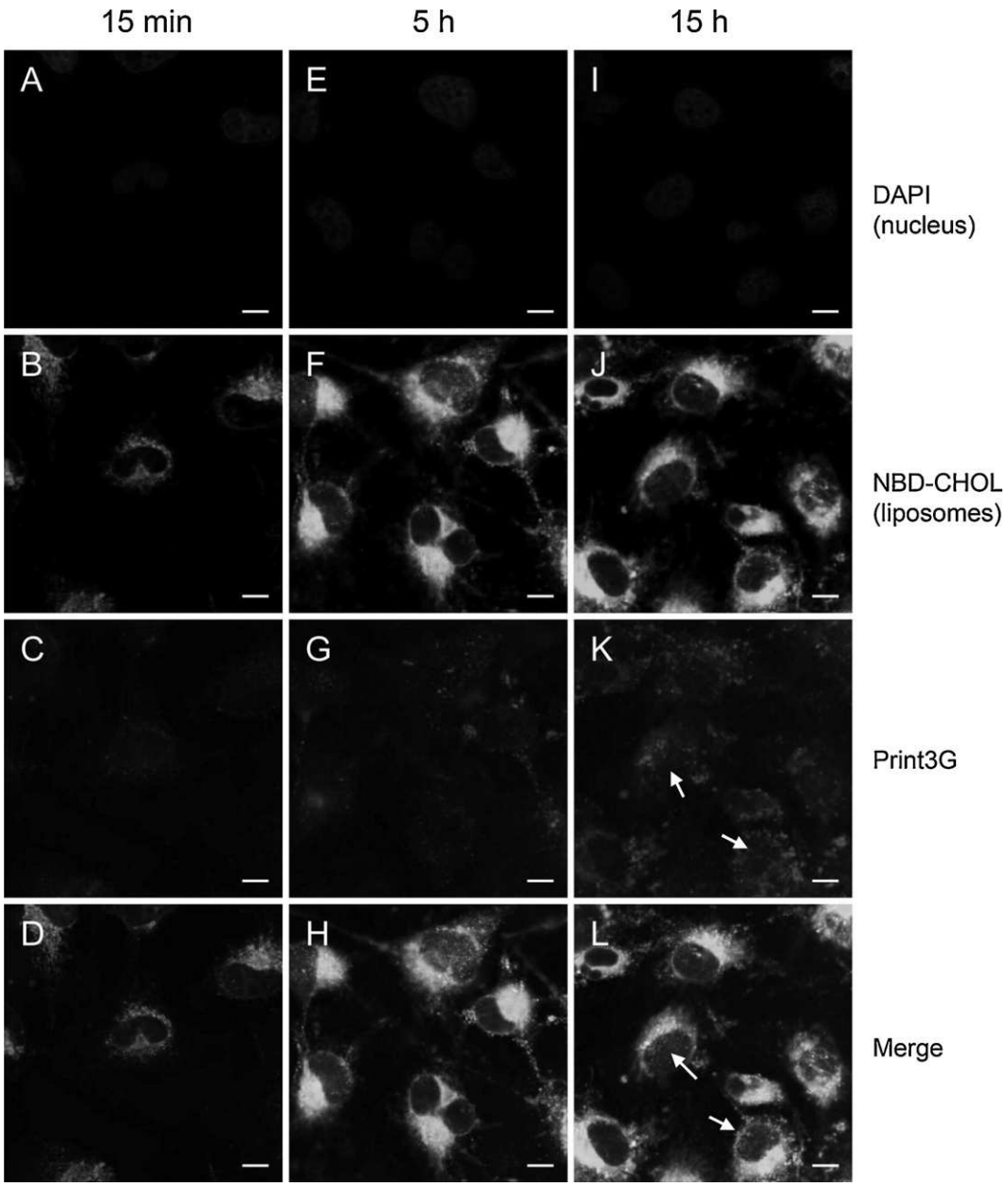

Fig. 11. Confocal laser microscopy analysis of Hs578t cells treated for 15 min (A–D), 5 h (E–H) and 15 h (I–L) with pH-sensitive stealth liposomes incorporating NBD-CHOL and encapsulating the biotinylated Print3G. (A, E, and I) Nuclei blue staining with DAPI; (B, F, and J) NBD-CHOL green staining of liposomes; (C, G, and K) biotinylated Print3G red staining; (D, H, and L) merge of blue, green and red channels. Bars represent 10 μm. (For interpretation of the references to colour in this figure legend, the reader is referred to the web version of the article.)

of vesicles and dilution in the exterior aqueous media. Regain of fluorescence happens when liposomes are taken up by cells and lysed.

Fig. 6 shows CLSM images illustrating the cellular uptake of calcein-loaded liposomes by Hs578t cells. As shown in Fig. 6B, calcein fluorescence is weak when using classical liposomes. By contrast, the majority of cells were found to be fluorescent when calcein-loaded pH-sensitive liposomes were applied onto cells (Fig. 6). Song et al. (2009) observed this fact using a classical formulation of doxorubicin in PEGylated liposomes. They evoked the possibility of self-quenched doxorubicin presenting a low fluorescence, not discernible in cells. In our study, calcein is encapsulated at a self-quenched concentration and may not be distinguished in the picture. Due to the lowering of the pH, a significant fraction of calcein is delivered from pH-sensitive stealth liposomes, from endosomes to cytoplasm, allowing observing a bright fluorescence.

As it can be also observed in Fig. 6E, fluorescence is sometimes doted, which might suggest that it remains some calcein entrapped in endosomes. But we can conclude that a significant amount of the dye is delivered in cytoplasm because of the bright fluorescence observed. If calcein remained totally in endosomes, the fluorescence should be significantly lower and pictures should be like Fig. 6B, obtained with the classical formulation.

FACS study was conducted on Hs578t cells and MDA-MB-231 cells to confirm results obtained by CLSM study (Fig. 7). Fluorescence intensities in positive Hs578t cells were respectively of $15{,}973 \pm 333$ for cells treated with pH-sensitive stealth liposomes and of 4217 ± 243 for cells treated with classical stealth liposomes. In positive MDA-MB-231 cells, fluorescence intensities amounted to $17{,}357 \pm 716$ for pH-sensitive stealth liposomes and to 4663 ± 96 for the classical formulation. Fluorescence intensity obtained for the pH-sensitive formulation was significantly higher

($p < 0.001$) comparing to the classical one, regardless of the type of cell observed. These results confirmed those obtained using CLSM, the calcein delivery is more efficient using the pH-sensitive formulation. Therefore, calcein is not released in the cytoplasm but remains sequestrated in classical stealth liposomes. On the contrary, pH-sensitive stealth liposomes escape from the endosome by disruption of their membrane, according to their mechanism of action, and then release their encapsulating material in the cytoplasm of cells. Then, calcein could be diluted in the cytoplasm and present a significant fluorescence on confocal pictures.

3.4.3. Liposomes encapsulating Print3G

The two first studies using both CLSM and FACS techniques allowed us to expect a better efficacy of PEGylated pH-sensitive liposomes as Print3G vectors than the classical formulation. However, calcein is not the perfect model molecule to predict the intracellular fate of the peptide and the next step of our study was to investigate the intracellular fate of the peptide, which has to reach the nucleus in order to interact with its target. Biotin was covalently grafted on Print3G in order to follow it to the cell nucleus using streptavidin conjugate Alexa Fluor 555.

3.4.3.1. Free Print3G. Firstly, the penetration of the free biotinylated peptide was evaluated at a concentration equivalent to that present in liposomes used for further experiments. Results are shown in Fig. 8, revealing the weak penetration of the unencapsulated biotinylated peptide.

3.4.3.2. Encapsulated Print3G. Long circulating pH-sensitive NBD-CHOL liposomes encapsulating biotinylated Print3G were then applied onto Hs578t cells for 2.5 h. Results are shown in Fig. 9. As it has been observed in our previous confocal experiments Fig. 9B shows a small region near the nucleus with a brighter fluorescence, indicating an accumulation of NBD-CHOL liposomes at this position. In Fig. 9C, an accumulation of the peptide clearly appears in some nuclei. The use of pH-sensitive liposomes allows to observe a significant amount of peptide escaping from the endosome by disruption of the liposomal membrane. The peptide can then diffuse freely from the cytoplasm to the nucleus of cells.

In order to discern a difference between classical and pH-sensitive long circulating liposomes in terms of sequestrated peptide delivery from the endosome to the cytoplasm and to investigate this phenomenon kinetic, Hs578t cells were incubated with classical or pH-sensitive liposomes for a period of 15 min, 5 h and 15 h. Confocal images obtained with the classical formulation of long circulating liposomes, incorporating NBD-CHOL in the phospholipid bilayer and the biotinylated peptide in their aqueous cavity, are shown in Fig. 10. Comparing Fig. 10B, F and J, the incursion of liposomes by themselves can be followed in the cytoplasm, peaking after 5 h then decreasing, providing an image comparable to those obtained in the first experiments with NBD-CHOL and classical liposomes. Penetration of the peptide (Fig. 10C, G and K) increases slightly but no fluorescence was observed in the cell nuclei.

These experiments were also performed with a formulation of stealth pH-sensitive liposomes. Results are shown in Fig. 11. Fig. 11B, F and J shows an increasing uptake of pH-sensitive liposomes as a function of time with a high fluorescence that remains intense for at least 15 h. The penetration of the peptide is also different from the one observed with classical liposomes: the peptide can enter the cell and reach the nucleus (Fig. 11C, G and K). The presence of Print3G in the nucleus of cells treated with pH-sensitive liposomes and its absence in cell nuclei when treated with the classical formulation still emphasize our arguments. So as for calcein experiments (see Sections 3.3 and 3.4.2), this difference could be explained by the particular mechanism of action of pH-sensitive liposomes, which is efficient to deliver the peptide, avoiding its degradation. While calcein or Print3G remain entrapped in endosome compartment when encapsulated in the classical formulation – observed respectively by a minimal fluorescence for calcein experiments and by a cytoplasm localization for peptide experiments – the pH-sensitive formulation allow the delivery of its encapsulated material in the cytoplasm, resulting respectively in a detectable fluorescence and in a nuclear localization of Print3G. The nucleus localization of the peptide after treatment with pH-sensitive formulation cannot be explained by the polysorbate permeabilization step. Indeed, the same permeabilization step was used when cells were treated with classical formulation but no peptide was observed in the nuclei even 15 h after liposomes delivery.

When experiments were conducted on MDA-MB-231 cell line, the presence of peptide in cells was observed after treatment with pH-sensitive stealth liposomes encapsulating Print3G (data not shown). The peptide was detected in the nucleus of the two cancerous cell lines.

4. Conclusion

Classical and pH-sensitive stealth liposomes possess acceptable size, shape, encapsulation efficiency and stability to be potential vectors for Print3G delivery. However, the use of CLSM and FACS in this study highlights the important benefit of pH-sensitive liposomes over classical ones. Indeed, stealth pH-sensitive liposomes can penetrate by themselves all the cell lines tested and deliver more efficiently hydrophilic materials to the cytoplasm of cancerous cells. This better efficacy could be explained by the particular composition of liposomes allowing a better interaction with cellular membrane and an endosomal escape of entrapped materials. The use of PEG_{750} replacing the widely used PEG_{2000} to formulate long-circulating liposomes is probably the key for the maintenance of a sufficient interaction with cellular membrane and pH-sensitivity. Most importantly, the better capacity of long circulating pH-sensitive liposomes to mediate intracellular delivery allow observing the delivery of the therapeutic peptide to the nucleus of tumorigenic and non tumorigenic breast cancer cells, something not observed with classical liposomes encapsulating Print3G. These results were obtained using liposomes formulated to maintain a long circulation lifetime and our study proved that the penetration of stealth pH-sensitive liposomes remains efficient in spite of their PEGylation. This study proves the benefit of developing stealth pH-sensitive formulations for peptide delivery.

Acknowledgements

This study was supported by the Région Wallonne. We are grateful to P. Compere for helping us to carry out the freeze-fracture electron microscopy study. We are also very thankful to the GIGA Cell Imaging and Flow Cytometry Platform for their technical help in CLSM and FACS studies.

References

Banga, A.K., Chien, Y.W., 1988. Systemic delivery of therapeutic peptides and proteins. Int. J. Pharm. 48, 15–50.

Bellavance, M.-A., Poirier, M.-B., Fortin, D., 2010. Uptake and intracellular release kinetics of liposome formulations in glioma cells. Int. J. Pharm. 395, 251–259.

Chen, R.F., Knutson, J.R., 1988. Mechanism of fluorescence concentration quenching of carboxyfluorescein in liposomes: energy transfer to nonfluorescent dimers. Anal. Biochem. 172, 61–77.

Dos Santos, N., Allen, C., Doppen, A.M., Anantha, M., Cox, K.A., Gallagher, R.C., Karlsson, G., Edwards, K., Kenner, G., Samuels, L., Webb, M.S., Bally, M.B., 2007. Influence of poly(ethylene glycol) grafting density and polymer length on liposomes: relating plasma circulation lifetimes to protein binding. Biochim. Biophys. Acta 1768, 1367–1377.

Ducat, E., Brion, M., Lecomte, F., Evrard, B., Piel, G., 2010. The experimental design as practical approach to develop and optimize a formulation of peptide-loaded liposomes. AAPS PharmSciTech 11, 966–975.

Duzgunes, N., Bagatolli, L.A., Meers, P., Oh, Y.-K., Straubinger, R.M., 2003. Fluorescence methods in liposome research. In: Torchilin, V., Weissig, V. (Eds.), Liposomes. , second ed. Oxford University Press, New York, pp. 105–147.

Hafez, I.M., Cullis, P.R., 2001. Roles of lipid polymorphism in intracellular delivery. Adv. Drug Deliv. Rev. 47, 139–148.

Hanato, J., Kuriyama, K., Mizumoto, T., Debari, K., Hatanaka, J., Onoue, S., Yamada, S., 2009. Liposomal formulations of glucagon-like peptide-1: improved bioavailability and anti-diabetic effect. Int. J. Pharm. 382, 111–116.

Hong, Y.-J., Pyo, C.G., Kim, J.-C., 2010. Liposomes incorporating hydrophobically modified silk fibroin: pH-dependent release. Int. J. Biol. Macromol. 47, 635–639.

Huth, U.S., Schubert, R., Peschka-Suss, R., 2006. Investigating the uptake and intracellular fate of pH-sensitive liposomes by flow cytometry and spectral bio-imaging. J. Control. Release 110, 490–504.

Johnsson, M., Edwards, K., 2001. Phase behavior and aggregate structure in mixtures of dioleoylphosphatidylethanolamine and poly(ethylene glycol)-lipids. Biophys. J. 80, 313–323.

Junior, A.D., Mota, L.G., Nunan, E.A., Wainstein, A.J., Wainstein, A.P., Leal, A.S., Cardoso, V.N., De Oliveira, M.C., 2007. Tissue distribution evaluation of stealth pH-sensitive liposomal cisplatin versus free cisplatin in Ehrlich tumor-bearing mice. Life Sci. 80, 659–664.

Katanasaka, Y., Ida, T., Asai, T., Maeda, N., Oku, N., 2008. Effective delivery of an angiogenesis inhibitor by neovessel-targeted liposomes. Int. J. Pharm. 360, 219–224.

Kirby, C., Clarke, J., Gregoriadis, G., 1980a. Cholesterol content of small unilamellar liposomes controls phospholipid loss to high density lipoproteins in the presence of serum. FEBS Lett. 111, 324–328.

Kirby, C., Clarke, J., Gregoriadis, G., 1980b. Effect of the cholesterol content of small unilamellar liposomes on their stability in vivo and in vitro. Biochem. J. 186, 591–598.

Klibanov, A.L., Torchilin, V.P., Zalipsky, S., 2003. Long-circulating sterically protected liposomes. In: Torchilin, V.P., Weissig, V. (Eds.), Liposomes, A Practical Approach. , second ed. Oxford University Press, New York, pp. 231–265.

Kono, K., Igawa, T., Takagishi, T., 1997. Cytoplasmic delivery of calcein mediated by liposomes modified with a pH-sensitive poly(ethylene glycol) derivative. Biochim. Biophys. Acta-Biomembr. 1325, 143–154.

Liu, D., Huang, L., 1989. Role of cholesterol in the stability of pH-sensitive, large unilamellar liposomes prepared by the detergent-dialysis method. Biochim. Biophys. Acta 981, 254–260.

Mady, M.M., Ghannam, M.M., Khalil, W.A., Muller, R., Fahr, A., 2009. Efficiency of cytoplasmic delivery by non-cationic liposomes to cells in vitro: a confocal laser scanning microscopy study. Phys. Med. 25, 88–93.

Maeda, H., Bharate, G.Y., Daruwalla, J., 2008. Polymeric drugs for efficient tumor-targeted drug delivery based on EPR-effect. Eur. J. Pharm. Biopharm. 71, 409–419.

Momekova, D., Rangelov, S., Yanev, S., Nikolova, E., Konstantinov, S., Romberg, B., Storm, G., Lambov, N., 2007. Long-circulating, pH-sensitive liposomes sterically stabilized by copolymers bearing short blocks of lipid-mimetic units. Eur. J. Pharm. Sci. 32, 308–317.

Obata, Y., Tajima, S., Takeoka, S., 2009. Evaluation of pH-responsive liposomes containing amino acid-based zwitterionic lipids for improving intracellular drug delivery in vitro and in vivo. J. Control. Release 142, 267–276.

Peschka-Suss, R., Schubert, R., 2003. pH-sensitive liposomes. In: Torchilin, V.P., Weissig, V. (Eds.), Liposomes, A Practical Approach. , second ed. Oxford University Press, New York, pp. 305–318.

Petrikovics, I., Budai, M., Baskin, S.I., Rockwood, G.A., Childress, J., Budai, L., Grof, P., Klebovich, I., Szilazi, M., 2009. Characterization of liposomal vesicles encapsulating rhodanese for cyanide antagonism. Drug Deliv. 16, 312–319.

Shi, G., Guo, W., Stephenson, S.M., Lee, R.J., 2002. Efficient intracellular drug and gene delivery using folate receptor-targeted pH-sensitive liposomes composed of cationic/anionic lipid combinations. J. Control. Release 80, 309–319.

Simoes, S., Moreira, J.N., Fonseca, C., Duzgunes, N., de Lima, M.C., 2004. On the formulation of pH-sensitive liposomes with long circulation times. Adv. Drug Deliv. Rev. 56, 947–965.

Simoes, S., Slepushkin, V., Duzgunes, N., Pedroso de Lima, M.C., 2001. On the mechanisms of internalization and intracellular delivery mediated by pH-sensitive liposomes. Biochim. Biophys. Acta 1515, 23–37.

Skalko, N., Peschka, R., Altenschmidt, U., Lung, A., Schubert, R., 1998. pH-sensitive liposomes for receptor-mediated delivery to chicken hepatoma (LMH) cells. FEBS Lett. 434, 351–356.

Song, C.K., Jung, S.H., Kim, D.D., Jeong, K.S., Shin, B.C., Seong, H., 2009. Disaccharide-modified liposomes and their in vitro intracellular uptake. Int. J. Pharm. 380, 161–169.

Straubinger, R.M., Duzgunes, N., Papahadjopoulos, D., 1985. pH-sensitive liposomes mediate cytoplasmic delivery of encapsulated macromolecules. FEBS Lett. 179, 148–154.

Torchilin, V., 2006. Anti-cancer proteins and peptides in liposomes. In: Torchilin, V. (Ed.), Delivery of Protein and Peptide Drugs in Cancer. Imperial College Press, London, pp. 155–182.

Torchilin, V., 2009. Multifunctional and stimuli-sensitive pharmaceutical nanocarriers. Eur. J. Pharm. Biopharm. 71, 431–444.

Weinstein, J.N., Yoshikami, S., Henkart, P., Blumenthal, R., Hagins, W.A., 1977. Liposome–cell interaction: transfer and intracellular release of a trapped fluorescent marker. Science 195, 489–492.

Zhou, X.H., Li Wan Po, A., 1991. Peptide and protein drugs: I. Therapeutic applications, absorption and parenteral administration. Int. J. Pharm. 75, 97–115.

Langmuir

Article

pubs.acs.org/Langmuir

Ursolic Acid Incorporation Does Not Prevent the Formation of a Non-lamellar Phase in pH-Sensitive and Long-Circulating Liposomes

Sávia C. A. Lopes,[†] Marcus V. M. Novais,[†] Diêgo S. Ferreira,[†] Fernão C. Braga,[†] Rogério Magalhães-Paniago,[‡] Ângelo Malachias,[‡] and Mônica C. Oliveira*,[†]

[†]Faculty of Pharmacy, and [‡]Physics Department, Institute of Exact Sciences, Universidade Federal de Minas Gerais, Belo Horizonte, Minas Gerais 31270-901, Brazil

ABSTRACT: Ursolic acid (UA) is a triterpene found in different plant species that has been shown to possess significant antitumor activity. However, UA presents a low water solubility, which limits its biological applications. In this context, our research group has proposed the incorporation of UA in long-circulating and pH-sensitive liposomes (SpHL−UA).These liposomes, composed of dioleylphosphatidylethanolamine (DOPE), cholesteryl hemisuccinate (CHEMS), and distearoylphosphatidylethanolamine−polyethylene glycol$_{2000}$ (DSPE−PEG$_{2000}$), were shown to be very promising carriers for UA. Considering that the release of UA from SpHL−UA and its antitumor activity depend upon the occurrence of the lamellar to non-lamellar phase transition of DOPE, in the present work, the interactions of UA with the components of the liposomes were evaluated, aiming to clarify their role in the structural organization of DOPE. The study was carried out by differential scanning calorimetry (DSC) and small-angle X-ray scattering (SAXS) under low hydration conditions. DSC studies revealed that DOPE phase transition temperatures did not shift significantly upon UA addition. On the other hand, in SAXS studies, a different pattern of DOPE phase organization was observed in the presence of UA, with the occurrence of the cubic phase *Im*3*m* at 20 °C and the cubic phase *Pn*3*m* at 60 °C. These findings suggest that UA interacts with the lipids and changes their self-assembly. However, these interactions between the lipids and UA were unable to eliminate the lamellar to non-lamellar phase transition, which is essential for the cytoplasmic delivery of UA molecules from SpHL−UA.

1. INTRODUCTION

Different lipid-based nanosystems, such as liposomes, nanoemulsions, nanocapsules, and solid lipid nanoparticles, can be used as carriers to improve anticancer treatments because of their capacity to increase the solubility of poorly water-soluble antitumor drugs. The encapsulation of anticancer drugs in these nanosystems increases the drug bioavailability and the fraction of drug delivered within the pathological area, thus improving efficacy and minimizing drug toxicity.[1−5] Among these nanosystems, the liposomes have been successfully used as carriers of many antitumor drugs, such as cisplatin,[6,7] doxorubicin,[8,9] and paclitaxel.[10,11]

Ursolic acid (UA) is a triterpene found in different plant species described to possess significant antitumor activity.[12−16] However, although UA presents the advantage of low toxicity, the clinical application of UA is limited because of its poor water solubility, which leads to a low bioavailability *in vivo* and, hence, restricts its effectiveness.[17−19] The use of nanosystems as carriers, such as liposomes, is a promising strategy to deliver this substance and allows for its intravenous administration. In this context, our research group proposed the incorporation of UA in long-circulating and pH-sensitive liposomes (SpHL−UA), which presented good stability in terms of mean vesicle size, ζ potential, and UA entrapment after storage for 1 year at 4 °C. Furthermore, SpHL−UA treatment significantly inhibited breast cancer cell line (MDA-MB-231) and prostate cancer cell line (LNCaP) proliferation, suggesting its applicability as a new and promising anticancer formulation.[2]

pH-sensitive liposomes have been designed to undergo destabilization when submitted to an acidic environment at the endosomal stage, thereby preventing drug degradation at the lysosomal level and promoting its release into the cytoplasm.[20,21] These liposomes are composed of unsaturated phosphatidylethanolamine, such as dioleylphosphatidylethanolamine (DOPE), and take advantage of their polymorphic phase behavior, which forms inverted hexagonal phases (H_{II}) rather than bilayers under physiological conditions of pH and temperature.[22,23] Liposome stabilization can be achieved using a titratable acid lipid, such as cholesteryl hemisuccinate (CHEMS), which is negatively charged at neutral pH. This carboxylated compound is homogeneously distributed among DOPE molecules and provides electrostatic repulsions that decrease intermolecular interactions, thus preventing a H_{II} phase formation and favoring the formation of bilayers (lamellar phase) under physiological conditions. The protonation of CHEMS molecules, in the acidic endosomal

Received: July 25, 2014
Revised: November 26, 2014
Published: November 27, 2014

compartment, suppresses charge repulsion in the bilayer, inducing the reversion of DOPE molecules into their H_{II} phase and, in turn, releasing the encapsulated drugs.[21,24]

Because the lamellar to non-lamellar DOPE phase transition plays a crucial role in drug delivery using pH-sensitive liposomes, it is interesting to investigate the self-assembly of these liposomes in the presence of a drug, such as UA. If UA molecules modify the lamellar to non-lamellar phase transition of DOPE, the pH-sensitivity of the liposomes might be altered.

Thus, in this paper, we investigated the effect of the addition of UA on the phase behavior of DOPE in the presence of other liposomal components, such as CHEMS and distearoylphosphatidylethanolamine−polyethylene $glycol_{2000}$ (DSPE−PEG_{2000}), aiming to clarify their structural organization. Thermal behavior of DOPE was examined by differential scanning calorimetry (DSC). Small-angle X-ray scattering (SAXS) measurements were recorded at different temperatures and used to characterize the phases involved. The study was performed with quasi-anhydrous preparations to be able to identify the lipid behavior at low temperatures in the absence of ice formation. This investigation in such concentrated and confined systems will shed some light on the behavior of more diluted preparations.

2. EXPERIMENTAL SECTION

2.1. Materials. DOPE and DSPE−PEG_{2000} were purchased from Lipoid GmbH (Ludwisgshafen, Germany). UA, CHEMS, and phosphate-buffered saline (PBS) were obtained from Sigma Chemical Company (St. Louis, MO). All other chemicals were of reagent grade and used as received.

2.2. Sample Preparation. Preweighted amounts of DOPE, CHEMS, and DSPE−PEG_{2000} were dissolved in chloroform, and aliquots of each (equal to 8.5, 3.7, and 2.8 mg, respectively) were added to DSC aluminum pans in different proportions to achieve the desired molar fractions of 5.7:0:0, 5.7:3.8:0, and 5.7:3.8:0.5, respectively. These samples were submitted to a gentle heating until solvent dryness. Aliquots of lyophilized PBS at pH 7.4 (12.7 mg) were added to the lipid film in all samples. When needed, an amount of UA (1 mg) was added. The liposomal components were mixed as follows: DOPE/PBS, DOPE/CHEMS/PBS, DOPE/CHEMS/DSPE−PEG_{2000}/PBS, and DOPE/CHEMS/DSPE−PEG_{2000}/UA/PBS.

The pans containing the liposomal components were hydrated over saturated solution of $MgCl_2{\cdot}6H_2O$ at 4 °C (34.6% relative humidity) until a constant weight. The water weight fraction for DOPE/PBS, DOPE/CHEMS/PBS, DOPE/CHEMS/DSPE−PEG_{2000}/PBS, and DOPE/CHEMS/DSPE−PEG_{2000}/UA/PBS was equal to 0.009, 0.052, 0.034, and 0.032, respectively. At equilibrium, the different pans were weighed, sealed, and analyzed by DSC. For SAXS measurements, these hydrated samples were transferred to metal rings and sealed with a polyimide film (Kapton).

2.3. DSC Measurements. DSC experiments were performed on a DSC 2910 modulated TA Instrument (New Castle, DE) at a heating rate of 5 °C/min. Indium was used for temperature and enthalpy calibration, and nitrogen was used as purging gas. The weighted samples were scanned from −50 to 80 °C. The samples were submitted to three consecutive runs, which allowed for their greater homogenization. Data acquisition and analysis were performed on a microcomputer using an isothermal software kit provided by TA Instruments. The transition temperatures were defined by the position of the DSC peak maximum.

2.4. SAXS Measurements. SAXS measurements were carried out at D1B-SAXS1 beamline of the Brazilian Synchrotron Light Laboratory (LNLS, Campinas, Brazil), at a fixed X-ray wavelength λ = 0.1488 nm. SAXS patterns were detected using a 300K Pilatus detector providing a q range of 0.15−4.0 nm^{-1}, where q is the momentum transfer calculated as $q = (4\pi/\lambda)\sin\theta$ and θ is the scattering angle. A sample holder with a DSC-linkam heating system was also used.

3. RESULTS AND DISCUSSION

The thermal behavior and SAXS patterns of liposomal component mixtures are described below. The lattice parameters (a) were calculated using the formula $a = 2\pi/q$, which is valid for the first-order peaks of all packing structure types analyzed in this work.

3.1. DOPE/PBS Mixtures. DOPE/PBS mixtures were first submitted to DSC analysis (Figure 1). Three endothermic

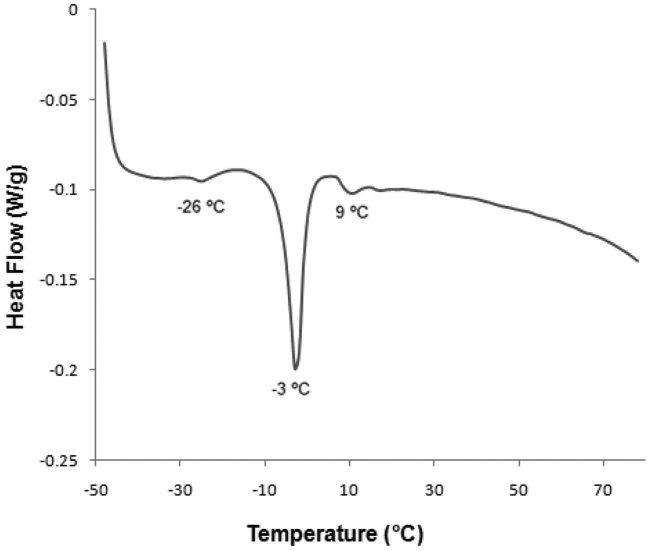

Figure 1. Thermal phase behavior of the DOPE/PBS sample.

peaks centered at −26, −3, and 9 °C could be observed. The intense DSC peak observed at −3 °C can be attributed to the ice melting, as previously described by De Oliveira and co-workers.[24]

SAXS patterns for the DOPE/PBS sample recorded at different temperatures are presented in Figure 2. Diffraction

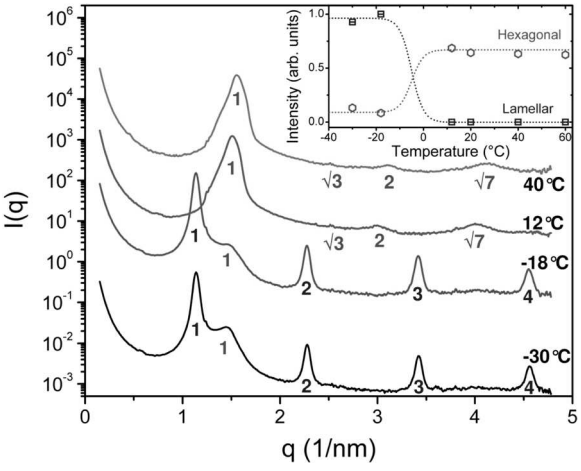

Figure 2. SAXS patterns of the sample DOPE/PBS at different temperatures. The indexes represent the periodicity of the Bragg reflections. Blue indexes are related to lamellar phases, while red indexes are related to hexagonal phases. The inset shows the normalized integrated intensity of the first-order SAXS peak of each phase. The solid lines are a guide to the eye.

dx.doi.org/10.1021/la502977j | Langmuir 2014, 30, 15083−15090

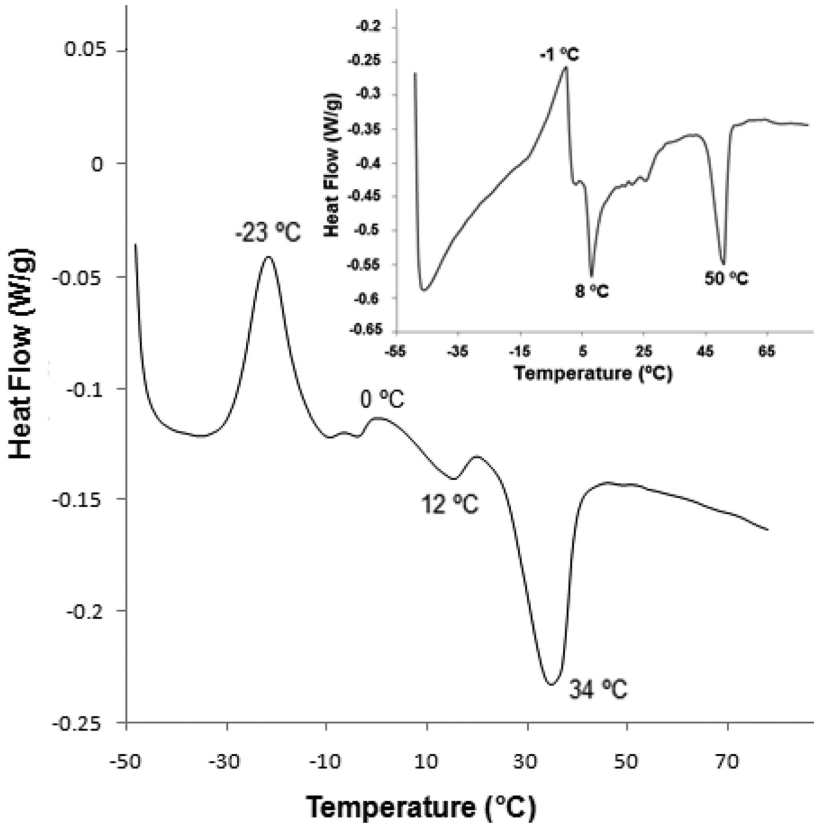

Figure 3. Thermal phase behavior of the DOPE/CHEMS/PBS sample. The inset shows the thermal phase behavior of the pure CHEMS sample.

patterns of DOPE at −30 and −18 °C showed SAXS peaks at q = 1.14, 2.28, 3.42, and 4.56 nm^{-1} with Bragg indexes 1, 2, 3, and 4, which characterizes the presence of lamellar phases (blue indexes). The lattice parameter was equivalent to 4.36 nm, at both temperatures. In addition, a broad SAXS peak at q = 1.44 nm^{-1} was observed, which presented a lower intensity at −18 °C compared to that obtained at −30 °C. This SAXS peak at q = 1.44 nm^{-1} is the first order of a hexagonal phase that developed upon heating and could be clearly identified at 12 and 40 °C. The occurrence of the structural changes of the hexagonal domains upon heating may be related to the appearance of the slight endotherm observed at −26 °C.

Concerning SAXS patterns acquired at 12 and 40 °C, peaks were identified at q = 1.52, 2.51, 2.98, and 4 nm^{-1} and q = 1.54, 2.51, 3.10, and 4.10 nm^{-1}, respectively. In both temperatures, the periodicity of Bragg reflections was equal to 1, $\sqrt{3}$, 2, and $\sqrt{7}$, indicating the existence of a hexagonal phase of DOPE. The lattice parameter found was equivalent to 4.1 nm. Therefore, the DSC peak observed at 9 °C (Figure 1) could be related to the lamellar to hexagonal (H_{II}) phase transition.

The inset of Figure 2 shows the temperature behavior of the normalized integrated intensity of the first-order SAXS peak of each phase. Clearly, one observes the coexistence of the hexagonal and lamellar phases throughout the working temperature range, showing that the phase transition is not of second order. Rather, the coexistence of phases reveals that the transition is of first order, with an activation energy (from one phase to the other) lower than the phase transition temperature. This means that the energy necessary for the transition from one phase to the other is lower than the thermal energy, allowing for the coexistence of both phases within the studied temperature range. This behavior was also observed for all other studied mixtures.

3.2. DOPE/CHEMS/PBS Mixtures. Figure 3 depicts the thermal behavior of the DOPE/CHEMS/PBS sample. Four DSC peaks centered at −23, 0, 12, and 34 °C were observed. The exothermic DSC peaks observed at −23 and 0 °C were attributed to the crystallization of CHEMS molecules, which are distributed heterogenously in the lipid bilayer. An exothermic peak was also observed in DSC analysis of pure CHEMS, where the DSC peak was centered at −1 °C (inset of Figure 3). The decrease of this crystallization temperature (−23 °C) might be related to the presence of PBS buffer salts.

SAXS measurements of the DOPE/CHEMS/PBS sample were obtained in different temperatures, as presented in Figure 4. At −30 °C, SAXS peaks were identified at q = 1.16, 2.27, 3.41, and 4.54 nm^{-1}, with periodicity of the Bragg reflections nearly equal to 1, 2, 3, and 4, which characterizes the presence of the lamellar phase of DOPE molecules. The lattice parameter found was equivalent to 5.41 nm. This structural dimension of the lamellar phase is in agreement with data reported in previous studies for anionic liposomes composed of DOPE, oleic acid, and cholesterol[22,24] as well as for liposomes made of DOPE and CHEMS.[23]

SAXS peaks were also observed at q = 1.37, 2.48, 2.86, and 3.59 nm^{-1}, with periodicity of Bragg reflections equal to 1, $\sqrt{3}$, 2, and $\sqrt{7}$, indicating the existence of a hexagonal phase of DOPE with the lattice parameter equivalent to 4.58 nm. This structural dimension of the hexagonal phase is also in agreement with data reported previously for liposomes composed of DOPE and CHEMS.[23]

SAXS patterns at −20 °C showed peaks with similar periodicity of Bragg reflections to those observed at −30 °C,

dx.doi.org/10.1021/la502977j | Langmuir 2014, 30, 15083−15090

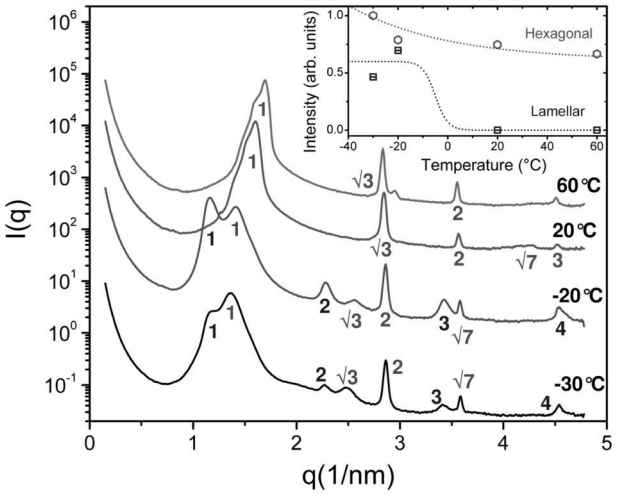

Figure 4. SAXS patterns of the sample DOPE/CHEMS/PBS at different temperatures. The indexes represent the periodicity of the Bragg reflections. Blue indexes are related to lamellar phases, while red indexes are related to hexagonal phases. The inset shows the normalized integrated intensity of the first-order SAXS peak of each phase. Notice the coexistence of the hexagonal phase over the whole temperature range.

indicating the existence of both lamellar and hexagonal phases of DOPE. Thus, the CHEMS crystallization (exothermic DSC peak at −23 °C) does not seem to compromise the integrity of the lipid bilayer, which maintains its lamellar organization. The coexistence of lamellar and hexagonal phases may be the result of a heterogeneous distribution of CHEMS molecules between the DOPE molecules in the lipid bilayer. The absence of CHEMS among DOPE molecules, in some regions, could allow for DOPE molecules to be brought close to each other, thus favoring hexagonal phase formation.[23]

At 20 °C, SAXS peaks were identified at q = 1.59, 2.84, 3.56, 4.29, and 4.52 nm^{-1}, with periodicity of the Bragg reflections nearly equal to 1, $\sqrt{3}$, 2, $\sqrt{7}$, and 3, indicating the presence of a hexagonal phase of DOPE molecules with lattice parameter equivalent to 3.95 nm. This result indicates the occurrence of the lamellar to hexagonal phase transition at 12 °C. The increase of the temperature of the lamellar to hexagonal phase transition of DOPE is explained by the appearance of electrostatic repulsions between the carboxylic groups of CHEMS and the phosphate groups of DOPE. This fact prevents the formation of phosphate−ammonium hydrogen bonds between DOPE molecules, which are responsible for their tendency to adopt the inverted hexagonal phase.[21,25]

SAXS patterns obtained at 60 °C presented peaks at q = 1.70, 2.84, and 3.56 nm^{-1}, with periodicity of the Bragg reflections nearly equal to 1, $\sqrt{3}$, and 2, indicating also the presence of the hexagonal phase of DOPE molecules with lattice parameter equivalent to 3.70 nm. The endotherm observed at 34 °C was attributed to the CHEMS melting. DSC analysis of pure CHEMS showed an endotherm at 50 °C (inset of Figure 3). The shift of the melting DSC peak of CHEMS toward a lower temperature is explained by the presence of other components (DOPE and PBS). DSC analysis of pure CHEMS showed also another endothermic peak at 8 °C, which could not be assigned.

3.3. DOPE/CHEMS/DSPE−PEG_{2000}/PBS Mixtures. The thermal behavior of the DOPE/CHEMS/DSPE−PEG_{2000}/PBS sample is presented in Figure 5. DSC peaks can be observed centered at −23, 0, 13, 36, and 42 °C. The exothermic DSC peaks at −23 and 0 °C can be attributed to CHEMS crystallization, as mentioned before.

SAXS patterns of DOPE/CHEMS/DSPE−PEG_{2000}/PBS are presented in Figure 6. At −25 °C, SAXS peaks were identified at q = 1.15, 2.27, 3.43, and 4.56 nm^{-1}, with periodicity of the Bragg reflections equal to 1, 2, 3, and 4, which characterizes the presence of the lamellar phase composed of DOPE molecules

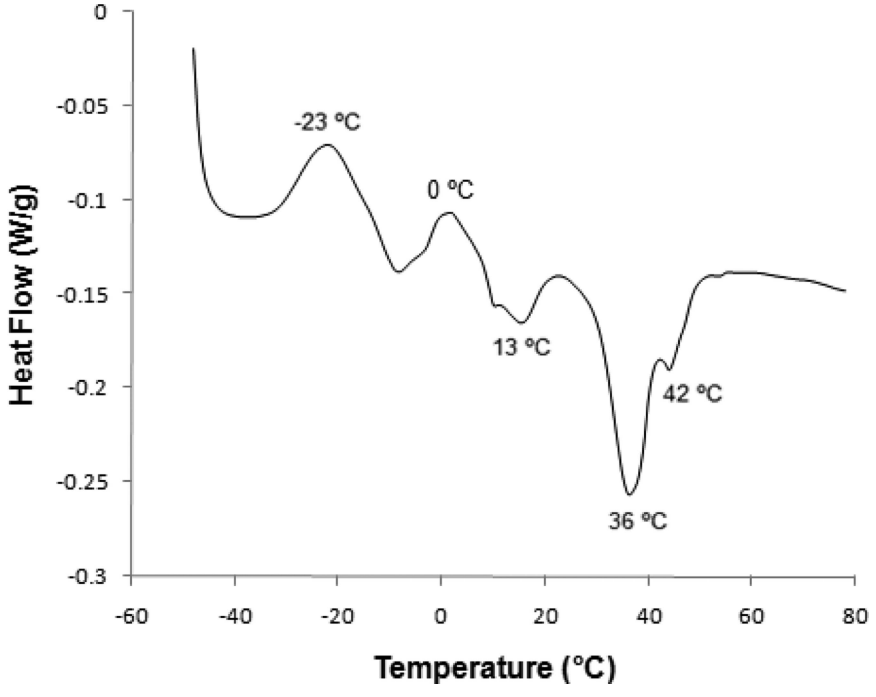

Figure 5. Thermal phase behavior of the DOPE/CHEMS/DSPE−PEG_{2000}/PBS sample.

dx.doi.org/10.1021/la502977j | *Langmuir* 2014, 30, 15083−15090

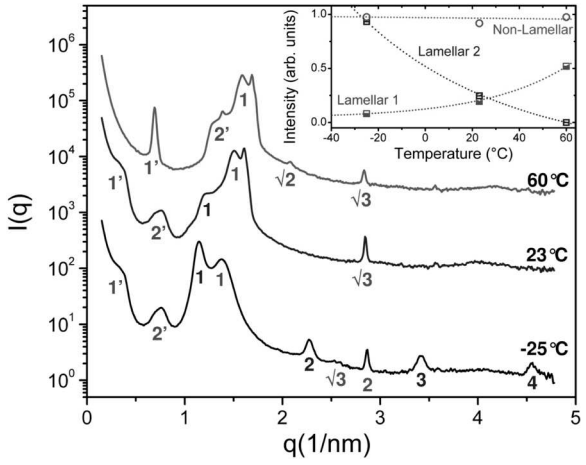

Figure 6. SAXS patterns of the sample DOPE/CHEMS/DSPE–PEG_{2000}/PBS at different temperatures. The indexes represent the periodicity of the Bragg reflections. Blue and green indexes are related to lamellar phases, while red indexes are related to non-lamellar phases. The inset shows the normalized integrated intensity of the first-order SAXS peak of each phase. The non-lamellar phase is present over the whole temperature range.

as the main structural lipid. The lattice parameter found was equivalent to 5.46 nm.

SAXS peaks related to a second lamellar system were observed with q values equal to 0.37 and 0.76 nm^{-1} (periodicity of Bragg reflections equal to 1′ and 2′) with lattice parameter equivalent to 16.9 nm. The increased thickness of the lipid bilayer (not observed in previous samples) might be associated with the presence of DSPE–PEG_{2000} molecules. The insertion of PEG derivatives has been shown to increase the bilayer thickness, which reached 15 nm depending upon the PEG conformation.[26,27] The observation of two lamellar domains may be the result of a heterogeneous distribution of DSPE–PEG_{2000} molecules located along the lipid bilayer. Diffraction patterns at −25 °C also showed periodicity of Bragg reflections equal to 1, $\sqrt{3}$, and 2, indicating the presence of non-lamellar domains at this temperature.

At 23 °C, the SAXS peaks associated with the main lamellar system (1, 2, 3, and 4) were not observed. However, the SAXS peaks related to the second lamellar system (1′ and 2′) remained present, which can be associated with the phase transitions in regions of the lipid bilayer with higher amounts of DSPE–PEG_{2000} molecules. SAXS peaks were also identified at q = 1.61 and 2.84 nm^{-1}, with periodicity of the Bragg reflections equal to 1 and $\sqrt{3}$, showing the presence of a non-lamellar phase of DOPE molecules with a lattice parameter equivalent to 3.9 nm. This result suggests the occurrence of a lamellar to non-lamellar phase transition at 13 °C. The endotherm related to the CHEMS melting was also observed at 36 °C.

SAXS patterns obtained at 60 °C presented peaks at q = 1.69, 2.08, and 2.83 nm^{-1}, with periodicity of Bragg reflections nearly equal to 1, $\sqrt{2}$, and $\sqrt{3}$ and lattice parameter equivalent to 3.7 nm, revealing the presence of a cubic phase of DOPE molecules (space group $Pn3m$).[18,19]

At 60 °C, the shift of the SAXS peaks to higher q values (0.69 and 1.38 nm^{-1}) was also observed, with periodicity of the Bragg reflections equal to 1′ and 2′ and lattice parameter equivalent to 9.1 nm. This result can be explained by the melting of DSPE–PEG_{2000} chains, leading to an increase of the bilayer fluidity. Thus, the DSC peak at 42 °C can be attributed to this melting of DSPE–PEG_{2000} molecules.

3.4. DOPE/CHEMS/DSPE–PEG_{2000}/UA/PBS Mixtures. Finally, the effect of UA on the thermal behavior of a DOPE/CHEMS/DSPE–PEG_{2000}/PBS system was investigated. DSC peaks centered at −20, 0, 15, 36, and 43 °C could be observed. The exothermic DSC peaks at −20 and 0 °C can be attributed to the crystallization of CHEMS molecules, as mentioned before (Figure 7).

SAXS patterns of the DOPE/CHEMS/DSPE–PEG_{2000}/UA/PBS sample are presented in Figure 8. At −20 °C, DSC peaks

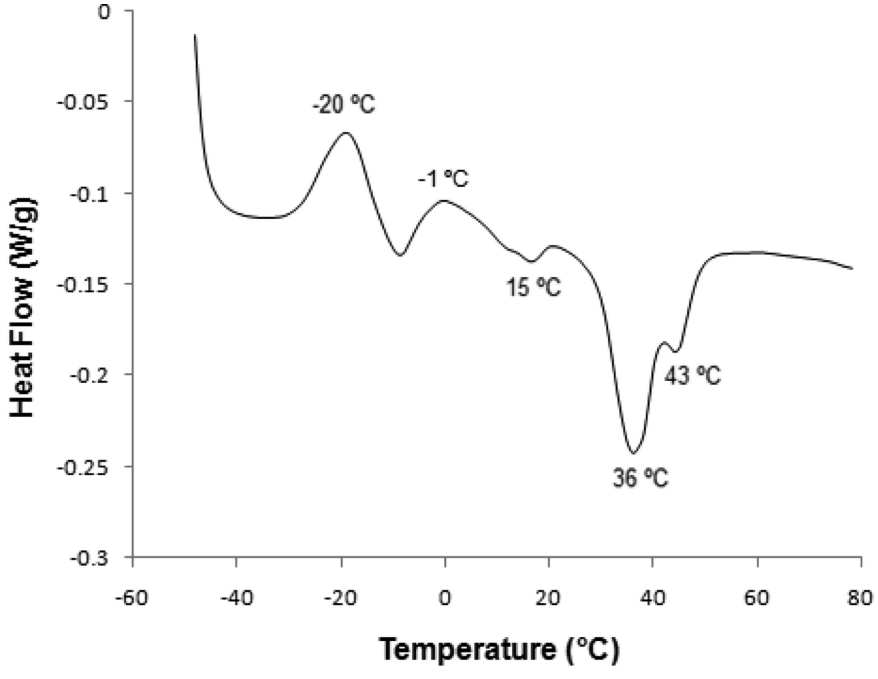

Figure 7. Thermal phase behavior of the DOPE/CHEMS/DSPE–PEG_{2000}/ UA/PBS sample.

dx.doi.org/10.1021/la502977j | *Langmuir* 2014, 30, 15083−15090

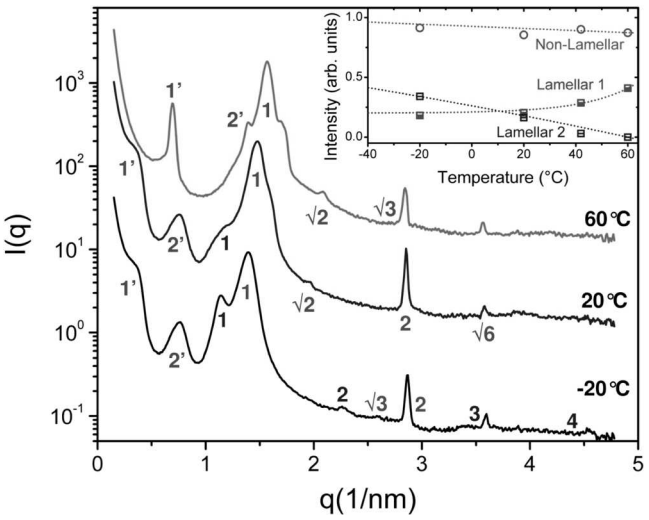

Figure 8. SAXS patterns of the sample DOPE/CHEMS/DSPE–PEG_{2000}/UA/PBS at different temperatures. The indexes represent the periodicity of the Bragg reflections. Blue and green indexes are related to lamellar phases, while red indexes are related to non-lamellar phases. The inset shows the normalized integrated intensity of the first-order SAXS peak of each phase. Again, the non-lamellar phase is present over the whole temperature range.

were identified at q = 1.14, 2.26, 3.59, and 4.52 nm^{-1}, with periodicity of the Bragg reflections equal to 1, 2, 3, and 4, which characterizes the presence of the lamellar phase of DOPE molecules with lattice parameter equivalent to 5.51 nm. SAXS peaks related to a second lamellar system were also observed at q = 0.38 and 0.77 nm^{-1}, with periodicity of Bragg reflections equal to 1′ and 2′ and lattice parameter equivalent to 16.5 nm. The observation of two lamellar domains may be the result of a heterogeneous distribution of DSPE–PEG_{2000} molecules located along the lipid bilayer, as previously mentioned. At −20 °C, SAXS peaks were observed at q = 1.42, 2.55, and 2.87 nm^{-1}, with periodicity of Bragg reflections equal to 1, $\sqrt{3}$, and 2 and lattice parameter equivalent to 4.42 nm, indicating the presence of non-lamellar domains at this temperature. As noted before, the coexistence of lamellar and hexagonal phases at this temperature might be associated with regions with lower amounts of CHEMS molecules.

At 20 °C, the SAXS peaks associated with the lamellar system (1, 2, 3, and 4) were not observed but the SAXS peaks related to the second lamellar system (1′ and 2′) were still present. SAXS peaks were also identified at q = 1.47, 1.96, 2.84, and 3.58 nm^{-1}, with periodicity of the Bragg reflections equal to 1, $\sqrt{2}$, 2, and $\sqrt{6}$ and lattice parameter equivalent to 4.27 nm, indicating the presence of a cubic phase of DOPE molecules (space group $Im3m$). In this bicontinuous cubic phase, the networks are constructed by joining bilayer units 6 × 6 along orthogonal axes.[28−30] This result indicates the occurrence of lamellar to non-lamellar phase transition at 15 °C. As observed in the previous sample, the melting of CHEMS molecules was also observed at 36 °C.

SAXS patterns obtained at 60 °C presented peaks at q = 1.57, 2.08, and 2.84 nm^{-1}, with periodicity of the Bragg reflections equal to 1, $\sqrt{2}$, and $\sqrt{3}$ and lattice parameter equivalent to 4.0 nm, indicating the presence of a cubic phase of DOPE molecules (space group $Pn3m$), where the bilayer units are joined tetrahedrally to form the water labyrinths.[28,29] It is interesting to note that the presence of UA contributed to the appearance of cubic phases of molecules of DOPE.

As observed with previous samples, at 60 °C, the SAXS peaks related to the second lamellar system (1′ and 2′) shifted to higher q values, equal to 0.69 and 1.39 nm^{-1}, with lattice parameter equivalent to 9.1 nm. This result can be explained by the melting of DSPE–PEG_{2000} chains, leading to an increase in the bilayer fluidity. Thus, the DSC peak at 43 °C can be attributed to this melting.

The results described before evidenced the effects related to the existence of interactions between UA and the lipids forming the long-circulating and pH-sensitive liposomes. SAXS patterns of samples containing UA (Figure 8) were different from those obtained for samples without UA (Figure 6) at all temperatures evaluated. These findings suggest that UA, a lipophilic drug (log P = 7.92),[31] could interact with the lipids, change their self-assembly, and consequently, alter the phase behavior of DOPE molecules.

Considering the lipophilic structure of UA, we can suggest the occurrence of hydrophobic interactions predominantly between the hydrophobic rings of UA and the fatty acyl chains of the lipids in the bilayer. The occurrence of electrostatic interactions between the carboxylic group of UA molecules and amino group of DOPE molecules is also possible (Figure 9). These kinds of interactions may play a crucial role for

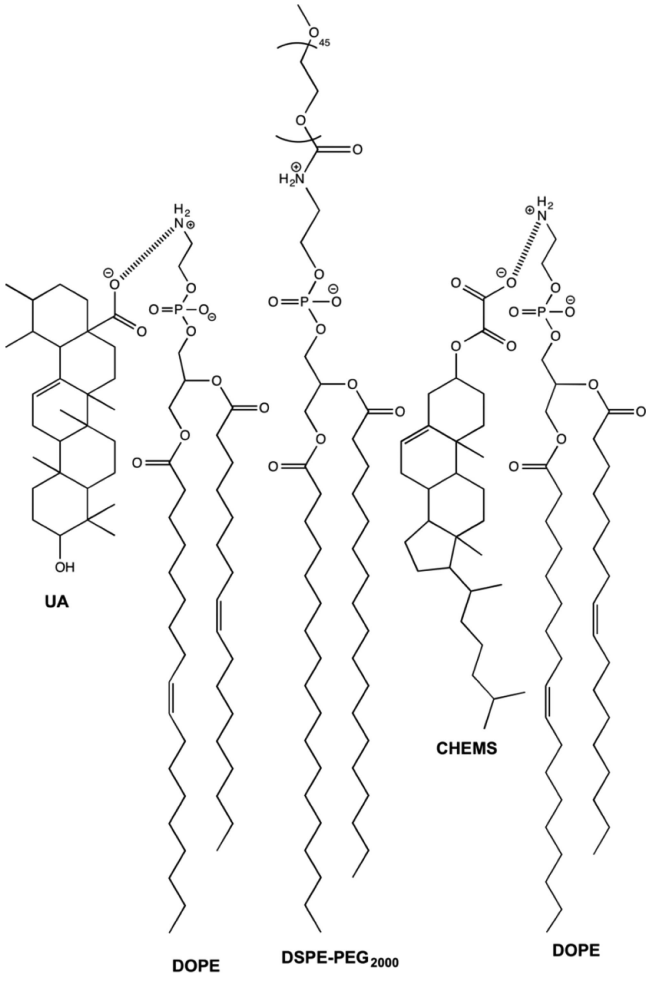

Figure 9. Schematic representation of interactions between UA and DOPE molecules in the lipid bilayer.

dx.doi.org/10.1021/la502977j | Langmuir 2014, 30, 15083−15090

controlling the lipid organization and, thus, for determining the phase behavior of DOPE molecules. However, it is important to note that the lamellar to non-lamellar phase transitions of DOPE were not prevented by these interactions.

It has also been demonstrated that the curvature of the lipid headgroup surfaces has an impact on their self-assembly. The inverted cubic phases (Q_{II}) have negative mean curvatures and are found to occur between the L_α and H_{II} regions in phase diagrams. The phase behavior appears not to depend upon molecular specifics but rather a collection of interactions that determine the preferred curvature of the system.[29,32] In this context, the different patterns of DOPE phase organization in the presence of UA molecules (Figure 8) may be associated with the specific interactions between UA and DOPE molecules, leading to a characteristic curvature associated with a structural organization of cubic type. Funari and co-workers[33] found similar results when investigating the interactions between two lipid-soluble hydroquinones with lipid model membranes composed of 1-palmitoyl-2-oleoyl-*sn*-glycero-3-phosphoethanolamine (POPE). They observed that only the more hydrophobic hydroquinone induced the formation of cubic phases (space groups $P_4 32$ and $Im3m$). It was suggested that the number of alkylthio chains attached to the ring on the hydroquinone, imbedded on the lipid matrix, presented a dramatic effect on the formation of these two cubic phases. Concerning interactions between UA and DOPE molecules, discussed previously, we can suggest that the anchoring of the hydrophobic tail of UA molecules into the SpHL−UA lipid matrix plays an essential role in the formation of the different cubic phases ($Im3m$ and $Pn3m$). The formation of cubic phases may be involved in processes of membrane fusion. The L_α−Q_{II} phase transition occurs via inverted micellar intermediates. These intermediates can merge with the outer monolayers to form interlamellar attachments, which are precursors of cubic phases.[25,34−36] In this context, it can be suggested that the tendency of the components of SpHL−UA to organize themselves in non-lamellar phases as in the cubic phases (Q_{II}) can favor the membrane fusion via that transient interlamellar attachment. This process should occur when the liposomal membrane merges with the endosomal membrane to release UA from SpHL−UA to the cytoplasm.

Regardless of our findings demonstrating that UA can interact with the lipids changing their self-assembly and, consequently, altering the phase behavior of DOPE molecules, these interactions were unable to eliminate the lamellar to non-lamellar phase transition of DOPE. This phase transition is essential for membrane fusion and cytoplasmic delivery of UA molecules from SpHL−UA.[21,23,24]

4. CONCLUSION

The incorporation of UA in pH-sensitive and long-circulating liposomes (SpHL) provides a promising strategy to deliver this substance and allow for its intravenous administration. However, to guarantee the efficiency of this system, the understanding of the structural organization of lipids after UA incorporation in SpHL is essential. Thus, in the present study, the interactions of UA with the SpHL components were evaluated to clarify their influence over self-assembly of lipids. DSC and SAXS findings demonstrated that UA interacts with liposomal membrane lipids and changes their self-assembly, resulting in the formation of the cubic phases $Im3m$ and $Pn3m$ at 20 and 60 °C, respectively. Nevertheless, these interactions between the lipids and UA do not interfere with the lamellar to non-lamellar phase transition of DOPE, which plays a crucial role for the cytoplasmic delivery of UA molecules from SpHL−UA. Owing to these results, studies in fully hydrated systems are currently in progress in our laboratory to clarify the behavior of SpHL−UA in the biological medium.

AUTHOR INFORMATION

Corresponding Author

*E-mail: itabra2001@yahoo.com.br and/or monicacristina@ufmg.br.

Notes

The authors declare no competing financial interest.

ACKNOWLEDGMENTS

The authors thank Dr. Mateus Borba Cardoso and his staff for their competence and support during the measurements at LNLS (Campinas, Brazil). The authors thank Fundação de Amparo à Pesquisa do Estado de Minas Gerais (FAPEMIG) for the financial support. The authors also thank Fundação Coordenação de Aperfeiçoamento de Pessoal de Nível Superior (CAPES), Brazil, for supporting Sávia Caldeira de Araújo Lopes with a scholarship.

REFERENCES

(1) Tapajos, E. C. C.; Longo, J. P.; Simioni, A. R.; Lacava, Z. G. M.; Santos, M. F. M. A.; Morais, P. C.; Tedesco, A. C.; Azevedo, R. B. In vitro photodynamic therapy on human oral keratinocytes using choloroaluminum-phtalocyanine. *Oral Oncol.* **2008**, *44*, 1073−1079.

(2) Lopes, S. C. A.; Novais, M. V. M.; Teixeira, C. S.; Honorato-Sampaio, K.; Pereira, M. T.; Ferreira, L. A. M.; Braga, F. C.; Oliveira, M. C. Preparation, physicochemical characterization, and cell viability evaluation of long-circulating and pH-sensitive liposomes containing ursolic acid. *BioMed Res. Int.* **2013**, *2013*, 1−7.

(3) Primo, F. L.; Michieleto, L.; Rodrigues, M. A. M.; Macaroff, P. P.; Morais, P. C.; Lacava, Z. G. M.; Bentley, M. V. L. B.; Tedesco, A. C. Magnetic nanoemulsions as drug delivery systems for Foscan: Skin permeation and retention *in vitro* assays for topical application in photodynamic therapy (PDT) of skin cancer. *J. Magn. Magn. Mater.* **2007**, *311*, 354−357.

(4) Estevanato, L. L. C.; Da Silva, J. R.; Falqueiro, A. M.; Mosinlewicz-Szablewska, E.; Suchocki, P.; Tedesco, A. C.; Morais, P. C.; Lacava, Z. G. M. C. Co-nanoencapsulation of magnetic nanoparticles and selol for breast tumor treatment: In vitro evaluation of cytotoxicity and magnetohyperthermia efficacy. *Int. J. Nanomed.* **2012**, *7*, 5287−5299.

(5) Mussi, S. V.; Carvalho, R. S.; Oliveira, M. C.; Lucci, C. M.; Azevedo, R. B.; Ferreira, L. A. M. New approach to improve encapsulation and antitumor activity of doxorubicin loaded in solid lipid nanoparticles. *Eur. J. Pharm. Sci.* **2012**, *48*, 282−290.

(6) Leite, E. A.; Souza, C. M.; Carvalho-Júnior, A. D.; Coelho, L. G. V.; Lana, A. M. Q.; Cassali, G. D.; De Oliveira, M. C. Encapsulation of cisplatin in long-circulating and pH-sensitive liposomes improves its antitumor effect and reduces acute toxicity. *Int. J. Nanomed.* **2012**, *7*, 5259−5269.

(7) Li, Q.; Tian, Y.; Li, D.; Sun, J.; Shi, D.; Fang, L.; Gao, Y.; Liu, H. The effect of lipocisplatin on cisplatin efficacy and nephrotoxicity in malignant breast cancer treatment. *Biomaterials* **2014**, *35*, 6462−6472.

(8) Wang, Z.; Yu, Y.; Dai, W.; Lu, J.; Cui, J.; Wu, H.; Yuan, L.; Zhang, H.; Wang, X.; Wang, J.; Zhang, X.; Zhang, Q. The use of tumor metastasis targeting peptide to deliver doxorubicin-containing liposomes to highly metastatic cancer. *Biomaterials* **2012**, *33*, 8451−8460.

(9) Biswas, S.; Dodwadkar, N. S.; Deshpande, P. P.; Parab, S.; Torchilin, V. P. Surface functionalization of doxorubicin-loaded liposomes with octa-arginine for enhanced anticancer activity. *Eur. J. Pharm. Biopharm.* **2013**, *84*, 517−525.

(10) Zhou, J.; Zhao, W.-Y.; Ma, X.; Ju, R.-J.; Li, X.-Y.; Li, N.; Sun, M.-G.; Shi, J.-F.; Zhang, C.-X.; Lu, W.-L. The anticancer efficacy of paclitaxel liposomes modified with mitochondrial targeting conjugate in resistant lung cancer. *Biomaterials* **2013**, *34*, 3626−3638.
(11) Liu, Y.; Ran, R.; Chen, J.; Kuang, Q.; Tang, J.; Mei, L.; Zhang, Q.; Gao, H.; Zhang, Z.; He, Q. Paclitaxel loaded liposomes decorated with a multifunctional tandem peptide for glioma targeting. *Biomaterials* **2014**, *35*, 4835−4847.
(12) Kim, K. H.; Seo, H. S.; Choi, H. S.; Choi, I.; Shin, Y. C.; Ko, S.-G. Induction of apoptotic cell death by ursolic acid through mitocondrial death pathway and extrinsic death receptor pathway in MDA-MB-231 cells. *Arch. Pharmacal Res.* **2011**, *34*, 1363−1372.
(13) Wang, X.; Zhang, F.; Yang, L.; Mei, Y.; Long, H.; Zhang, X.; Zhang, J.; Qimuge-Suyila; Su, X. Ursolic acid inhibits proliferation and induces apoptosis of cancer cells *in vitro* and *in vivo*. *J. Biomed. Biotechnol.* **2011**, *2011*, 1−8.
(14) Zhang, H.; Li, X.; Ding, J.; Xu, H.; Dai, X.; Hou, Z.; Zhang, K.; Sun, K.; Sun, W. Delivery of ursolic acid (UA) in polymeric nanoparticles effectively promotes the apoptosis of gastric cancer cells through enhanced inhibition of cyclooxygenase 2 (COX-2). *Int. J. Pharm.* **2013**, *441*, 261−268.
(15) Shanmugam, M. K.; Rajendran, P.; Li, F.; Nema, T.; Vali, S.; Abbasi, T.; Kapoor, S.; Sharma, A.; Kumar, A. P.; Ho, P. C.; Hui, K. M.; Sethi, G. Ursolic acid inhibits multiple cell survival pathways leading to suppression of growth of prostate cancer xenograft in nude mice. *J. Mol. Med.* **2011**, *89*, 713−727.
(16) Shanmugam, M. K.; Dai, X.; Kumar, A. P.; Tan, B. K. H.; Sethi, G.; Bishayee, A. Ursolic acid in cancer prevention and treatment: Molecular targets, pharmacokinetics and clinical studies. *Biochem. Pharmacol.* **2013**, *85*, 1579−1587.
(17) Liu, J. Oleanolic acid and ursolic acid: Research perspectives. *J. Ethnopharmacol.* **2005**, *100*, 92−94.
(18) Tian, Z.; Lin, G.; Zheng, R. X.; Huang, F.; Yang, M. S.; Xiao, P. G. Anti-hepatoma activity and mechanism of ursolic acid and its derivatives isolated from *Aralia decaisneana*. *World J. Gastroenterol.* **2006**, *12*, 874−879.
(19) Gao, D.; Tang, S.; Tong, Q. Oleanolic acid liposomes with polyethylene glycol modification: Promising antitumor drug delivery. *Int. J. Nanomed.* **2012**, *7*, 3517−3526.
(20) Junior, A. D. C.; Mota, L. G.; Nunan, E. A.; Wainstein, A. J.; Wainstein, A. P.; Leal, A. S.; Cardoso, V. N.; De Oliveira, M. C. Tissue distribution evaluation of stealth pH-sensitive liposomal cisplatin versus free cisplatin in Ehrlich tumor-bearing mice. *Life Sci.* **2007**, *80*, 659−664.
(21) Ferreira, D. S.; Lopes, S. C. A.; Franco, M. S.; Oliveira, M. C. pH-sensitive liposomes for drug delivery in cancer treatment. *Ther. Delivery* **2013**, *4* (9), 1−24.
(22) De Oliveira, M. C.; Fattal, E.; Couvreur, P.; Lesieur, P.; Bourgaux, C.; Ollivon, M.; Dubernet, C. pH-sensitive liposomes as a carrier for oligonucleotides: A physico-chemical study of the interaction between DOPE and a 15-mer oligonucleotide in quasi-anhydrous samples. *Biochim. Biophys. Acta* **1998**, *1372*, 301−310.
(23) Silva, S. M. L; Coelho, L.; Malachias, A.; Perez, C. A.; Pesquero, J. L.; Paniago, R. M.; De Oliveira, M. C. Study of the structural organization of cyclodextrin−DNA complex loaded anionic and pH-sensitive liposomes. *Chem. Phys. Lett.* **2011**, *506*, 66−70.
(24) De Oliveira, M. C.; Rosilio, V.; Lesieur, P.; Bourgaux, C.; Couvreur, P.; Ollivon, M.; Dubernet, C. pH-sensitive liposomes as a carrier for oligonucleotides: A physico-chemical study of the interaction between DOPE and a 15-mer oligonucleotide in excess water. *Biophys. Chem.* **2000**, *87*, 127−137.
(25) Seddon, J. M. Structure of the inverted hexagonal (H_{II}) phase, and non-lamellar phase transitions of lipids. *Biochim. Biophys. Acta* **1990**, *1031*, 1−69.
(26) Garbuzenko, O.; Barenholz, Y.; Priev, A. Effect of grafted PEG on liposome size and on compressibility and packing of lipid bilayer. *Chem. Phys. Lipids* **2005**, *135*, 117−129.
(27) Varga, Z.; Wacha, A.; Vainio, U.; Gummel, J.; Bóta, A. Characterization of the PEG layer of sterically stabilized liposomes: A SAXS study. *Chem. Phys. Lipids* **2012**, *165*, 387−392.
(28) Lindblom, G.; Rilfors, L. Cubic phases and isotropic structures formed by membrane lipids—Possible biological relevance. *Biochim. Biophys. Acta* **1989**, *288*, 221−256.
(29) Tate, M. W.; Eikenberry, D. C.; Turner, D. C.; Shyamsunder, E.; Gruner, S. M. Nonbilayer phases of membrane lipids. *Chem. Phys. Lipids* **1991**, *57*, 147−164.
(30) Zeng, X.; Cseh, L.; Mehl, G. H.; Ungar, G. Testing the triple network structure of the cubic $Im\bar{3}m$ (I) phase by isomorphous replacement and model refinement. *J. Mater. Chem.* **2008**, *18*, 2953−2961.
(31) Ramos, A. A.; Lima, C. F.; Pereira, M. L.; Fernandes-Ferreira, M.; Pereira-Wilson, C. Antigenotoxic effects of quercetin, rutin and ursolic acid on HepG2 cells: Evaluation by the comet assay. *Toxicol. Lett.* **2008**, *177*, 66−73.
(32) Guner, S. M.; Cullis, P. R.; Hope, M. J.; Tilcock, C. P. S. Lipid polymorphism: The molecular basis of nonbilayer phases. *Annu. Rev. Biophys. Biophys. Chem.* **1985**, *14*, 211−238.
(33) Funari, S. S.; Rebbin, V.; Marzorati, L.; Di Vitta, C. Membrane morphology modifications induced by hydroquinones. *Langmuir* **2011**, *27*, 8257−8262.
(34) Siegel, D. P. Inverted micellar structures in bilayer membranes: Formation rates and half-lives. *Biophys. J.* **1984**, *45*, 399−420.
(35) Siegel, D. P. Inverted micellar intermediates and the transitions between lamellar, cubic, and inverted hexagonal lipid phases—II. Implications for membrane−membrane interactions and membrane fusion. *Biophys. J.* **1986**, *49*, 1171−1183.
(36) Marsh, D. General features of phospholipids phase transitions. *Chem. Phys. Lipids* **1991**, *57*, 109−120.

ELSEVIER

Journal of Controlled Release 80 (2002) 309–319

journal of controlled release

www.elsevier.com/locate/jconrel

GENE DELIVERY

Efficient intracellular drug and gene delivery using folate receptor-targeted pH-sensitive liposomes composed of cationic/anionic lipid combinations

Guangfeng Shi, Wenjin Guo, Stacy M. Stephenson, Robert J. Lee*

Division of Pharmaceutics and Pharmaceutical Chemistry, College of Pharmacy, The Ohio State University, Rm 542 LM Parks Hall, 500 W. 12th Ave., Columbus, OH 43210, USA

Received 28 November 2001; accepted 9 January 2002

Abstract

pH-sensitive liposomes are designed to promote efficient release of entrapped agents in response to low pH. In this study, novel pH-sensitive liposomes consisting of cationic/anionic lipid combinations are evaluated for intracellular drug and gene delivery. First, liposomes composed of egg phosphatidylcholine, dimethyldioctadecylammonium bromide (DDAB), cholesteryl hemisuccinate (CHEMS), and Tween-80 (25:25:49:1, mol/mol) were shown to stably entrap calcein at pH 7.4 and undergo rapid content release and irreversible aggregation under acidic pH. Compared to pH-sensitive liposomes incorporating dioleoylphosphatidylethanolamine, these liposomes showed improved retention of pH-sensitivity in the presence of serum. The folate receptor (FR), which is amplified in a wide variety of human tumors, could be targeted by incorporating 0.1 mol% folate-polyethyleneglycol-phosphatidylethanolamine (f-PEG-PE) into liposomes. f-PEG-PE has been shown to facilitate FR-mediated endocytosis of liposomes into KB human oral cancer cells, which express amplified FR. FR-targeted pH-sensitive liposomes produced increased cytosolic release of entrapped calcein, as shown by fluorescence microscopy, and enhanced cytotoxicity of entrapped cytosine-β-D-arabinofuranoside, as shown by an 11-fold reduction in the IC_{50} in KB cells, compared to FR-targeted non-pH-sensitive liposomes. Furthermore, FR-targeted pH-sensitive liposomes composed of DDAB/CHEMS/f-PEG-PE, combined with polylysine-condensed plasmid DNA, were shown to mediate FR-specific delivery of a luciferase reporter gene into KB cells in the presence of 10% serum. These findings suggest that cationic lipid-containing pH-sensitive liposomes, combined with FR targeting, are effective vehicles for intracellular drug and gene delivery.

Keywords: pH-sensitive liposomes; Folate receptor; Drug targeting; Cytosine-β-D-arabinofuranoside; Gene therapy

1. Introduction

Liposomes are phospholipid bilayer vesicles with potential application in drug and gene delivery. Cellular uptake of liposomes generally follows an endocytic pathway. pH-sensitive liposomes are designed to undergo rapid destabilization in acidic environments like those found in endocytic vesicles [1]. These liposomes are typically composed of a neutral cone-shaped lipid dioleoylphosphatidyl-

*Corresponding author. Tel.: +1-614-292-4172; fax: +1-614-292-7766.

E-mail address: lee.1339@osu.edu (R.J. Lee).

0168-3659/02/$ – see front matter
PII: S0168-3659(02)00017-2

ethanolamine (DOPE) and a weakly acidic amphiphile, such as cholesteryl hemisuccinate (CHEMS) [2,3]. A key limitation for DOPE-based pH-sensitive liposomes is the loss of acid-induced fusogenicity in the presence of serum, possibly due to interactions between the DOPE-rich lipid bilayer and serum opsonins. Therefore, development of novel liposomal formulations that retain pH-sensitivity in the presence of serum is necessary if pH-sensitive liposomes are to be adopted in an in vivo setting.

In a step toward this goal, Hafez et al. [4] recently reported the preparation of non-DOPE-based pH-sensitive liposomes composed of combinations of cationic and anionic lipids including dioleoyldimethylammonium chloride (DODAC) combined with cholesteryl hemisuccinate (CHEMS) and 3-α-[*N*-(*N′N′*-dimethylaminoethane) carbamoyl] cholesterol (DC-Chol) combined with dioleoylphosphatidic acid (DOPA). These liposomes carried net negative charges at neutral pH and contain a titratable lipid component consisting of either a weakly acidic (anionic) or a weakly basic (cationic) amphiphile. The lipids formed a stable bilayer at neutral or basic pH. At acidic pH, where the weakly acidic or the weakly basic amphiphile within the bilayer was partially protonated, the liposomes became charge neutral and underwent rapid aggregation and membrane fusion due to the removal of electrostatic colloidal stabilization. The pH required for triggering liposomal fusion was dependent on the cationic to anionic lipid ratio and the pK_a of the titratable component (e.g. CHEMS and DC-Chol) in the liposomes [4]. Liposomes composed solely of charged lipids, however, may not be suitable for drug delivery since they do not form vesicles that are capable of stably entrapping drug molecules.

Since pH-sensitive liposomes can facilitate the cytosolic release of membrane impermeable molecules, it might be feasible to combine their use with a targeting ligand that promotes receptor-mediated endocytosis. The folate receptor (FR) is a 38-kDa glycosyl phosphatidylinositol (GPI)-anchored glycoprotein with highly restricted normal tissue distribution and amplified expression in a wide variety of human tumors including over 95% of non-mucinous ovarian carcinomas [5–7]. Liposomes incorporating a lipophilic folate derivative, such as folate-PEG-DSPE or folate-PEG-Chol, have been shown to efficiently deliver antitumor agents into FR-bearing tumor cells via receptor-mediated endocytosis [8–11]. Therefore, combining pH-sensitive formulations with FR targeting could potentially improve drug or gene delivery to tumor cells possessing amplified levels of FR.

In this report, two novel liposomal formulations were investigated with pH-sensitive formulations consisting of cationic/anionic lipid combinations and including an FR targeting ligand for pH-dependent destabilization and for drug and gene delivery efficiency in tumor cells with amplified FR expression [11]. Our findings indicate that liposomes based on cationic/anionic combinations and FR targeting are highly efficient vehicles for intracellular drug and gene delivery.

2. Materials and methods

2.1. Materials

Egg phosphatidylcholine (PC) and dioleoylphosphatidylethanolamine (DOPE) were obtained from Avanti Polar Lipids (Alabaster, AL). Poly-L-lysine (PLL, M_r ~29,000), calcein, cholesteryl hemisuccinate (CHEMS), cytosine-β-D-arabinofuranoside (araC), dimethyldioctadecylammonium bromide (DDAB), distearoylphosphatidylethanolamine (DSPE), 3-(4,5-dimethylthiazol-2-yl)-2,5-diphenyltetrazolium (MTT), folic acid dihydrate, polyoxyethylenesorbitan monooleate (Tween-80), Sepharose CL-4B resin and Triton X-100 were purchased from Sigma (St. Louis, MO). Folate-polyethyleneglycol (MW ~3,350)-distearoylphosphatidylethanolamine (f-PEG-PE) was synthesized as described previously [9]. Luciferase assay reagents were obtained from Promega (Madison, WI). Polycarbonate membranes and a handheld LiposoFast™ lipid extruder were obtained from Avestin (Ottawa, Canada). BCA protein assay reagents were purchased from Pierce Chemical (Rockford, IL). Tissue culture media were purchased from Life Technologies (Rockville, MD).

2.2. Cell culture

KB human oral carcinoma cells, which exhibit amplified FR expression, were kindly provided by Dr

Philip Low at Purdue University (West Lafayette, IN). The cells were cultured as monolayers in 75-cm^2 flasks in folate-free RPMI 1640 media supplemented with antibiotics and 10% FBS in a humidified atmosphere containing 5% CO_2 at 37 °C.

2.3. Liposome preparation

Liposomes were prepared using a previously described polycarbonate membrane extrusion method [12]. Briefly, a chloroform solution of a lipid mixture with the desired lipid composition was dried into a thin film on the wall of a glass tube under a stream of nitrogen gas. Residual chloroform was removed by vacuum desiccation for an additional 60 min. The lipids were then resuspended in a buffer solution containing the molecule of interest, such as calcein or araC, by vortexing and periodic sonication in a bath sonicator (model 50 HT, VWR Scientific Product). The lipidic suspension was then subjected to six cycles of freezing and thawing followed by ten cycles of extrusion through a 100-nm pore-size polycarbonate membrane using a handheld LiposoFast™ extruder. FR-targeted liposomes were prepared by including 0.1 mol% of f-PEG-PE in the initial lipid mixture [9]. Un-entrapped drug was separated from the liposomes by gel filtration on a 10-ml Sepharose CL-4B column equilibrated in phosphate buffered saline (PBS, 136.9 mM NaCl, 2.68 mM KCl, 8.1 mM Na_2HPO_4, 1.47 mM KH_2PO_4, pH 7.4). Drug concentration in the liposome preparations was determined by measuring absorption (at 495 nm for calcein and 273 nm for araC) of the liposomes dissolved in methanol/water (3:1, v/v) based on the molar extinction coefficient of the free drug. Liposome mean diameter and size distribution were determined by photon correlation spectroscopy using a NICOMP Particle Sizer Model 370.

2.4. Calcein dequenching assays

Liposomal formulations were evaluated for their ability to stably entrap membrane impermeable molecules by determining the percentage of liposomal calcein release of various formulations following a 2-week incubation at 4 °C or 10 min at 37 °C in the presence of 10% fetal bovine serum (FBS) determined by fluorescence dequenching, as previously described [13]. Furthermore, the liposomes were characterized for low pH-triggered calcein release using the following procedure. Freshly column-purified liposomes entrapping 80 mM calcein and containing 50 nmol of lipid were added to 2 ml PBS or sodium acetate buffer (100 mM NaCl, 10 mM Na acetate, pH 4.0, 4.5, 5.0, 5.5, 6.0 and 6.5) with or without 90% FBS in disposable cuvettes. After a 10-min incubation at 37 °C, buffer pH was adjusted to pH 7.4 and calcein fluorescence was measured before and after addition of 0.15% Triton X-100, which defines 100% calcein leakage from the liposomes. The percentage of low pH-triggered calcein release was calculated using the formula below:

$$\% \text{ low pH-triggered calcein release} = ((F_{pH} - F_{7.4})/(F_{TX} - F_{7.4}))*100\%$$

where F_{pH} is fluorescence intensity following incubation in the low pH buffer, $F_{7.4}$ is fluorescence intensity after incubation at pH 7.4 and F_{TX} is fluorescence intensity after the addition of Triton X-100.

All fluorescence measurements were performed on a Perkin Elmer LS-5B spectrofluorometer operated with FTWinlab software (Morena Valley, CA). The excitation and emission wavelengths were set at 490 and 520 nm, respectively.

2.5. pH-induced liposomal aggregation

Liposomal aggregation in response to reduced buffer pH was measured by increase in particle size. Some 40-μl samples of the liposomes containing 200 nmol of lipid were diluted in 4 ml of sodium acetate buffer of various pH values and incubated at 37 °C. At various time points, aliquots of the samples were withdrawn and the mean particle diameter was determined by photon correlation spectroscopy on a NICOMP Particle Sizer Model 370.

2.6. Uptake of calcein containing liposomes by cultured KB cells

Cellular uptake of calcein-containing liposomes was examined by fluorescence microscopy. KB cells cultured as a monolayer were harvested by a brief treatment with trypsin/EDTA. The suspended KB cells were gently pelleted by centrifugation, resus-

pended in fresh culture media at a density of 10^6 cells/ml, and aliquoted into 1.5-ml centrifuge tubes. A 1-ml aliquot of the cell suspension was incubated for 3 h at 37 °C under gentle shaking with liposomes at a final calcein concentration of 20 μM. For a competitive binding assay, 1 mM free folic acid was included in the incubation media. After the incubation, the cells were washed three times with cold PBS and examined on a Leica DMLS Epifluorescence Microscope with a fluorescein dichroic filter set and a photo attachment. The level of cellular liposomal uptake was quantified based on calcein fluorescence by flow cytometry on a Coulter Elite flow cytometer.

2.7. Cytotoxicity assay

Liposomal drug delivery was assessed by comparing the cytotoxicity of various formulations of liposomal araC and free araC in KB cells. The effect of pH-sensitivity on liposomal araC delivery efficiency was evaluated by comparing pH-sensitive and non-pH-sensitive liposomes that are targeted to the FR. Empty pH-sensitive liposomes in combination with free araC were also included as a control to investigate the possibility of inherent liposomal cytotoxicity. The cytosolic delivery of araC was evaluated in KB cells using an MTT cytotoxicity assay, as described previously [9]. For liposome preparation, 400 mM araC was used to hydrate the dried lipid mixture. Liposomes were then prepared by polycarbonate membrane extrusion as described in Section 2.3.

KB cells were seeded in 96-well plates to reach ~25% confluence at the time of the study. The cells were incubated in triplicate with serial dilutions of the various formulations of liposomal araC or free araC for 2 h at 37 °C in media containing 10% FBS. In free folate blockade studies, 1 mM folic acid was added to the incubation media. The cells were washed four times with PBS (pH 7.4), and fresh media was then added. After an additional 48 h of incubation, MTT was added and cells were incubated for 1 h at 37 °C. The cells were then dissolved in HCl acidified isopropanol, and cellular viability was determined by measuring absorption at 570 nm using an automated plate reader. The concentrations of araC leading to 50% cell kill (IC_{50}) were then derived from the concentration dependent cell viability curves.

2.8. Plasmid DNA preparation

Plasmid containing a firefly luciferase reporter gene under the cytomegalovirus promoter, pCMV-Luc, was obtained as a gift from Dr Leaf Huang at the University of Pittsburgh. The DNA was purified using the Qiagen mega kit (Qiagen, Santa Clarita, CA). Plasmid DNA was quantified by measuring UV absorbance at 260 nm and analyzed for structural integrity and percentage of supercoiled DNA by electrophoresis on a 0.9% agarose gel.

2.9. Preparation of LPDII

pH-sensitive liposomes were prepared as described in Section 2.3 using 20 mM HEPES (pH 8.0) as the buffer of hydration and lipid compositions of DDAB/CHEMS/f-PEG-PE (30:70:0.1) and DDAB/CHEMS/PEG-PE (30:70:0.1) for the targeted and the non-targeted formulation, respectively. For LPDII preparation, 3 μg plasmid DNA was diluted in 60 μl serum-free RPMI 1640 medium and vortexed with an appropriate amount of poly-L-lysine (PLL) dissolved in an equal volume of the same media. Following a 10-min incubation at room temperature, the resulting polyplexes were then mixed with the desired amount of liposomes to prepare LPDII complexes.

2.10. Transfection procedure

Gene delivery efficiency was evaluated using a plasmid construct carrying a luciferase reporter gene. Targeted and non-targeted pH-sensitive liposomes were used as components of an LPDII vector to transfect KB cells with and without the presence of serum. Again, blocking assays were performed with free folate to ascertain that differences seen in targeted liposomes were due to FR targeting. KB cells were seeded in 24-well plates 24 h prior to transfection, which allowed cells to reach 60–80% confluence at the time of transfection. Unless otherwise specified, all transfection experiments were performed in regular growth media containing 10% FBS. Cells were incubated in triplicate with vector

formulations containing 1 μg plasmid DNA in 500 μl culture media for 4 h at 37 °C. The transfection media was replaced with fresh culture media containing 10% FBS and the cells cultured for 24 h. Cells were then rinsed three times with PBS and lysed with a lysis buffer (0.5% Triton X-100, 100 mM Tris–HCl, 2 mM EDTA, pH 7.8). The lysates were centrifuged and the supernatants analyzed for protein content using a BCA protein assay and luciferase activity on a Mini-Lum luminometer (Bioscan, Washington, DC). Relative light unit (RLU) values were converted to picograms of luciferase using a standard curve generated under identical assaying conditions with a firefly luciferase standard. Luciferase activity was presented as relative light units (RLUs) calibrated by cellular lysate protein content, which was determined by the BCA protein assay.

3. Results

3.1. Effect of formulation on the stability of pH-sensitive liposomes

Several lipid compositions, incorporating combinations of cationic lipid DDAB and anionic lipid CHEMS, were evaluated for entrapment of calcein, an anionic membrane impermeable fluorescent dye. Liposomes composed of DDAB/CHEMS (33:66, all ratios are molar ratios) or PC/DDAB/CHEMS (40:20:40) were unable to retain entrapped calcein in the presence of 10% FBS, showing 38% release after a 10-min incubation at 37 °C. Tween-80, which contains a polyoxyethylene headgroup, is known to increase liposomal stability by providing a steric barrier on the surface of liposomes. We evaluated the effect of Tween-80 addition on the stability of the above pH-sensitive liposomes. Liposomes composed of PC/DDAB/CHEMS/Tween-80 (25:25:49:1) showed improved stability at neutral buffer pH, showing only 1.3% calcein release after 2-week storage at 4 °C and 4.1% calcein release after 10-min incubation at 37 °C in buffer containing 10% FBS. Therefore, this liposome formulation was further evaluated for pH-sensitivity and intracellular drug delivery.

3.2. Low pH-triggered calcein release and liposomal aggregation

Liposomes composed of PC/DDAB/CHEMS/Tween-80 (25:25:49:1) and reference control liposomes composed of DOPE/CHEMS (60:40) entrapping 80 mM calcein were evaluated for low pH-triggered calcein release. As shown in Fig. 1, both liposome formulations showed increased calcein release at low buffer pH relative to pH 7.4. However, the presence of 90% serum rendered the DOPE/CHEMS liposomes much less responsive to the lowering of the pH showing only 20–30% additional calcein release. In contrast, PC/DDAB/CHEMS/Tween-80 showed ~55% additional calcein release under the same conditions.

The above liposomes were further evaluated for pH-dependent aggregation. As shown in Fig. 2a, the mean diameter of the liposomes was greatly increased at lower buffer pH values, indicating vesicle aggregation and/or membrane fusion. The time course of liposome aggregation at pH 4.0 is shown in Fig. 2b. The observed particle size increase could not be reversed by adjusting the pH back to 7.4.

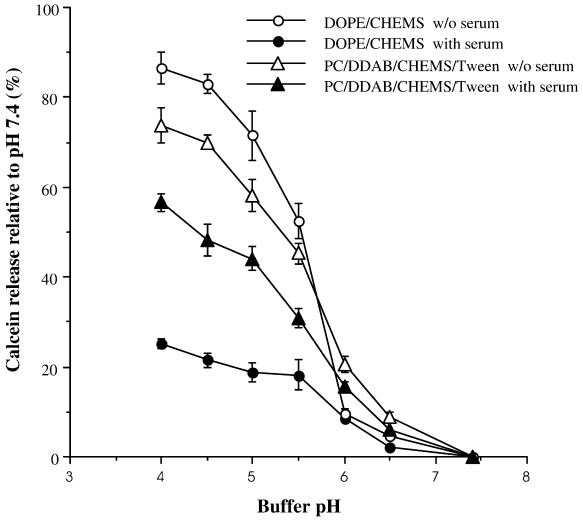

Fig. 1. Calcein release from liposomes triggered by low buffer pH. Calcein-loaded liposomes were incubated in buffers of varying pH, with or without 90% serum, for 10 min at 37 °C. The percentage of calcein dequenching was measured as described in Materials and methods.

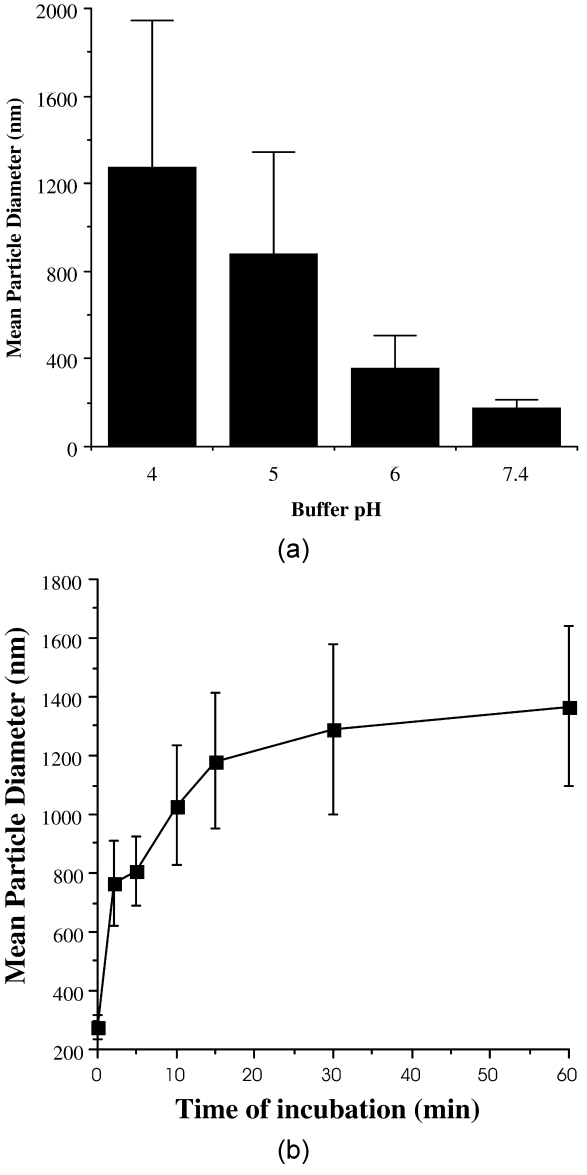

Fig. 2. Increase in liposome size in response to buffer pH. (a) The mean diameter of the liposomes following a 30-min incubation at 37 °C at various buffer pH; (b) time-dependent increase in liposome size at pH 4. The liposome composition used was PC/DDAB/CHEMS/Tween-80 (25:25:49:1); error bar represents 1 S.D.; $n=3$.

3.3. FR-targeting of pH-sensitive liposomes

Flow cytometry demonstrated, as shown in Fig. 3, that FR-targeted liposomes containing calcein had a

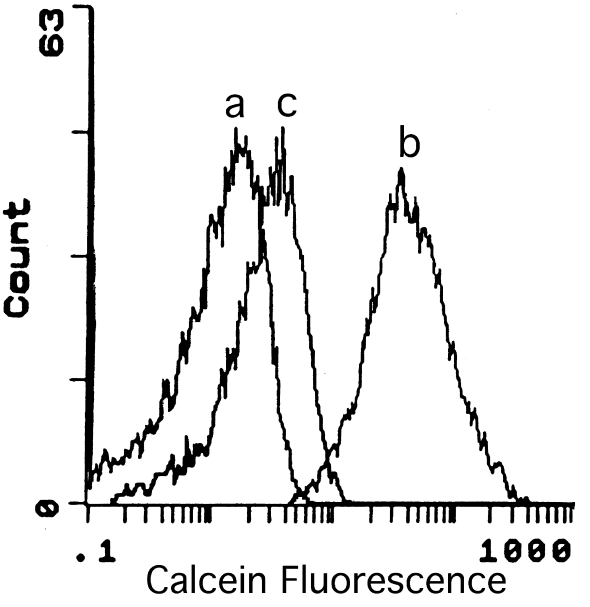

Fig. 3. FR-dependent uptake of PC/DDAB/CHEMS/Tween-80 (25:25:49:1) liposomes entrapping calcein. KB cells were incubated with 20 μM calcein entrapped in (a) non-targeted, (b) FR-targeted liposomes (containing 0.1 mol% f-PEG-PE), or (c) FR-targeted liposomes plus 1 mM free folate for 1 h at 37 °C. Cellular uptake of the liposomes was measured by flow cytometry as described in Materials and methods.

34-fold greater uptake than the non-targeted control liposomes. This increase in liposome uptake could be blocked by 1 mM free folate. Fluorescence microscopy demonstrated differing intracellular fluorescence distributions for targeted pH-sensitive and non-pH-sensitive liposomes. As shown in Fig. 4, KB cells treated with FR-targeted non-pH-sensitive liposomes, composed of PC/Chol/f-PEG-PE (60:40:0.1), had a punctate cytoplasmic distribution indicating endosomal sequestration of calcein. In contrast, cells treated with FR-targeted pH-sensitive liposomes, composed of PC/DDAB/CHEMS/Tween-80/f-PEG-PE (25:25:49:1:0.1), displayed diffuse cytoplasmic fluorescence indicating significant cytosolic release of the fluorescent dye.

3.4. Cytotoxicity of FR-targeted liposomal araC

The IC_{50} for free araC, araC entrapped in pH-sensitive liposomes, non-pH-sensitive liposomes, and free araC plus empty pH-sensitive liposomes were

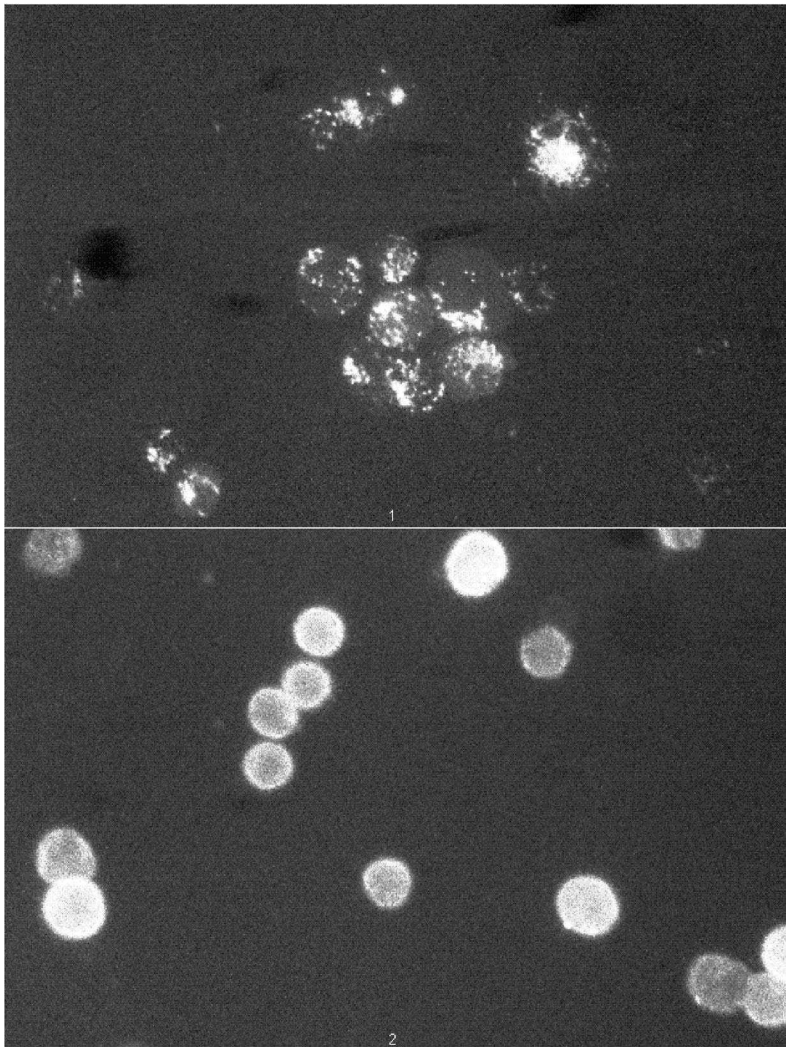

Fig. 4. Fluorescence micrograph of KB cells treated with FR-targeted calcein-containing liposomes. (Upper panel) Cells treated with FR-targeted non-pH-sensitive liposomes composed of PC/CHEMS/f-PEG-PE (60:40:0.1). (Lower panel) Cells treated with FR-targeted pH-sensitive liposomes composed of egg PC/DDAB/CHEMS/Tween-80/f-PEG-PE (25:25:49:1:0.1).

compared for cytotoxicity based on an MTT assay in KB cells. As shown in Table 1, araC showed low cytotoxicity ($IC_{50}=5{,}625$ μM) when added to the cells as a free drug. Entrapment of araC in FR-targeted non-pH-sensitive liposomes increased drug cytotoxicity ($IC_{50}=991$ μM). Delivery of araC in FR-targeted pH-sensitive liposomes enhanced cytotoxicity a further 11 times ($IC_{50}=89$ μM). In addition, the cytotoxicity of FR-targeted pH-sensitive liposomes was reduced by ~6-fold by 1 mM free folic acid, indicating FR-dependence of the observed cytotoxicity. Furthermore, the cytotoxicity was very low ($IC_{50}>10{,}000$ μM) when araC was delivered in non-targeted pH-sensitive liposomes. Finally, free araC in the presence of empty FR-targeted pH-sensitive liposomes also showed very limited cytotoxicity compared to araC entrapped in FR-targeted pH-sensitive liposomes (IC_{50} of 3,966 vs. 89 μM), indicating that efficient intracellular araC delivery required liposomal encapsulation.

Table 1
Cytotoxicity of araC formulations to KB cells determined by MTT assay

Formulation	IC_{50} (μM) ($n=3$)
AraC in FR-targeted pH-sensitive liposomes	89±17
AraC in FR-targeted pH-sensitive liposomes+1 mM folic acid	523±150
AraC in FR-targeted non-pH-sensitive liposomes	991±231
AraC in non-targeted pH-sensitive liposomes	>10,000
Free araC	5,620±1130
Free araC+FR-targeted pH-sensitive liposomes	3,970±530

3.5. FR-dependent gene delivery using targeted LPDII vectors

LPDII vectors are composed of a polycation-condensed plasmid DNA core complexed with anionic pH-sensitive liposomes via electrostatic interactions [14]. In the present study, cationic lipid containing pH-sensitive liposomes composed of DDAB/CHEMS/f-PEG-PE (30:70:0.1) were incorporated into the LPDII formulation and investigated as an FR-targeted vector for in vitro gene transfer in KB cells. LPDII vectors prepared using liposomes composed of DDAB/CHEMS/PEG-PE (30:70:0.1) were used as a non-targeted control. The liposomes exhibited acidic pH-triggered aggregation similar to that observed with above-described drug carrying liposomes (data not shown). KB cells were transfected with these vectors carrying a luciferase reporter gene. As shown in Fig. 5, the FR-targeted LPDII vectors displayed a 13-fold greater transfection activity when compared to the non-targeted LPDII vector, which could be blocked by 1 mM free folic acid. In contrast to DOPE-based LPDII vectors, which were inactivated by serum, the cationic lipid-based LPDII vectors showed excellent gene transfer activity in the presence of 10% FBS.

4. Discussion

pH-sensitive liposomes are designed to undergo rapid destabilization in acidic environments such as those inside the endosomal compartment. However, current formulations using DOPE as the fusogenic lipid lose their pH-sensitivity in the presence of serum. Hafez et al. have recently reported pH-sensitive liposome formulations composed of mixtures of cationic and anionic lipids such as DODAC and CHEMS. Lipid mixing assays with these liposomes demonstrated strong pH-dependent membrane fusion, which occurred as a result of liposomal charge neutralization in response to pH reduction [4]. In the present study, liposomes composed of cationic/anionic lipid pairs consisting of DDAB and CHEMS failed to effectively entrap molecules as demonstrated by the 38% calcein release seen after a 10-min incubation at 37 °C. Therefore, we have modified the formulation by adding PC and Tween-80 to improve liposomal stability while maintaining the basic pH-sensitive properties of the cationic/anionic lipid combination. A liposome composition of PC/DDAB/CHEMS/Tween-80 (25:25:49:1) provided optimal liposomal stability as evidenced by the minimal release after 2-week storage at 4 °C.

Both DOPE-based and cationic/anionic lipid-based liposomes exhibited similar pH-sensitive properties in the absence of serum. While serum did reduce calcein release by cationic/anionic lipid liposomes, the effect was not as pronounced as with the DOPE-based liposomes. At pH 4.0, cationic/anionic lipid-based liposome calcein release dropped from 75 to 55% with the presence of 90% FBS, while DOPE-based liposome calcein release was reduced from 85 to only 25%. Therefore, the cationic/anionic lipid-based liposomes exhibited superior 'serum-stability' compared to traditional DOPE-based pH-sensitive liposomes. Furthermore, these findings showed that pH-triggered destabilization of the cationic/anionic liposomes was also not abolished by the incorporation of moderate amounts of PC and Tween-80.

In response to acidic buffer pH, the mean particle size became progressively larger as pH decreased and could not be reduced by adjustment of pH back to 7.4. This permanent change in particle size with the decrease in pH suggests the occurrence of

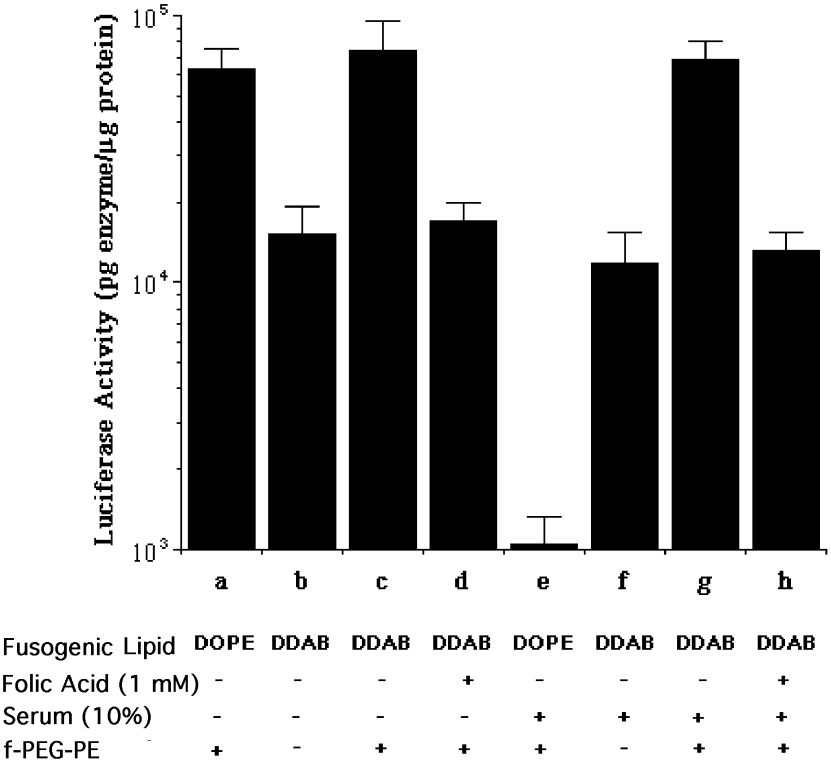

Fig. 5. Gene transfer properties of FR-targeted LPDII vectors in KB cells. KB cells were transfected with LPDII vectors carrying a luciferase reporter gene composed of a PLL/DNA (with a 1.5 to 1 weight ratio) core and pH-sensitive liposomes with the indicated composition at a lipid-to-DNA ratio of 12:1, as described in Materials and methods. a–d were carried out in serum free media; e–h were carried out in media containing 10% FBS. The liposome compositions were: a and e, DOPE/CHEMS/f-PEG-PE (60:40:0.1); b and f, DDAB/CHEMS (30:70); c, d, g, and h, DDAB/CHEMS/f-PEG-PE (30:70:0.1); d and h, transfection was performed in media containing 1 mM free folate ($n=3$).

membrane fusion. At pH 4.0, particle size increased rapidly within the first 10 min of incubation and continued to increase at a slower rate upon prolonged incubation. These trends in pH-dependent particle size were similar to those observed with the DOPE-based liposomes (data not shown).

Besides pH-induced membrane destabilization, the presence of cationic lipids in the liposome bilayer might provide a novel mechanism for increasing interaction between the liposomal and endosomal membranes, as illustrated in Fig. 6. Inside the endosome, the liposomes might display a net positive charge due to protonation of the anionic lipid CHEMS. Since the endosomal membrane presumably carries a net negative charge, the reversal of the liposomal net charge might lead to liposomal fusion with the endosomal membrane based on electrostatic interactions and release of liposomal content into the cytoplasm. Fluorescence micrographs (Fig. 4) of KB cells exposed to targeted pH-sensitive and non-pH-sensitive liposomes containing calcein provided evidence for the ability of these pH-sensitive liposomes to increase cytosolic delivery of entrapped calcein. The diffuse cytosolic fluorescence occurring in cells exposed to pH-sensitive liposomes, as opposed to the punctate fluorescence seen with non-pH-sensitive liposomes, indicated release of calcein into the cytoplasm.

Since the FR is highly amplified in a wide range of human tumors while possessing a narrow normal tissue distribution, it has been investigated as a target for the selective delivery of therapeutic compounds to tumor cells [15]. Uptake of folate-derivatized liposomes has been previously shown to proceed via

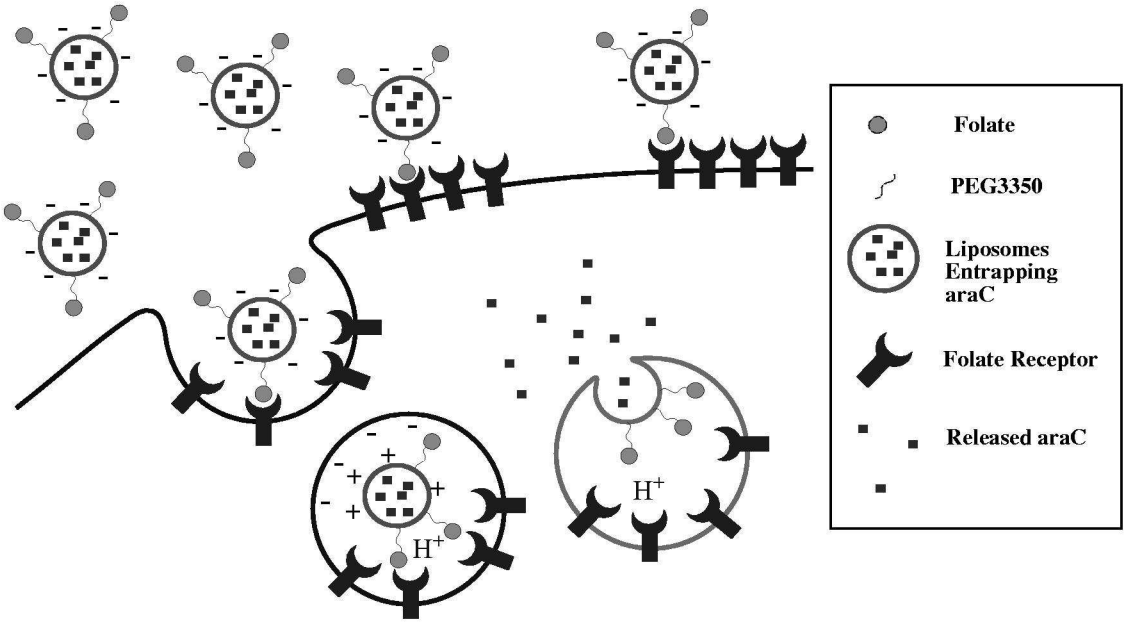

Fig. 6. Possible mechanism of intracellular araC delivery by FR-targeted cationic lipid-based pH-sensitive liposomes. At first, the folate-derivatized liposomes are taken into the cell via binding to the FRs on the plasma membrane and FR-mediated endocytosis. This is followed by acidification of the endosome, which results in protonation of the anionic lipid component and generation of a net positive surface charge on the liposomes. Finally, the electrostatic interactions between the liposomal and endosomal membranes result in bilayer fusion and the cytosolic delivery of the encapsulated araC.

receptor-mediated endocytosis in FR-bearing tumor cells [8,9]. In addition, the endosomal compartment in this delivery pathway has been shown to be highly acidified [11]. Therefore, FR-targeting of pH-sensitive liposomes could provide an ideal mechanism for cell-specific delivery of therapeutic agents that are membrane impermeable.

The cytotoxicity data clearly indicate that optimal activity of liposomal araC required both FR-targeting and pH-sensitive liposome formulation. Interestingly, araC delivered by non-targeted non-pH-sensitive liposomes showed greatly reduced cytotoxicity compared to free araC. A possible explanation is that free araC can access the cell via a nucleoside transporter, whereas liposomal encapsulation without FR-targeting adds an additional barrier to cellular uptake. The relatively high IC_{50} value of free araC might be due to the short incubation time (2 h) used, combined with the fact that araC is an S-phase specific agent. Liposomal araC is expected to have greatly extended systemic circulation time compared to free araC. It might, therefore, have the added advantage of prolonging tumor cell exposure to the drug during in vivo administration, which might lead to improved therapeutic efficacy.

In addition to drug delivery, pH-sensitive liposomes can be used with polycation-condensed DNA to construct LPDII gene transfer vectors [14]. Since fusogenicity rather than drug retention is the key for efficient gene delivery, liposomes composed of DDAB/CHEMS (30:70) were evaluated as the lipidic component for formulating LPDII vectors. Targeted pH-sensitive vectors attained similar levels of transfection to DOPE-based LPDII vectors. In contrast to DOPE-based vectors, which were completely inactivated by serum, the cationic/anionic lipid-based LPDII vectors were highly efficacious in transfecting cells in the presence of serum. These vectors also exhibited FR-dependent gene transfer that could be blocked with free folate.

In summary, FR-targeted pH-sensitive liposomes based on cationic/anionic lipid pair, with the appropriate composition, can facilitate highly efficient intracellular drug and gene delivery. In contrast to

DOPE-based pH-sensitive liposomes, the pH-sensitivity of cationic/anionic liposomes is maintained in the presence of serum. Since retaining activity in the presence of serum is required for use in systemic delivery, these liposomes might potentially be suitable for systemic administration. Further studies are warranted to evaluate the potential use of these formulations for in vivo drug and gene delivery.

Acknowledgements

This work was supported in part by a grant (RPG-99-097-01-MGO) from the American Cancer Society and grant R01 CA79758-01A1 from the National Institute of Health.

References

[1] R.M. Straubinger, pH-sensitive liposomes for delivery of macromolecules into cytoplasm of cultured cells, Methods Enzymol. 221 (1993) 361–376.
[2] M.Z. Lai, W.J. Vail, F.C. Szoka, Acid- and calcium-induced structural changes in phosphatidylethanolamine membranes stabilized by cholesteryl hemisuccinate, Biochemistry 24 (1985) 1654–1661.
[3] J. Connor, M.B. Yatvin, L. Huang, pH-sensitive liposomes: acid-induced liposome fusion, Proc. Natl. Acad. Sci. USA 81 (1984) 1715–1718.
[4] I.M. Hafez, S. Ansell, P.R. Cullis, Tunable pH-sensitive liposomes composed of mixtures of cationic and anionic lipids, Biophys. J. 79 (2000) 1438–1446.
[5] P. Garin-Chesa, I. Campbell, P.E. Saigo, J.L. Lewis Jr., L.J. Old, W.J. Rettig, Trophoblast and ovarian cancer antigen LK26. Sensitivity and specificity in immunopathology and molecular identification as a folate-binding protein, Am. J. Pathol. 142 (1993) 557–567.
[6] S.D. Weitman, R.H. Lark, L.R. Coney, D.W. Fort, V. Frasca, V.R. Zurawski Jr., B.A. Kamen, Distribution of the folate receptor GP38 in normal and malignant cell lines and tissues, Cancer Res. 52 (1992) 3396–3401.
[7] J.F. Ross, H. Wang, F.G. Behm, P. Mathew, M. Wu, R. Booth, M. Ratnam, Folate receptor type-β is neutrophilic lineage marker and is differentially expressed in myeloid leukemia, Cancer 85 (1999) 348–357.
[8] R.J. Lee, P.S. Low, Delivery of liposomes into cultured KB cells via folate receptor-mediated endocytosis, J. Biol. Chem. 269 (1994) 3198–3204.
[9] R.J. Lee, P.S. Low, Folate-mediated tumor cell targeting of liposome-entrapped doxorubicin in vitro, Biochim. Biophys. Acta 1233 (1995) 134–144.
[10] A. Gabizon, A.T. Horowitz, D. Goren, D. Tzemach, F. Madelbaum-Shavit, M.M. Qazen, S. Zalipsky, Targeting folate receptor with folate linked to extremities of poly-(ethylene glycol)-grafted liposomes: in vitro studies, Bioconjug. Chem. 10 (1999) 289–298.
[11] R.J. Lee, S. Wang, P.S. Low, Measurement of endosome pH following folate receptor-mediated endocytosis, Biochim. Biophys. Acta 1312 (1996) 237–242.
[12] W. Guo, T. Lee, J. Sudimack, R.J. Lee, Receptor-targeted delivery of liposomes via folate-PEG-Chol, J. Liposome Res. 10 (2000) 179–195.
[13] K.M. Vogel, S. Wang, R.J. Lee, J.A. Chmielewski, P.S. Low, Peptide-mediated release of folate-targeted liposome content from endosomal compartments, J. Am. Chem. Soc. 118 (1996) 1581–1586.
[14] R.J. Lee, L. Huang, Folate-targeted, anionic liposome-entrapped polylysine-condensed DNA (LPD II) for tumor cell-specific gene transfer, J. Biol. Chem. 271 (1996) 8481–8487.
[15] J. Sudimack, R.J. Lee, Drug targeting via the folate receptor, Adv. Drug Deliv. Rev. 41 (2000) 147–162.

European Journal of Pharmaceutical Sciences 43 (2011) 290–296

Contents lists available at ScienceDirect

European Journal of Pharmaceutical Sciences

journal homepage: www.elsevier.com/locate/ejps

Liposomes radiolabeled with ^{159}Gd: *In vitro* antitumoral activity, biodistribution study and scintigraphic image in Ehrlich tumor bearing mice

Daniel Crístian Ferreira Soares, Mônica Cristina de Oliveira, André Luís Branco de Barros, Valbert Nascimento Cardoso, Gilson Andrade Ramaldes *

Universidade Federal de Minas Gerais, Faculdade de Farmácia, Avenida Presidente Antônio Carlos, 6627 Pampulha, 31270-901 Belo Horizonte, Minas Gerais, Brazil

ARTICLE INFO

Article history:
Received 31 January 2011
Received in revised form 18 April 2011
Accepted 7 May 2011
Available online 14 May 2011

Keywords:
Gadolinium-159 liposomes
In vitro antitumoral activity
Biodistribution study
Scintigraphic image

ABSTRACT

PEG-coated pH-sensitive and PEG-folate-coated pH-sensitive liposomes containing the Gd-DTPA-BMA complex were prepared and radiolabeled by neutron activation. The radiolabeled liposomes presented significant *in vitro* cytotoxic activity against Ehrlich tumor cells when compared with controls. The biodistribution profile of these liposomes and free ^{159}Gd-DTPA-BMA were studied in mice bearing a previously-developed solid Ehrlich tumor. The results demonstrated an important uptake of the formulations by the tumor tissue, with a tissue/blood partition coefficient (Kp) 3.88 and 14.16 times higher than that of the free complex for pH-sensitive PEG-coated and PEG-folate-coated liposomes containing the ^{159}Gd-DTPA-BMA complex, respectively. Both formulations accumulated in the liver and spleen, thereby revealing some difficulty in escaping the action of the MPS cells. The formulation without folate presented a lower renal uptake, which is desirable in patients with chronic renal failure due to the potential risk of nephrogenic systemic fibrosis (NFS). The scintigraphic study revealed that the target/non-target ratio is always greater than three for pH-sensitive PEG-coated liposome formulations and above nine for pH-sensitive PEG-folate-coated liposome formulations. The results obtained in this study demonstrated that the formulations employed can be considered to be a potential alternative for the treatment of cancer, including patients with chronic renal failure.

1. Introduction

Different therapeutic radiopharmaceuticals containing the ^{32}P, ^{188}Re, ^{89}Sr, and ^{90}Y radioisotopes have been used effectively in alleviating bone pain resulting from metastases, synovectomy, and tumors (Vallabhajosula, 2001; Ferro-Flores and Arteaga De Murphy, 2008). These radioisotopes all present the ability to emit high doses of beta radiation, leading to the death of tumor cells. Similarly, according to Saha (1998), the ^{159}Gd isotope emits negative beta (1001 keV) and gamma radiation (main energy: 363.54 keV) suitable for therapeutic applications in nuclear medicine. *In vitro* studies conducted by Soares et al. (2010) showed that free ^{159}Gd-DTPA-BMA presents a high *in vitro* cytotoxicity against Ehrlich tumor cells. However, when administered alone and internally, this radioisotope does not accumulate in target tissues. Thus, to meet these requirements, different pharmaceutical formulations consisting of nanostructured carriers, such as liposomes, have been proposed to reduce the toxicity in non-target organs, especially in patients with chronic kidney disease (Thomsen, 2006), while increasing the effective concentration and contact time in target tissues (Vemuri and Rhodes, 1995; Tokumitsu et al., 2000; Watanabe et al., 2002; Le and Cui, 2006a,b).

The in vivo behavior of "classical or conventional" liposomes showed that they accumulate rapidly in cells of the monocytic phagocyte system (MPS), especially in the liver, spleen, and bone marrow (tissues rich in macrophages), and are quickly eliminated. This elimination limits their use in other tissues. Seeking to overcome these problems, advances in the biophysics of membranes have allowed for the development of liposomes with a modified surface so that the vesicles can undergo a lesser extent of serum protein opsonization, in turn leading to a low degree of recognition by MPS cells. These liposomes are referred to as "stealth", "long circulating", or "sterically stabilized" and represent important advances in in vivo applications due to their ability to evade MPS action cells. Moreover, these liposomes tend to circulate longer in the bloodstream, which in turn facilitates the selection of the targeted tumor regions. Since the pH of oncogenic tissues is lower than that observed in normal tissues, the use of pH-sensitive liposomes has been suggested as a new therapeutic strategy (Carvalho Júnior et al., 2007). This system is capable of releasing, for example, an antineoplastic drug directly into the tumor, thereby decreasing absorption by non-target tissues. In studies conducted by this group, a stable radiolabeled gadolinium complex

* Corresponding author. Tel./fax: +55 31 3409 69 34.
E-mail address: ramaldes@farmacia.ufmg.br (G.A. Ramaldes).

0928-0987/$ - see front matter © 2011 Elsevier B.V. All rights reserved.
doi:10.1016/j.ejps.2011.05.006

(^{159}Gd-DTPA-BMA), suitable for *in vitro* studies in stealth PEG-coated pH-sensitive liposomes (^{159}Gd-SpHL), was produced using a neutron-activation technique in a nuclear reactor and was successfully characterized. In addition, the ^{159}Gd-SpHL presented an *in vitro* cytotoxic activity of 1170 times greater than that of the free complex in RT2 tumor cells (mouse glioma) (Soares et al., 2011).

Several tumor cell lines (OVCAR-3, IGROV1, SKOV3, ovarian cancer, SW626, human adenocarcinoma, and Ehrlich tumor) express receptors for folic acid on their cell surfaces. Thus, seeking better target results for the application of drugs and radioisotopes in tumor tissues, studies have been conducted that involved the immobilization of folic acid molecules on the surface of liposomes and other nanostructures to increase the specificity of liposome action when interacting with receptors located on tumor cell surfaces (Sikora and Grzelakowska-Sztabert, 1984; Parker et al., 2005; Gosselin and Lee, 2002; Sen et al., 1996). In the present work, the preparation of pH-sensitive PEG-coated and PEG-folate-coated liposomes containing the ^{159}Gd-DTPA-BMA complex, the characterization of the *in vitro* cytotoxic activity of these formulations against Ehrlich tumor cells, as well as a biodistribution study and scintigraphic imaging in mice bearing a solid Ehrlich tumor were performed.

2. Experimental

2.1. Materials

The Gd-DTPA-BMA complex, commercially known as Gadodiamide (Omniscan® – General Electric Healthcare Company), was purchased from FARMASA (São Paulo, Brazil). The lipids dioleoylphosphatidylethanolamine (DOPE), distearoylphosphatidylethanolamine-polyethyleneglycol 2000 (DSPE-PEG$_{2000}$), and cholesteryl hemisuccinate (CHEMS) were purchased from Lipoid GmbH (Ludwigshafen, Germany) and Sigma (St. Louis, USA), respectively. The DSPE-PEG-Folate lipid was purchased from Avanti Polar Lipids (Alabaster, USA). The MTT [3-(4,5-dimethyl-2-thiazolyl-2,5-diphenyl)-2*H*-tetrazolium bromide] salt was purchased from Sigma (St. Louis, MO, USA), and the DMEM culture medium was purchased from Gibco BRL (Grand Island, NY, USA). All the solvents used were of analytical grade, while the relevant chemicals were of commercially available reagent grade and were used without further purification. MilliQ® water (simplicity 185, Millipore, Bedford, USA) was used throughout. For quantification of caspase-3, the *CleavaLite® Caspase 3 Activity Assay Kit* was purchased from Millipore (Billerica, USA).

2.2. Methods

2.2.1. Liposome preparation

The pH-sensitive PEG-coated and PEG-folate-coated liposomes containing the Gd-DTPA-BMA complex (Gd-SpH and Gd-FTSpHL, respectively) were prepared according to the procedure described for Soares et al. (2011). For the Gd-SpHL formulation, the DOPE, CHEMS, and DSPE-PEG$_{2000}$ lipids, in a molar ratio of 5.7/3.8/0.5 were employed. For the Gd-FTSpHL formulation, the lipids of DOPE, CHEMS, DSPE-PEG$_{2000}$, and DSPE-PEG$_{2000}$-folate presented a molar ratio of 5.7/3.8/0.45/0.05 in a total lipid concentration of 40 mM, adopted according to studies conducted by Gabizon et al. (1999).

2.2.2. Gd-DTPA-BMA labeling procedure

The procedure for labeling the Gd-DTPA-BMA complex encapsulated in liposomes was performed in polystyrene containers in a TRIGA MARK-I IPR-R1 nuclear reactor at the Division for Radiation Technology, Nuclear Technology Development Centre/National Commission for Nuclear Energy (CDTN–CNEN, Brazil). Liposome samples (1 mL) containing Gd-DTPA-BMA were irradiated at 100 kW with a thermal neutron flux of 6.6×10^{11} n cm^{-2} s^{-1} for 8 h, reaching an activity of 13.8 ± 1.4 GBq.

To verify whether the ^{159}Gd radioisotope had been formed, the gamma spectroscopy procedure was conducted in a hyper-pure germanium detector (Canberra, France) with a resolution (FWHM) of 1.75 keV at 1332 keV and a 15% relative efficiency. All counts were obtained through a constant geometry in a position where the analyzer dead-time indicator registered less than 5% decay correction. The Genie-2000 software was used to process the spectra and determination of the peak area.

2.2.3. In vitro cytotoxic evaluation

In previous studies conducted by Soares et al. (2010), the IC_{50} values of free 134 mM Gd-DTPA-BMA and 1.4 mM ^{159}Gd-DTPA-BMA were determined against the Ehrlich tumor model. In the present study, the *in vitro* cytotoxic activity of samples containing blank liposomes (encapsulating Hepes buffer), PEG-coated (^{159}Gd-SpHL), and PEG-folate-coated (^{159}Gd-FTSpHL) pH-sensitive liposomes were determined using the same tumor model. The Ehrlich tumor cells were obtained from ascites tumors previously induced in Swiss mice. The cells were extracted at the appropriate time for tumor development in animal donors and placed on a 96-well culture plate (500/well), totaling 120,000 cells. After serial dilution to obtain a maximum radioactivity concentration of 650 MBq mL^{-1} well^{-1} in a volume of 100 μL, the cells were treated for 48 h (5% CO_2 – Pol-Eko Aparatura – ST line) in a humid atmosphere at 37 °C in a CO_2 incubator. A culture medium of Dulbecco's modified eagle medium (DMEM), supplemented with sodium bicarbonate (3.7 g/L), penicillin (5000 U/mL), and 10% w/w sterile fetal calf serum, was used. A total of eight replicates were used for appropriate statistical evaluation. By means of an MTT assay, metabolic feasibility tests were performed to evaluate the efficacy of the treatment. The IC_{50} curve, comparing the percentage of cell survival to the molar concentration of samples, was obtained by employing a non-linear regression model (sigmoid dose–response option) using the GraphPad Prism, version 5.0 software. Data were analyzed by a two-way ANOVA, and the means were compared by applying the Bonferroni test (Post-hoc), where $P \leqslant 0.05$ was considered to be statistically significant.

2.2.4. Ehrlich solid tumor development

One milliliter of the ascitic fluid containing viable Ehrlich tumor cells was transferred to a 50 mL Falcon tube. The Ehrlich cells were centrifuged at 3000*g* for 5 min. The supernatant was removed and sediment was dissolved in sufficient saline solution (0.9%) to obtain the original volume. This process was repeated, and the cells were stained with a solution of Trypan blue (0.4%) and counted using a Newbauer chamber with a microscope at a magnification of 400×.

A suspension of viable cells with an average density of 5.0×106 cells/mL was prepared for the development of the Ehrlich solid tumor, and a 100-μL volume of this suspension was implanted in the right flank of female Swiss mice, with a body mass of approximately 25 g ($n = 36$). The mice were kept in an area with controlled lighting and had free access to food and water. Twenty days after implantation, the solid Ehrlich tumor was visible and palpable.

All the protocols involving animal experiments in this study were approved by the Ethics Committee on Animal Experimentation at the Federal University of Minas Gerais (CETEA), under the Code No. 019/09, and comply with the requirements of the Guide for Care and Use of Laboratory Animals recommended by the Institute of Laboratory Animal Resources (USA).

2.2.5. Determination of apoptosis in Ehrlich tumor cells

This test was performed by applying the method of the CleavaLite® Caspase 3 Activity Assay Kit (Millipore). For this study, Ehrlich cells were placed on 96-well culture plates and incubated for 24 h for adhesion. Then, 3.0×10^6 cells were divided into three different groups, each containing 1.0×10^6 cells. The cells of group 1 (the control group) were treated with saline. The cells of group 2 and 3 were treated with Gd-DTPA-BMA and ^{159}Gd-DTPA-BMA at 1.0×10^{-1} and 1.0×10^{-3} mM, respectively. After the treatment period, the cells of group 2 and 3 were lysed with 500 μL of lysis buffer, provided by the kit's manufacturer, and incubated in an ice bath for a period of 10 min.

The cells were centrifuged at 10,000 rpm (9600*g*) for 5 min at 4 °C and the supernatant (cytosolic extract) was transferred to an Eppendorf tube. This cytosolic extract was used to test the activity of caspases 3. A 20-μL volume of extract was incubated with 100 μL of assay buffer (supplied in the kit) in the presence or absence of the caspase 3 inhibitor. The samples were then transferred and incubated at 37 °C on a 96-well microplate for 1 h. The concentration of pNA (p-nitroaniline) formed was monitored by a 96-well card reader at 405 nm and compared with the control group, using a previously-standardized reference curve of optical density versus pNA concentration.

2.2.6. Biodistribution studies

Biodistribution studies were conducted using two different protocols: (1) ex vivo biodistribution study and (2) scintigraphic study and subsequent sacrifice. The studies were conducted based on the presence of radioactive gadolinium in the formulations, and the animals received implants of Ehrlich solid tumors with an average development time of 20 days prior to the study.

2.2.6.1. Ex vivo biodistribution study. Samples of ^{159}Gd-DTPA-BMA (100 μL; 0.5 mmol/mL), ^{159}Gd-SpHL and ^{159}Gd-FTSpHL (236 mg/kg) were injected intravenously into the tail of Swiss mice. After periods of 10 min and 1, 8, and 24 h, each animal (three per group) was anesthetized intraperitoneally with a mixture of Ketamine and Xylazine at a dose of 100 and 8 mg/kg, respectively. The blood was collected immediately by cardiac puncture, and the mice were sacrificed by cervical dislocation. The lungs, stomach, spleen, liver, kidneys, and solid Ehrlich tumor were collected, washed with distilled water, dried on filter paper, and weighed. The determination of radioactivity present in the organs was achieved through automatic scintillation (ANSR-Abott, USA). The readings were conducted at the 350–380 keV energy window for 4 min. The radioactivity contained in each organ was divided by its mass to furnish the radioactivity in counts per minute per gram of tissue (cpm/g). To set the radioactive decay of ^{159}Gd, a separate tube with the standard dose containing the same activity and volume of the dose injected into animals was defined as 100% of radioactivity. The % ID/g ratio of tissue was obtained from the relationship between the radioactivity measured in tissue and the radioactivity measured in the standard. The data were statistically analyzed by analysis of variance (ANOVA) using a PRISM 5.0 software. The tissue-blood partition coefficient (Kp) was determined by dividing the area under the tissue concentration versus the time curve by the area under the blood concentration versus time curve.

2.2.6.2. Scintigraphic biodistribution study. For the scintigraphic study, ^{159}Gd-SpHL and ^{159}Gd-FTSpHL with 125 MBq activity were produced to obtain enough activity to acquire the images. The animals were anesthetized intraperitoneally with a Ketamine and Xylazine solution at a dose of 40 and 5 mg/kg, respectively, and were then placed on the table in a supine position so that the detector was positioned on the anterior region of the animal. The images were obtained with a gamma camera with a collimator-type High Energy General Purpose (HEGP) $128 \times 128 \times 32$ array and an acquisition time of 900 s. Nine animals were used, with the Ehrlich tumor implanted in the back of the left thigh. Images were obtained from the same animals 8 h after the administration of 11 MBq of the radiolabeled sample.

2.3. Statistical analysis

The results were calculated and presented as the mean for each group ± the standard error of the mean (mean ± SD). Statistical evaluation of the data was performed using analysis of variance (ANOVA), followed by the Bonferroni's test (post-hoc), where $P \leqslant 0.05$ was considered to be statistically significant.

3. Results and discussion

3.1. Liposome labeling

The ^{159}Gd isotope is unavailable on the market. Therefore, the only way to produce this isotope is by irradiating a natural gadolinium sample with a neutron flux in a suitable nuclear reactor or by obtaining it from a ^{252}Cf source (Alfassi, 1985). In a previous study, the Gd-DTPA-BMA complex was irradiated with neutrons to obtain the ^{159}Gd-DTPA-BMA isotope. It was concluded that this complex was stable and that no significant change in the structure of the complex could be observed after 8 h of irradiation (Soares et al., 2010). The preparation of liposomes containing radioisotopes involves complex operations that require licensing from government agencies as well as the handling of radioactive material in liquid form, which is typically performed by highly trained personnel. Faced with these difficulties, Gd-SpHL was prepared in a previous study and irradiated with neutrons for 8 h to produce a radioactive liposome (^{159}Gd-SpHL) (Soares et al., 2011). The results showed that the neutron activation process resulted in no changes in the size distribution, Zeta potential, and morphology of the liposomes, thus indicating that their physical integrity was maintained (Mumper and Jay, 1992; Ostrowsky, 1993).

In the present study, Gd-SpHL and Gd-FTSpHL were irradiated for 8 h using the same procedures described above. The PCS technique aided us in determining the mean size and Zeta potential of vesicles nearly at 100 nm and -47 ± 2.3 mV, respectively, for both formulations. The characteristic peaks of the ^{159}Gd radioisotope were determined at 58.7, 79.5, 137.5, 305.5, 348.2, and 363.5 keV, and the specific activity of 12.6 ± 2.1 MBq mg^{-1} was calculated and confirmed through gamma spectroscopy. The energies and their intensities were consistent with the values published by Soares et al. (2011).

3.2. In vitro cytotoxic study

The cytotoxic activity of the blank liposomes and the Gd-SpHL were evaluated as a control of the cytotoxic activity of the ^{159}Gd-SpHL formulation. The results revealed an IC_{50} of 13.8 ± 0.4 mM for blank liposomes. Research published since the 1970s demonstrate the cytotoxic activity of liposomes (Panzner and Jansons, 1979; Cortesi et al., 1996). Because of the similarity of chemical structures in the cell membranes and liposomes, fluidization phenomena and a destabilization of the cytoplasmic membrane, which can lead to apoptosis, especially in tumor cells, can be observed. Furthermore, the results also showed that the use of blank liposomes containing a total lipid concentration of lower than 9 mM can lead to a more than 90% viability of the Ehrlich cells (data not presented). Therefore, lipid concentrations of lower than 9 mM were employed for all the experiments, thereby avoiding the contribution of the phospholipid constituents within the

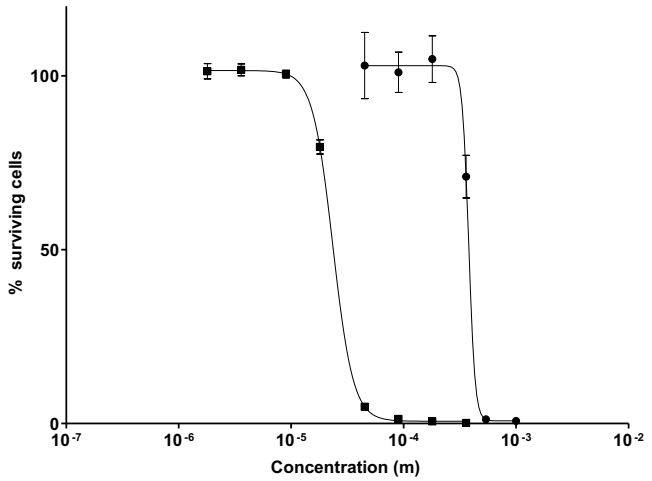

Figure 1. Cytotoxity of ^{159}Gd-SpHL (■) and Gd-SpHL (●) formulations in Ehrlich cells (n = 8). The curve fit presents R^2 = 0.981 and degrees of freedom = 30.

preparations of cytotoxic activity of formulations containing the Gd-DTPA-BMA.

IC_{50} values of 0.39 ± 0.40 and 0.024 ± 0.004 mM, respectively, were observed for Gd-SpHL and ^{159}Gd-SpHL samples (Fig. 1). The radioactivity caused a 16-fold enhancement of the cytotoxic activity of the formulation against Ehrlich tumor cells. By comparing these results with data published by Soares et al. (2010), where Gd-DTPA-BMA and ^{159}Gd-DTPA-BMA presented IC_{50} values of 134 and 1.4 mM, respectively, it can be verified that, regardless of the form used (radioactive or not), the encapsulation of Gd-DTPA-BMA in liposomes enhanced the *in vitro* cytotoxic effect against the Ehrlich tumor model. Furthermore, when comparing the results for the IC_{50} values of Gd-DTPA-BMA and ^{159}Gd-SpHL, the radioactivity proved to supplement the action of the liposomes as carriers and lead to a 5580-fold increase in the cytotoxic activity.

The molecular mechanisms of liposome cell interactions are not well-understood. However, many studies in the literature report that liposomes can fuse with the cell membrane or undergo endocytosis, thus internalizing substances of interest, as is the case in endocytic vesicles with slightly acidic pH levels (Düzgünes and Nir, 1999; Simões et al., 2004). The structure of Gd-DTPA-BMA is very hydrophilic. Thus, it may be difficulty for this liposome to access the intracellular environment. The present studies' results indicate that the encapsulation of the gadolinium complex in liposomes facilitated their internalization within the cytosol of Ehrlich cells, thus contributing to improving their cytotoxic activity. This discussion can be supported by the results obtained by Simões et al. (2001) which shows that DOPE containing liposomes are essentially internalized by endocytosis.

3.3. A study of apoptosis in Ehrlich cells

The determination of caspase-3 activity in Ehrlich cells was employed in a study of the apoptosis process in Ehrlich cells. The results for the activity of caspase-3 in four groups of samples are presented in Fig. 2. These results revealed that the presence of a non-radioactive metal complex and blank liposomes (total lipid concentration of 9 mM) did not alter the activity of caspase-3. However, there was a significant increase in the caspase-3 group, when compared to control cells, when they were under the influence of ^{159}Gd-DTPA-BMA, indicating that apoptosis is most likely the main means of death suffered by the cells.

Although malignant tumor cells exhibit various characteristics, evidence shows that resistance to apoptosis is a distinguishing

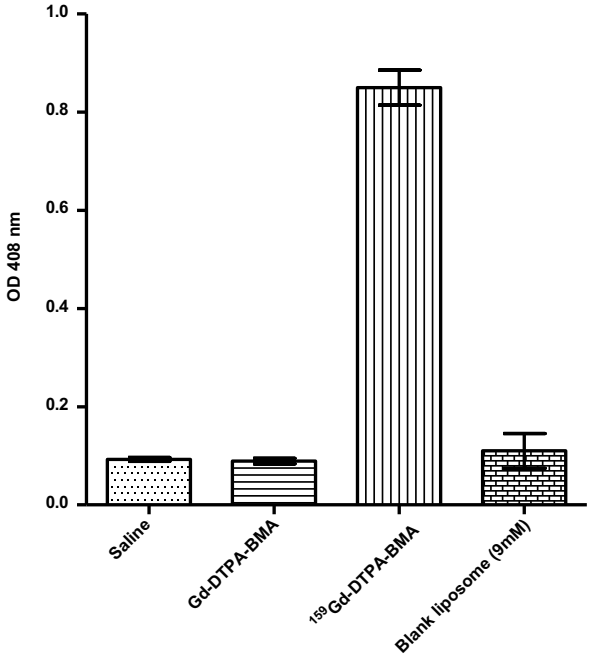

Figure 2. Caspase-3 activity in Ehrlich cells treated with saline, Gd-DTPA-BMA, ^{159}Gd-DTPA-BMA and blank liposome (9 mM total lipid concentration). Values expressed in optic density ± standard deviation.

characteristic of most malignant tumors and is an important goal of therapeutic approaches (Okada and Mak, 2004). Studies indicate that the p53 protein plays a key role in regulating the G1 phase checkpoint in response to DNA damage (Millau et al., 2008). The relationship between the p53 protein and carcinogenesis has been widely confirmed by the high rate of mutation of the gene in malignant tumors from different tissues (Khan et al., 2000; Baker et al., 1990). Experimental procedures revealed that ionizing radiation can promote the activation of the p53 protein, thereby increasing its concentration in the cell nucleus and leading to apoptosis. These observations have contributed greatly to the elucidation of the action mechanism of ionizing radiation against tumor cells (Burger et al., 1998; Choi et al., 2004; Zambetti, 2005). The migration of pro-apoptotic proteins (BAX and BID) from the cytoplasm to the mitochondria can occur in the presence of intracellular stress, such as exposure to ionizing radiation from ^{159}Gd, thereby altering the permeability and allowing for the release of other pro-apoptotic proteins as well as the activation of caspase-9. This activation triggers the caspase-3 effector identified in this study. These results suggest that the cytotoxic effect triggered by ^{159}Gd-DTPA-BMA is associated with the activation of apoptotic pathways that lead cells to Ehrlich death.

3.4. Biodistribution studies

3.4.1. Ex vivo biodistribution study

The results of ex vivo biodistribution studies are shown in Fig. 3. The values found in the lungs and stomach were suppressed, since these values were lower than 0.01% ID/g and were considered negligible. For the other organs investigated (blood, liver, spleen, and kidneys), a rapid blood clearance within 1 h after administration was observed for ^{159}Gd-DTPA-BMA. This result is in agreement with those presented in the monograph of the drug (GE Healthcare, 2006). The values observed for the formulations after 1 h were significantly higher than those found for the free drug. The values for the area under the curve (AUC) were 6.55 and 5.81 times higher for the ^{159}Gd-SpHL and ^{159}Gd-FTSpHL formulations, respectively.

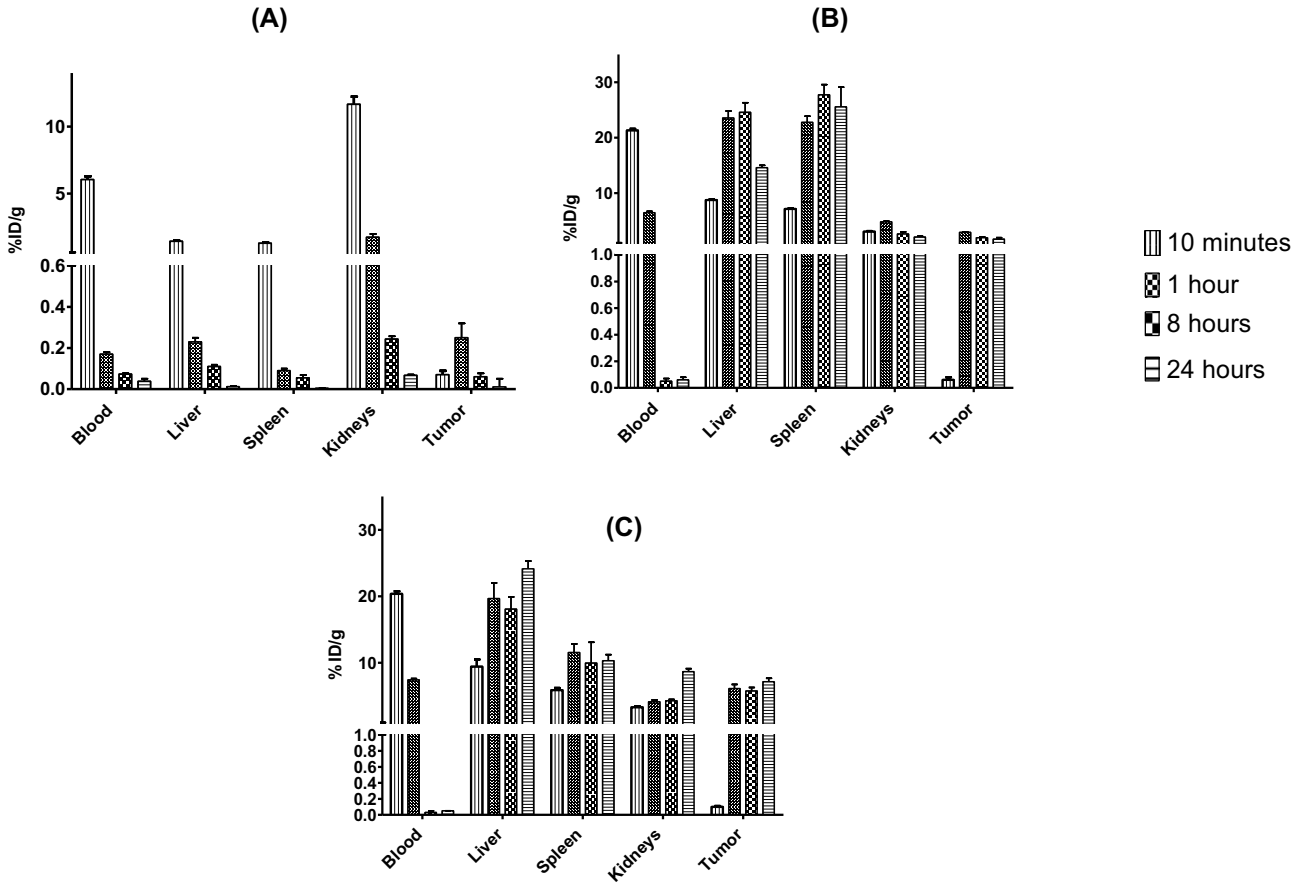

Figure 3. Biodistribution profile in different tissues at the times: 10 min, 1, 8 and 24 h. (A) ^{159}Gd-DTPA-BMA, (B) ^{159}Gd-SpHL, (C) ^{159}Gd-FTSpHL. Values expressed as mean ± SD.

Thus, the circulation time of the formulations in the bloodstream (Table 1) is greater. The biodistribution studies of the liver and spleen showed that the concentration of free drug was lower than those of the formulations. According to Zong et al. (2008), the Gd-DTPA-BMA complex does not undergo hepatic metabolism and is eliminated, mainly in the form of the original complex. This fact may well explain the low hepatic uptake observed. Moreover, it is known that liposomes are taken up by MPS cells, which are widely present in the liver and spleen, although the formulations also contain PEG or PEG-folate chains.

A significantly higher uptake of the ^{159}Gd-FTSpHL formulation by the liver than the formulation without folate after 24 h could be observed. This finding can be explained by the fact that the liver has cells that express receptors for folic acid (FR) (Parker et al., 2005). The formulation containing folate presented a lower uptake by the spleen than that of the ^{159}Gd-SpHL formulation. It is known that the addition of hydrophilic polymers to the surface of liposomes results in a lower serum protein opsonization of the vesicles, thus reducing uptake by MPS cells. It is believed that the addition of folic acid, a very hydrophilic molecule, to the surface of liposomes contributed in further reducing the process of opsonization and led to a lower uptake by MPS cells. This fact may well explain the results for uptake by the spleen (Torchilin, 2006). All the results obtained for the biodistribution of the formulations in the liver and spleen are in agreement with the findings of Carvalho Júnior et al. (2007). The biodistribution values for free ^{159}Gd-DTPA-BMA are consistent with the results published by Tweedle et al. (1995).

Similar to the results obtained for the hepatic uptake, a significant increase in the renal uptake of ^{159}Gd-SpHL and ^{159}Gd-FTSpHL during a 24 h period could be observed. These results revealed that this is an important elimination route for the two formulations. However, the increased uptake observed for the ^{159}Gd-FTSpHL formulation concerning ^{159}GdSpHL can be explained by the presence of folate receptors in this organ (Parker et al., 2005). Adverse effects, especially in patients suffering from chronic renal

Table 1
Partition coefficient tissue/blood (Kp) in mouse different tissues after I.V. administration of ^{159}Gd-DTPA-BMA, ^{159}Gd-SpHL and ^{159}Gd-FTSpHL.

Tissue	AUC			Kp (A)	Kp (B)	Kp (C)	Kp (B)/Kp (A)	Kp (C)/Kp (A)
	^{159}Gd-DTPA-BMA (A)	^{159}Gd-SpHL (B)	^{159}Gd-FTSpHL (C)					
Blood	4.27	27.98	24.81					
Liver	2.86	495.00	481.60	0.67	19.41	26.44	17.69	29.01
Spleen	1.55	615.20	244.50	0.36	9.85	60.45	21.99	27.10
Kidneys	14.95	57.45	139.20	3.50	4.97	0.66	2.31	1.42
Tumor	1.79	45.52	147.30	0.42	5.93	3.88	1.63	14.16

Kp calculated from ratio AUC_{0-24h}/tissue and AUC_{0-24h} blood.

insufficiency, were observed after the administration of the Gd-DTPA-BMA complex in MRI procedures (Thomsen, 2006). For this reason, the FDA requested that a warning be added to the descriptions of the product (Omniscan®) regarding the potential risk of NFS in patients with chronic renal failure (US FDA, 2010).

The ^{159}Gd-SpHL formulation contains a Kp of 2.31, versus 3.50 for the free drug (Table 1). A lower renal uptake may result in fewer possibilities for the development of NFS in patients with renal failure. However, a Kp of 4.97 was observed for the ^{159}Gd-FTSpHL formulation, as compared to 3.50 for the free drug, which indicates that the former presented a higher renal accumulation (Table 1). Therefore, the possible use of the ^{159}Gd-FTSpHL formulation for the treatment of cancer by patients with severe chronic kidney disease still warrants further investigation.

The biodistribution studies in solid Ehrlich tumors revealed a low uptake of the free drug, which presented a maximum value of 0.25 ± 0.7% ID/g after 1 h (Fig. 3). The formulations presented a higher uptake by tumor tissue during the same period. The uptake of the ^{159}Gd-SpHL formulation (2.92 ± 0.1% ID/g) was 11.7 times higher, while that of the ^{159}Gd-FTSpHL formulation (6.12 ± 0.3% ID/g) was 24.5 times higher. As regards other times, the maintenance of levels of tumor uptake for both formulations could be identified. Several studies have been published showing that folic acid receptors are expressed in a broad spectrum of tumors (Sudimack et al., 2000; Gabizon et al., 2003). In the present study, the formulation containing folic acid presented an uptake by solid Ehrlich tumors which were significantly higher than that of the formulation without folic acid. This result is consistent with the fact that Ehrlich tumor cells, according to Sikora and Grzelakowska-Sztabert (1984), show receptors for folic acid on their surface. More detailed studies regarding the quantity and avidity of folic acid receptors in these cells can serve as guidelines for the development of more effective formulations of therapeutic drugs for targeting these cells.

By using the AUC/tissue and AUC/blood ratios for the period studied, the partition coefficient was calculated and revealed that the formulations present a more expressive perfusion in the liver, spleen, kidneys, and tumor with Kp values of 17.69, 21.99, 2.31, and 1.63, respectively, for ^{159}Gd-SpHL (Table 1), as well as Kp values of 19.41, 9.85, 4.97, and 5.93, respectively, for ^{159}Gd-FTSpHL (Table 1). These results showed that the formulation containing folate induced a greater perfusion in all the tissues studied, except for the spleen, where a 2.2-fold reduction in splenic accumulation was observed, with Kp values varying from 21.99 to 9.85 (Table 1). With regard to the tumor, the free complex had a low degree of perfusion. However, a Kp value of 1.63 was obtained for the ^{159}Gd-SpHL formulation. This value represents an increase of approximately 3.88-fold over that of the free complex (Table 1). The ^{159}GdFTSpHL presented a Kp value of 5.93, which represents an increase of approximately 14.41-fold more than that of the free complex (Table 1). When comparing the Kp of the two formulations, the addition of folate led to a 3.63-fold increase in tumor tissue permeation and an improvement in the delivery of the radioactive complex to these cells.

3.4.2. Scintigraphy biodistribution study

Scintigraphic images of mice that received ^{159}Gd-SpHL or ^{159}Gd-FTSpHL are shown in Fig. 4. Since the amounts of radiation were insufficient, it was impossible to acquire images of animals that received ^{159}Gd-DTPA-BMA.

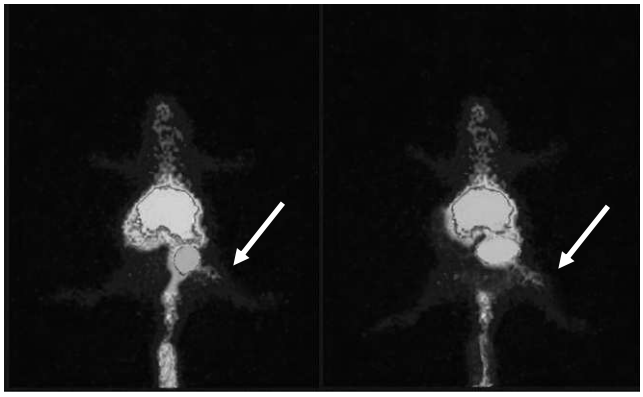

Figure 4. Scintigraphic image obtained after I.V. administration of ^{159}Gd-SpHL (left image) and ^{159}Gd-FTSpHL (right image).

The quantitative analysis of the images revealed that the region of interest (ROI) showed that the target/non-target ratio tended to be greater than three for the ^{159}Gd-SpHL formulation. This fact indicates that the tumor region presented at least a 300% greater radioactivity than that of the control (muscle) (Table 2). These results support data obtained from the biodistribution study, confirming that the Gd-SpHL formulation has a greater affinity for the tumor region than for muscle tissue. The ROI determined for the ^{159}Gd-FTSpHL formulation showed that the target/non-target ratios tended to be greater than nine (Table 2). This fact shows that the tumor region presented at least a 900% greater radioactivity than the control (muscle) and that the formulation presented a high affinity for the tumor tissue. By comparing the results of the target/non-target ratio for ^{159}Gd-SpHL and ^{159}Gd-FTSpHL formulations, an increase of approximately 3-fold in the tumor uptake for the formulation containing folate was calculated. This result is in agreement with the findings obtained in the ex vivo biodistribution study.

4. Conclusion

Stealth pH-sensitive PEG-coated and PEG-folate-coated liposomes containing the ^{159}Gd-DTPA-BMA complex were successfully prepared and radiolabeled. These formulations presented significant cytotoxic activities against Ehrlich tumor cells, and the apoptosis was determined to be the most probable mechanism that mediated the death of the cells. The biodistribution study revealed that free ^{159}Gd-DTPA-BMA has a low affinity for the tissues studied, including the solid Ehrlich tumor, being eliminated mainly by renal excretion. However, the formulations exhibited different biodistribution profiles. The accumulation in the tumor tissue was significantly greater than that observed in the liver, spleen, and kidney tissues. The immobilization of folate on the liposome surface resulted in a 3-fold increase in the uptake of the radioactive complex by the tumor, in addition to a significant reduction in uptake by the spleen. This increase resulted in the delivery of higher

Table 2
Ratio target/non-target obtained in gamma camera (%dose/cm^2).

Sample	1 h	4 h	6 h	8 h	18 h	24 h
^{159}Gd-SpHL	3.19 ± 0.04	3.03 ± 0.08	3.21 ± 0.03	3.18 ± 0.02	3.16 ± 0.09	3.14 ± 0.02
^{159}Gd-FTSpHL	9.14 ± 0.06	9.00 ± 0.03	9.45 ± 0.12	9.58 ± 0.11	9.67 ± 0.08	9.75 ± 0.17

Results expressed as mean ± standard deviation. The values are not statistically different ($P > 0.05$).

radiation doses to the tumor region and improved the chances of the successful treatment of cancer with this formulation.

Due to the presence of folate receptors in liver and kidney cells, the increase in the uptake of the formulation by these tissues resulted in an increase in the radiation dose in these organs. More detailed studies to evaluate whether the radiation doses received by these organs may impair their functions should be conducted. Finally, the investigation of the scintigraphic image showed that the ^{159}Gd-SpHL formulation presented a target/non-target ratio of above three, while ^{159}Gd-FTSpHL presented a target/non-target ratio of above nine, thereby demonstrating that these represent promising therapeutic cancer formulations.

Acknowledgements

The authors thank FAPEMIG (Fundação de Amparo a Pesquisa do Estado de Minas Gerais), CNPQ (Conselho Nacional de Desenvolvimento Científico e Tecnológico), and CNEN (Comissão Nacional de Energia Nuclear) for their financial support.

References

Alfassi, Z.B., 1985. Epithermal neutron activation analysis. J. Radioanal. Nucl. Chem. 90, 151–165.

Baker, S.J., Markowitz, S., Fearon, E.R., Willson, J.K., Vogelstein, B., 1990. Suppression of human colorectal carcinoma cell growth by wild-type p53. Science 249, 912–915.

Burger, H., Nooter, K., Boersma, A.W.M., Kortland, C.J., Van den Berg, A.P., Stoter, G., 1998. Expression of P53, P21/WAF/CIP, BCL-2, BAX, BCL-X, and BAK in radiation-induced apoptosis in testicular germ cell tumor lines. Int. J. Radiat. Oncol. Biol. Phys. 4, 415–424.

Carvalho Júnior, A.D., Mota, L.G., Nunan, E.A., Wainstein, A.J.A., Wainstein, A.P.D.L., Leal, A.S., Cardoso, V.N., De Oliveira, M.C., 2007. Tissue distribution evaluation of stealth pH-sensitive liposomal cisplatin versus free cisplatin in Ehrlich tumor-bearing mice. Life Sci. 80, 659–664.

Choi, E.K., Roberts, K.P., Griffin, R.J., Han, T., Park, H., Song, C.W., Park, H.J., 2004. Effect of pH on radiation-induced p53 expression. Int. J. Radiat. Oncol. Biol. Phys. 60, 1264–1271.

Cortesi, C.R., Esposito, A.E., Menegatti, A.E., Gambari, B.R., Nastruzzi, C., 1996. Effect of cationic liposome composition on in vitro cytotoxicity and protective effect on carried DNA. Int. J. Pharm. 139, 69–78.

Düzgünes, N., Nir, S., 1999. Mechanisms and kinetics of liposome-cell interactions. Adv. Drug Deliv. Rev. 40, 3–18.

Ferro-Flores, G., Arteaga De Murphy, C., 2008. Pharmacokinetics and dosimetry of ^{188}Re-pharmaceuticals. Adv. Drug Deliv. Rev. 60, 1389–1401.

Gabizon, A., Horowitz, A.T., Goren, D., Tzemach, D., Shmeeda, H., Zalipsky, S., 2003. Invivo fate of folate-targeted polyethylene-glycol liposomes in tumor-bearing mice. Clin. Cancer Res. 9, 6551–6559.

Gabizon, A., Horowitz, A.T., Goren, D., Tzemach, D., Mandelbaum-Shavit, F., Qazen, M.M., Zalipsky, S., 1999. Targeting folate receptor with folate linked to extremities of poly(ethylene glycol)-grafted liposomes: in vitro studies. Bioconjug. Chem. 10, 289–298.

GE Healthcare. Ominiscan, Contrast Enhancement Agent for Magnetic Resonance Imaging (MRI). Product Monograph. Ontario Canadá, 2006, 25pp.

Gosselin, M.A., Lee, R.J., 2002. Folate receptor-targeted liposomes as vectors for therapeutic agents. Biotechnol. Annu. Rev. 8, 103–131.

Khan, Z.A., Jonas, S.K., Le-Marer, N., Patel, H., Wharton, R.Q., Tarragona, A., Ivison, A., Allen-Mersh, T.G., 2000. P53 mutations in primary and metastatic tumors and circulating tumor cells from colorectal carcinoma patients. Clin. Cancer Res. 6, 3499–3504.

Le, U.M., Cui, Z., 2006a. Biodistribution and tumor-accumulation of gadolinium (Gd) encapsulated in long-circulating liposomes in tumor-bearing mice for potential neutron capture therapy. Int. J. Pharm. 320, 96–103.

Le, U.M., Cui, Z., 2006b. Long-circulating gadolinium-encapsulated liposomes for potential application in tumor neutron capture therapy. Int. J. Pharm. 312, 105–112.

Millau, J.F., Bastien, N., Drouin, R., 2008. P53 transcriptional activities: a general overview and some thoughts mutation research. Rev. Mutat. Res. 681, 118–133.

Mumper, R.J., Jay, M., 1992. Poly(L-lactic acid) microspheres containing neutron-activatable holmium-165: a study of the physical characteristics of microspheres before and after irradiation in a nuclear reactor. Pharm. Res. 9, 149–154.

Okada, H., Mak, T.W., 2004. Pathways of apoptotic and nonapoptotic death in tumour cells. Nat. Rev. Cancer 4, 592–603.

Ostrowsky, N., 1993. Liposome size measurements by photon correlation spectroscopy. Chem. Phys. Lipids 64, 45–56.

Panzner, E.A., Jansons, V.K., 1979. Control of in vitro cytotoxicity of positively charged liposomes. J. Cancer Res. Clin. Oncol 95, 29–37.

Parker, N., Turk, M.J., Westrick, E., Lewis, J.D., Low, P.S., Leamon, C.P., 2005. Folate receptor expression in carcinomas and normal tissues determined by a quantitative radioligand binding assay. Anal. Biochem. 338, 284–293.

Saha, G.B., 1998. Fundamentals of Nuclear Pharmacy. Springer, New York, 34–170pp.

Sen, S., Erba, E., D'Incalci, Bottero, M.F., Canevari, S., Tomassetti, A., 1996. Role of membrane folate-binding protein in the cytotoxicity of 5,10-dideazatetrahydrofolic acid in human ovarian carcinoma cell lines in vitro. Br. J. Cancer 73, 525–530.

Sikora, E., Grzelakowska-Sztabert, B., 1984. Quinazoline CB 3717 and CB 3703 inhibition of folate retention and metabolism in Ehrlich ascites carcinoma cells and some organs of the host-mouse. Cancer Lett. 23, 289–295.

Simões, S., Moreira, J.N., Fonseca, C., Düzgünes, N., Pedroso de Lima, M.C., 2004. On the formulation of pH-sensitive liposomes with long circulation times. Adv. Drug Deliv. Rev. 56, 947–965.

Simões, S., Slepushkin, V., Düzgünes, N., Pedroso de Lima, M.C., 2001. On the mechanisms of internalization and intracellular delivery mediated by pH-sensitive liposomes. Biochim. Biophys. Acta 1515, 23–37.

Soares, D.C.F., Menezes, M.A.B.C., Santos, R.G., Ramaldes, G.A., 2010. ^{159}Gd: preparation and preliminary evaluation as a potential antitumoral radionuclide. J. Radioanal. Nucl. Chem. 284, 315–320.

Soares, D.C.F., Oliveira, M.C., Santos, R.G., Andrade, M.S., Vilela, J.M.C., Cardoso, V.N., Ramaldes, G.A., 2011. Liposomes radiolabeled with ^{159}Gd-DTPA-BMA: preparation, physicochemical characterization, release profile and in vitro cytotoxic evaluation. Eur. J. Pharm. Sci. 42, 462–469.

Sudimack, J., Robert, J., Lee, P., 2000. Target drug delivery via the folate receptor. Adv. Drug Deliv. Rev. 41, 147–162.

Thomsen, H.S., 2006. Nephrogenic systemic fibrosis: a serious late adverse reaction to gadodiamide. Eur. Radiol. 16, 2619–2621.

Tokumitsu, H., Hiratsuka, J., Sakurai, Y., Kobayashi, T., Ichikawa, H., Fukumori, Y., 2000. Gadolinium neutron-capture therapy using novel gadopentetic acid ± chitosan complex nanoparticles: in vivo growth suppression of experimental melanoma solid tumor. Cancer Lett. 150, 177–182.

Torchilin, V.P., 2006. Multifunctional nanocarries. Adv. Drug Deliv. Rev. 58, 1532–1555.

Tweedle, M.F., Wedeking, P., Krishan, K., 1995. Biodistribuition of radiolabeled, formulated gadopentetate, gadoteridol, gadoterate and gadodiamide in mice and rats. Invest. Radiol. 6, 372–380.

US FDA – Food and Drug Administration. Information for Healthcare Professionals: Gadolinium-based Contrast Agents for Magnetic Resonance Imaging Scans. Available from: http://www.fda.gov/Drugs/DrugSafety/ucm223966.htm (accessed 15.12.10).

Vallabhajosula, S., 2001. Radiopharmaceuticals in oncology. In: Khalkhali, I., Maublant, J.C., Goldsmith, S.J. (Eds.), Nuclear Oncology Diagnosis and Therapy. Lippincott Williams and Williams, Philadelphia, pp. 31–59.

Vemuri, S., Rhodes, C.T., 1995. Preparation and characterization of liposomes as therapeutic delivery systems. A review. Pharm. Acta Helv. 70, 95–111.

Watanabe, T., Ichikawa, H., Fukumori, Y., 2002. Tumor accumulation of gadolinium in lipid-nanoparticles intravenously injected for neutron-capture therapy of cancer. Eur. J. Pharm. Biopharm. 54, 119–124.

Zambetti, G.P., 2005. The p53 Tumor Suppressor Pathway and Cancer. Springer, New York, 254p.

Zong, Y., Wang, X., Jeong, E.K., Parker, D.L., Lu, Z.R., 2008. Structural effect on degradability and in vivo contrast enhancement of polydisulfide Gd(III) complexes as biodegradable macromolecular MRI contrast agents. Magn. Reson. Imaging 27, 503–511.